Studies on Charge-Transfer Interactions toward Efficient and Stable Blue Organic-Light Emitting Diodes

グエン バ タイン

2023

Doctor thesis

Studies on Charge-Transfer Interactions toward Efficient and Stable Blue Organic-Light Emitting Diodes

(高効率で安定な青色有機発光ダイオードの実現を目指した電荷移動相互作用に関する研究)

Thanh Ba Nguyen

Department of Chemistry and Biochemistry

Graduate School of Engineering

Kyushu University

Content

Chapter 1

Introduction

1-1. General introduction

The research on semiconducting and photophysical properties of purely organic molecules such as anthracene and naphthalene has been ongoing for over 60 years. This area of research has made significant progress and has led to the development of consumer products in optoelectronics, such as displays based on organic light-emitting diodes (OLEDs). Notably, OLED-based displays have been used as display applications for smartphones and a distinguished panel of large-sized OLED TVs, and the OLED technology improved the basics of our daily human life. Nowadays, it is not difficult to find organic semiconductors in modern consumer electronics, particularly display applications. Additionally, organic semiconductors offer distinctive qualities, like ultra-flexibility, making further advancements in organic electronics through fundamental research a promising path toward a bright future.

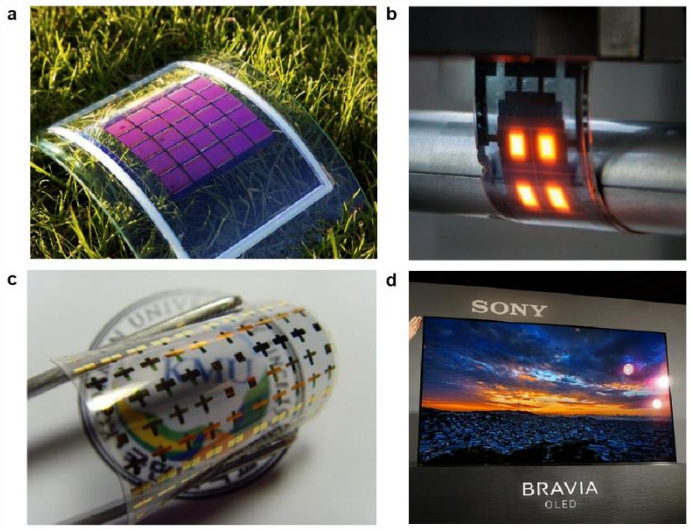

Figure 1.1. Several application fields of organic semiconductor-based devices. (a) Organic solar cells from sciencedaily.com. (b) Flexible OLEDs from news.cnrs.fr. (c) Flexible organic transistors from phys.org. (d) SONY OLED BRAVIA television from cdrinfo.com.

1-2. Brief introduction of organic semiconductor

Conventional inorganic materials exhibit two energy bands[1,2] for the most-outer electrons: the valance band and conduction band (**Fig. 1.2**). The gap between these two classifies materials into insulators (such as rubber), conductors (such as metal), and semiconductors (such as silicon). The material is considered an insulator if the band gap exceeds 5 eV and the Fermi level is within the gap. If the valance band and the conduction band overlap each other, they form a continuous band which

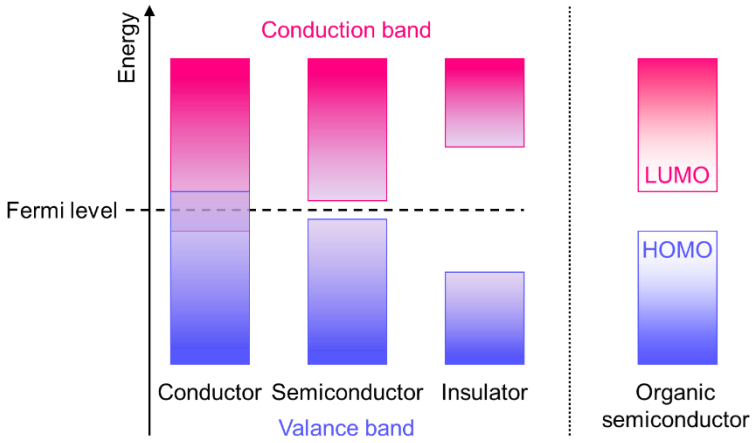

Figure 1.2. Left: Valance band and conduction band of inorganic material. Right: HOMO-LUMO level of organic material.

has the Fermi level lying inside, creating a conductor. Inorganic semiconductors can be achieved when there is a relatively small band gap (< 4 eV) and the Fermi level lies in the gap.

On the contrary, organic semiconductors possess a feature that can imitate the valence-conduction band gap. Due to its intrinsic properties, an organic molecule has the Highest Occupied Molecular Orbital (HOMO) and the Lowest Unoccupied Molecular Orbital (LUMO)[3]. These MOs act like the valance band and conducting band, respectively. Since electrons can be taken from or injected into these MOs, charges can hop between organic molecules. In practice, such a process takes a very long time and suffers from low carrier mobilities of organic materials for holes and electrons. With sufficient technology, it was thought to be possible to realize industrial organic semiconductors. History had to wait until the thin-film fabricating technique, including material development, was invented, resulting in sub-nanometer organic layers. The state-of-the-art thin organic films can sufficiently transport carriers, allowing organic semiconductors to be practically used[4].

It took a short time until people realized that two different processes (often contradicting each other) occur during charge transportation inside the organic semiconductors. They are illustrated in **Fig. 1.3**. As can be seen, both formation of radial anion and radical cation influence the electron-hoping process. To identify them, thinking about electrons and holes transporting through the organic semiconductors is more productive. In detail, we think of electron transport when electrons hop in and out of LUMO. A material favoring this process can be classified as an *n*-type semiconductor. Reversely, when electrons hop in and out of HOMO, we think of it as a positive-charge quasi-particle called “hole”. A material favoring hole transportation can be classified as a *p*-type semiconductor. In principle, however, note that any organic molecule should be able to transport both electrons and holes, i.e., classified as an intrinsic semiconductor. Examples of all types can be found in **Fig. 1.4**[5–11].

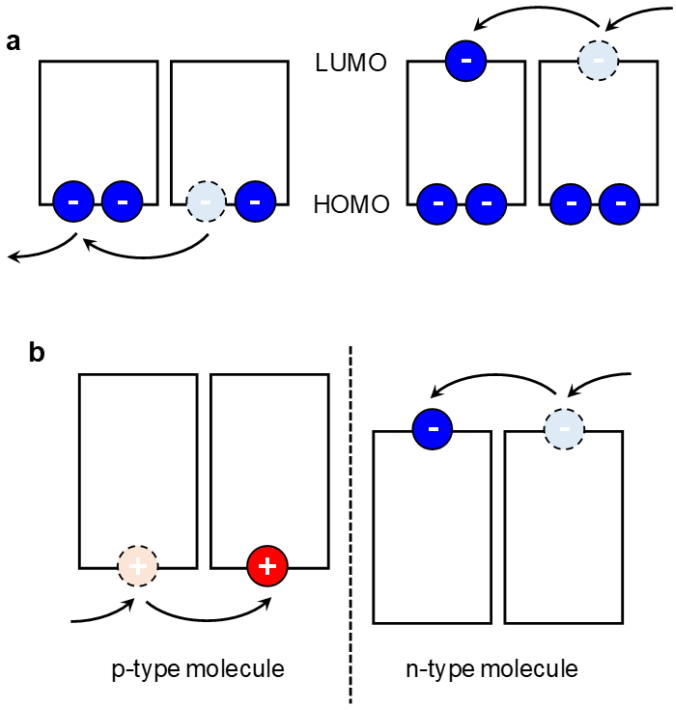

Figure 1.3. (a) Holes and electrons transport through HOMO level and LUMO level, respectively. (b) Two types of organic materials.

Organic semiconductors offer several significant advantages over inorganic-based semiconducting devices. Firstly, due to lacking ionic bonds and metal components, they possess relatively low boiling and sublimation temperatures which will be an advantage for the possibility of low-cost fabrication of the film-making processes with low-temperature processes. Besides, the device fabrication based on solution processes is enabled even for large polymer chains, reducing the cost considerably[3]. Moreover, since its semiconducting property lies behind the conjugated π-system, many organic molecules could be designed and synthesized to fit each semiconducting device's requirements[12]. Among all the applications of organic semiconductors, OLEDs contribute a significant proportion thanks to directly applying to the commercial market of high-performance flat panel displays.

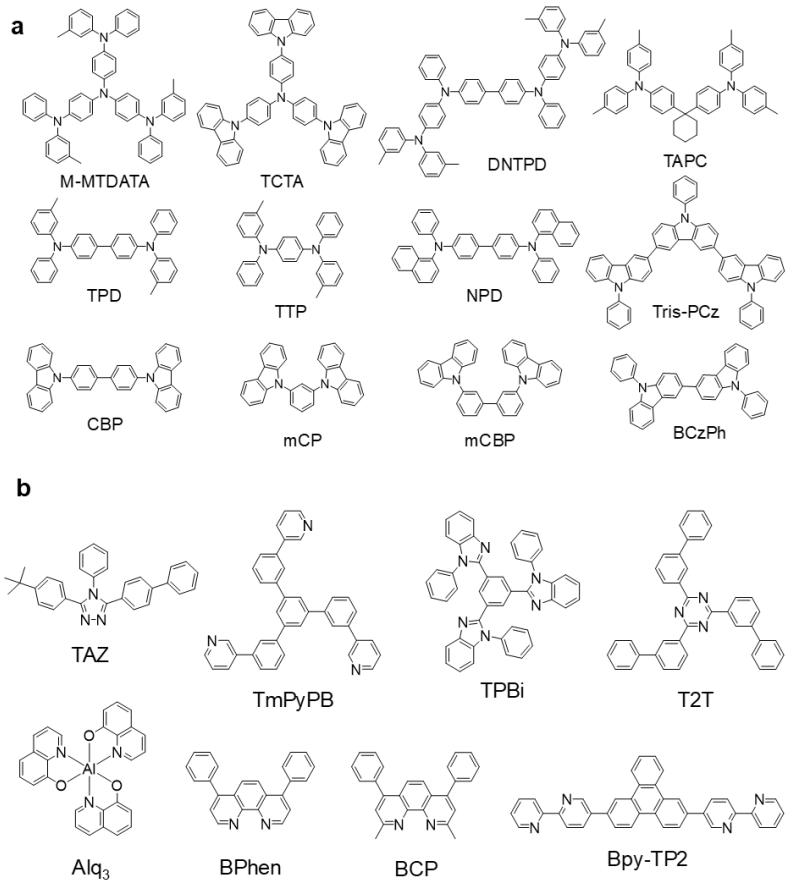

Figure 1.4. Some examples of (a) *p*-type of organic materials. (b) *n*-type of organic materials.

Table 1.1. Summary of current OLEDs situation with three primary colors: red, green, and blue.

Devices	E Q E (%)	Device lifetime (h)	References
Blue Flu.	~10	LT_{95}~1000	T. Sato. et al., *Org. Elec*. **2019**, 74, 118
Blue Phos.	~23	LT_{95}~150	J. Sun, et al., *Nat. Photon.* **2022**, 29, 1903068
Blue TADF	~32	LT_{95}~18	C. Y. Chan, et al., *Nat. Photon.* 20201, 15, 203
Green Phos.	~25	LT_{95}~21,000	D. J. Kim, et al., *J. Mater. Chem. C.* **2021**, 9, 12102
Green TADF	~20	LT_{95}~4500	R. M. Ciarnain, et al., *Adv. Mater.*, **2022**, 34, 2201409
Red Phos.	~27	LT_{95}~55,000	E. A. Margulies, et al., *SID. Sym. Dig. Tech.* **2019**, 65-1, 911
Red TADF	~24	LT_{90}~1,000	S. Kothavale, et al., *J. Mater. Chem. C* **2021**, 9, 528

1-3. Brief introduction of Organic Light-Emitting Diodes

It is undeniable that OLEDs have become a crucial element of displays in today's world. These OLEDs are now an indispensable part of modern display technology. It offers a variety of beneficial characteristics, including the possibility of low-cost production, ultra-flexible panel, high electroluminescence (EL) efficiency, and lightweight property. Notably, the OLEDs have been used as real display applications for smartphones and a distinguished panel of large OLED-TVs, and the OLED technology improved the basics of daily human life. Since the first report about modern OLED by Prof. C. W. Tang in 1987[13], OLEDs have gone through nearly 50 years of development. The original paper has laid the foundation for fully color-controlled OLEDs thanks to the usage of the stacked and stable ultra-thin amorphous organic layers. Since then, all sorts of emission wavelengths have been realized, ranging from near ultra-violet to near-infrared[14–20]. Sharp and pure spectrum is reported in all visible colors, making OLED display extremely vivid and eye-pleasing[21]. Two critical factors to consider when evaluating OLED studies are EL efficiency and operational stability. These are crucial for successful commercialization. Researchers must address two challenges: achieving ideal EL efficiency (100%) and ensuring an ultra-long operating lifetime (typically over 10,000 hours).

1-4. General mechanism of exciton harvesting as light emission

During hole-electron recombination events in organic semiconducting molecules, generally, excitons generated by a formation of polaron pairs are spin-statistically split into a 25% singlet excited state and a 75% triplet excited state[22,23]. However, triplet exciton is essentially a “dark” excited state because of the spin-forbidden nature of an electron transition from the triplet state to a ground state. The first generation of OLEDs focused on harvesting excited singlet excitons as electro-fluorescence. For example, TBPe (the chemical structure is illustrated in **Fig. 1.5**) is a well-known efficient blue emitter that shows intense emission at around 460nm[24]. Thanks to that, OLEDs with TBPe offer maximum current efficiency of 3.4 cd/A. However, unfortunately, this efficiency

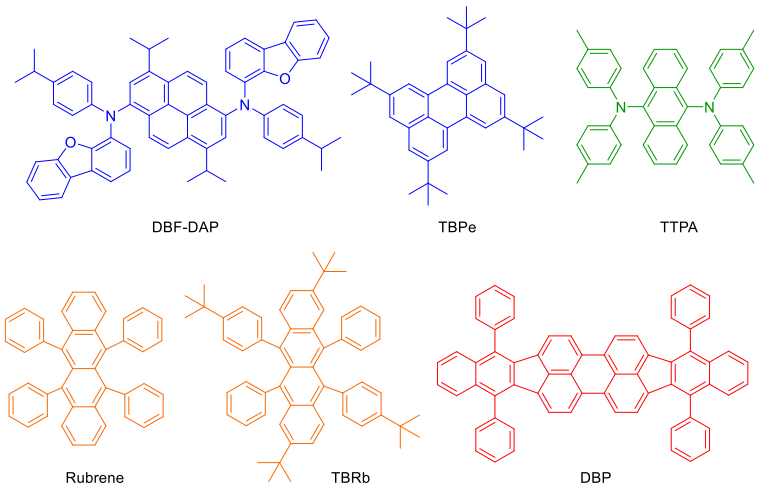

Figure 1.5. Some examples of fluorescent materials.

is far from the true potential of OLEDs. Therefore, the harvesting triplet excitons as "bright" EL plays a critical role in 100% internal EL quantum efficiency (IQE) in organic light-emitting diodes (OLEDs). To harvest triplet exciton energy as light emission, the intense mixing of wave function between the singlet and triplet excited states is required to escape the spin multiplicity restriction. Mixing the singlet and triplet states' wavefunctions makes it possible to create a triplet wavefunction involving the singlet character as described in Equation 1, where ψ_T is the triplet wavefunction, ψ_{S_i} is the *i*-energy-level singlet wavefunction, λ_i is the mixing coefficient between the triplet state and the *i*-th level singlet state, Ψ_T' is the overall triplet wavefunction that can be harvested as a photon[25,26].

$$\psi_T{}' = \alpha\psi_T + \sum_{i=0}^{n} \lambda_i \psi_{S_i} \tag{1}$$

It is clear from the equation that λ_I play a vital role in allowing wavefunction mixing. It is controlled by a Hamiltonian matrix of spin-orbit coupling (H_{SOC}) as well as the energy gap between the single excited state and triplet excited state ($\Delta E_{S\text{-}T}$) as described in Equation 2.

$$\lambda_i \approx \frac{H_{SOC}}{\Delta E_{S_i - T}} \tag{2}$$

This circumstance, therefore, yields two excitonic paths to achieve intense singlet-triplet mixing: I) By maximizing the H_{SOC}, harvesting of all electrically generated excitons through emissive triplet states can be possible, i.e., room-temperature phosphorescence, and II) Reducing the $\Delta E_{S\text{-}T}$ to nearly 0 can open additional intersystem crossing (ISC) channel from the triplet to the singlet state, i.e., reverse ISC (RISC). By the utilization of the RISC process, "dark" triplet exciton can be converted to "bright" singlet exciton, i.e., thermally-activated delayed fluorescence (TADF).

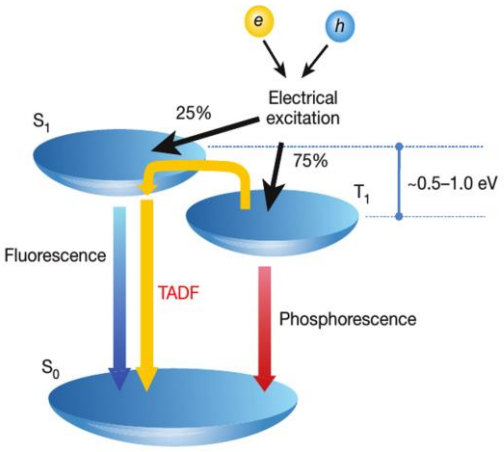

Figure 1.6. Light emitting processes of fluorescence, phosphorescence, and TADF materials.

Most common room-temperature phosphorescence materials are rare-earth metal complexes such as Iridium or Platinum complex[27,28]. Because these elements possess a large atomic number (Z_{Ir} = 77, Z_{Pt} = 78), it is naturally expected that these complexes have a large H_{SOC}, i.e., heavy atom effect. For instance, a well-known example is $Ir(ppy)_3$, which emits green phosphorescence with a photoluminescence quantum yield (PLQY) of nearly 100%, even at room temperature[27,29]. Therefore,

the IQE of $Ir(ppy)_3$-based OLEDs have reached almost 100%. Here note that the EL mechanism in the OLED consists of two distinct processes. The 25% electrically generated singlet excitons will undergo a fast intersystem crossing (ISC) step to produce 100% triplet excitons. These excitons then radiatively decay as phosphorescence thanks to the internal heavy atom effect.

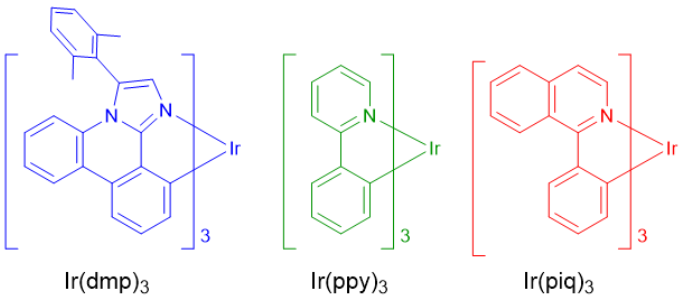

Figure 1.7. Some examples of phosphorescent materials.

The TADF, on the other hand, is a novel class of purely organic material designed to have degenerated excited states between the singlet and triplet state[22,30]. Theoretically, the ΔE_{S-T} is expressed by an overlapping integral of the wavefunctions between the highest occupied molecular orbital (HOMO) and the lowest unoccupied molecular orbital (LUMO) as described in Eq. 3.

$$\Delta E_{S1-T1} = 2\iint \phi_{HOMO}(1)\phi_{LUMO}(2)\frac{1}{r_{12}}\phi_{HOMO}(2)\phi_{LUMO}(1)d\tau_1\tau_2 \qquad (3)$$

Therefore, a small HOMO-LUMO overlap in a molecule can provide a small $\Delta E_{S\text{-}T}$. Thus, electron donor (D) and electron acceptor (A) moieties are typically introduced to design molecules exhibiting TADF. The molecular structure containing D and A fragments results in a strong charge-transfer (CT) character for excited states, spatially separating HOMO on the donor part from LUMO on the acceptor part. As a result, $\Delta E_{S\text{-}T}$ is reduced to near zero, enabling the RISC process. TADF can harvest "dark" triplet excitons as "bright" delayed fluorescence. Upon electrically excited, 25% singlet excitons will first decay as prompt EL. Meanwhile, 75% of triplet excitons will undergo the RISC process to convert the singlet excited state before decaying as delayed EL. It implies that 100% IQE OLEDs are achievable even without expensive rare-earth metal elements, highlighting the benefit of TADF over the Ir complex. One prominent example is a TADF named 4CzIPN which

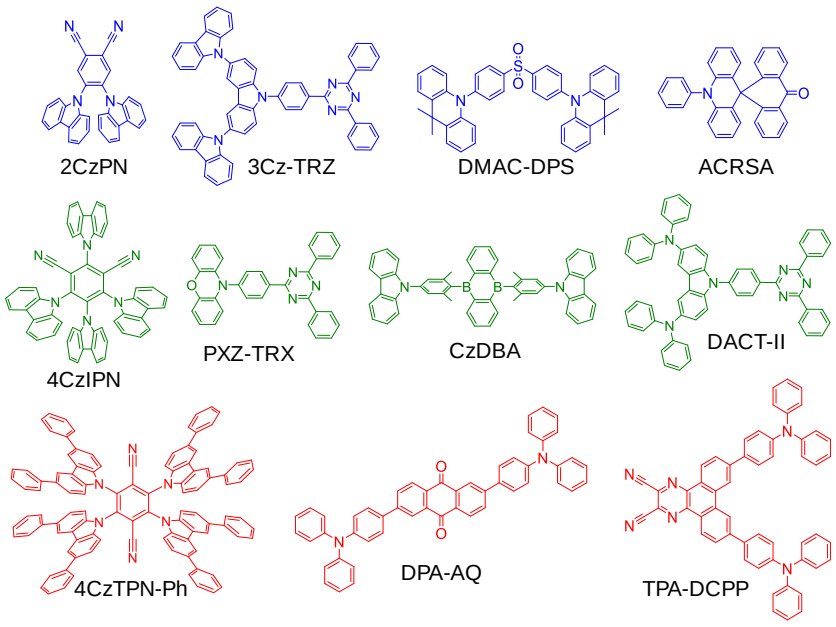

Figure 1.8. Several examples of TADF molecules.

exhibits not only near-unity PLQY but also great promising EL performance[22,23]. It is clear that these two excitonic pathways are fully capable of realizing 100% IQE OLEDs. In fact, **Table 1** proves the highly efficient property of modern RGB OLED with over 20% EQE, i.e., nearly 100% IQE.

Another method of achieving TADF characteristics is through the formation of an excited complex, also known as an exciplex. This is a well-known concept in photochemistry, where two molecules interact to form an excited dimer state, either through aggregation, stacking, or close-distance interaction. If not inhibited by steric hindrance, an electron cloud can be shared between two species, leading to a possibility of charge transfer between them. If the excited state is formed between two different types of material, it is considered an exciplex. This interaction can be enhanced further by using a pair of *n*-type and *p*-type materials according to a large HOMO-LUMO offset. Like the TADF molecular design mentioned above, the exciplex system contains an electron-donating molecule and an electron-accepting molecule[31]. This combination allows spatial separation of the HOMO-LUMO overlapping, naturally leading to a small energy gap between ^{1}CT and ^{3}CT. However, TADF-active exciplex was not discovered until 2012 because of missing a crucial condition[31]. In order for exciton to confine at ^{3}CT, all triplet energy levels of exciplex's donor and exciplex's acceptor (localized excited triplet state, *i.e.*, ^{3}LE) must be higher than that of the ^{3}CT. In

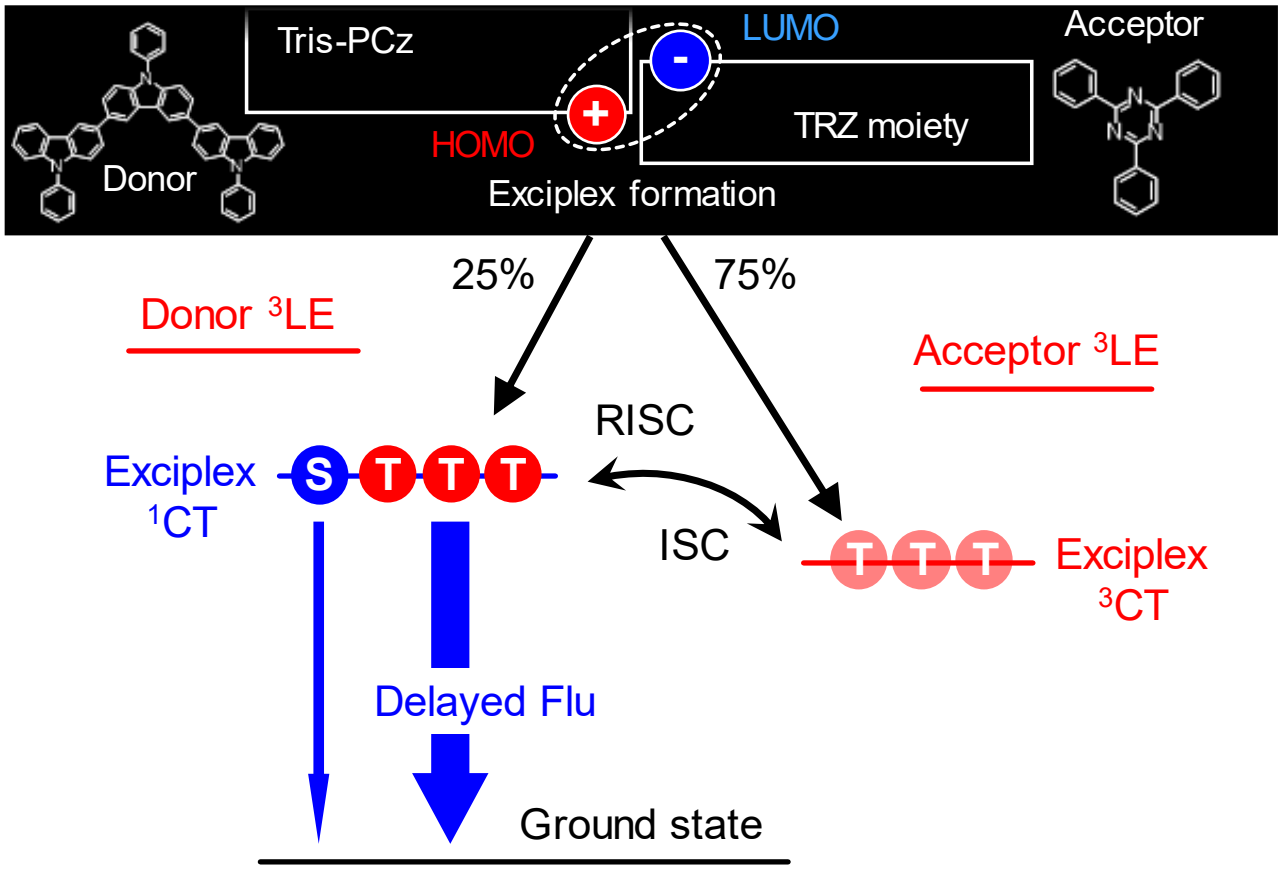

Figure 1.9. Schematic of TADF-active exciplex formation.

2021, K. Goushi et al. demonstrated a combination containing *m*-MTDATA (donor) and *t*-Bu-PBD (acceptor), specifically satisfying the triplet energy level requirement. Since then, various similar combinations have been reported to exhibit TADF property[32,33], but the underlying mechanism remained unclear. This criterion was then further studied by M. Mamada et al., showing that the gap between ^{3}LE and ^{3}CT is vital to enhance RISC efficiency[34]. Conversely, M. Chapran et al. reported a counter-example where the ^{3}LE-^{3}CT gap is sufficiently large, but hyperfine coupling between ^{3}CT and ^{1}CT still allows for efficient TADF property[35]. Other researchers explore the possibility of using TADF-type exciplex as a host matrix for OLEDs because of its suitable charge carrier transporting characteristic. L. Zhang and K. W. Cheah reported a system of TCTA-Tm3PYBPZ which can facilitate a good host for the fluorescent emitter, i.e., rubrene[36]. H. Sasabe and J. Kido also studied the host for phosphorescent emitters, who reported TAPC-BTPS-based exciplex as a good candidate for blue material like FIrpic[37]. In addition, fundamental studies on exciplex also progressed since then. In particular, researchers pay great attention to the donor-acceptor distance because it determines how HOMO-LUMO can be effectively separated. Theoretically, the exciplex energy is determined by the coulombic interaction between hole and electron.

$$E_{coulombic} = \frac{e^2}{4\pi\varepsilon\varepsilon_0 r} \tag{4}$$

where e is the elementary charge, ε is the relative permittivity of organic materials (~3.5), ε_0 is the permittivity of free space, and r is the distance between the charges, respectively. H. Nakanotani et al. introduced a thin spacer layer between exciplex components to demonstrate long-range CT interaction between the donor and acceptor molecule in solid-state, allowing for functionalization of spacer layer such as non-polaron-injecting emitting layer[38]. Prof. Pu and his team later found a unique spacer material allowing for over 10 nm-long CT interaction[39]. P. Monkman group tried to increase D-A distance by diluting exciplex inside another host material such as UGH-3[40]. Noticeably, D. Zhang and L. Duan's group modifies the distance *via* donor-acceptor molecular design. By adding bulky spirofluorene, they could blue-shift their exciplex system to construct highly efficient and stable white OLEDs [41].

1-5. Last obstacle of OLED stability: the stability of blue OLEDs

Green and red PHOLEDs or TADF-OLEDs have been up-to-date with modern standards. By 2019, many research groups reported high performance in such PHOLEDs and TADF-OLEDs. For example, Fukagawa et al. demonstrated a green PHOLED exhibiting over 20% EQE and LT_{90} (device

operational duration corresponding to luminance dropping from 100% to 90%) of 1000 hours even at high brightness (1,000 cd m^{-2})[42]. In addition, Song and his co-worker presented a red PHOLED with 19% EQE and LT50 ~1,400 hours at, impressively, initial luminance of 3,000 cd m^{-2}, which is three times higher than common standard[43]. Needless to say, green and red PHOLEDs are capable of commercialization. Green TADF-OLEDs such as 4CzIPN were also recently reported to achieve LT95 ~4500 hours as well as 20% EQE[18]. Also, with the introduction of TADF assisting fluorescence OLEDs (TAF OLEDs), the device stability is enhanced even further thanks to the "one-way" singlet energy transfer process[44]. Aligning TADF's emitting spectrum with the fluorescence emitter's absorption makes rapid exciton radiative relaxation possible. For instance, 4CzIPN-Me and TBRb were reported to function well with each other to produce highly efficient and stable yellow/orange OLEDs[45]. In conclusion, green and red OLEDs have reached the requirement for mass industrial production.

Researchers have been focusing on improving the operational lifetime in blue OLEDs while maintaining high EL efficiency. However, the progress in this target has been limited in recent years. For blue Flu-OLED, while H. Fukagawa et al. reported an over 1,000,000 hours lifetime, and the maximum EQE was only 9%[46]. On the other side, record-breaking blue PHOLED was demonstrated by a Korean research group, showing over 23% EQE, but LT95 is only 150 hours[15]. C. Y. Chan and M. Tanaka from our group also propose a blue tandem-type TAF-OLED reaching nearly 40% EQE, yet LT95 was just ~20 hours[16]. Researchers worldwide have been working hard to develop stable and efficient blue OLED, but it remains an ongoing challenge. The question arises as to why blue OLED is so unstable.

A "death mechanism" for blue phosphorescence OLEDs was suggested by Prof. Forrest and his colleague in 2017[47]. **Figure 1.10** clearly illustrates the idea behind blue OLED degradation. There are two trivial points applying to both blue PHOLEDs and blue TADF-OLEDs: the high triplet energy (> 3 eV) and the long triplet exciton lifetime (from μs to ms). The first point directly results in the danger of chemical degradation. Because a bonding dissociation energy in an organic molecule is typically ~ 5 eV, it lies right under a

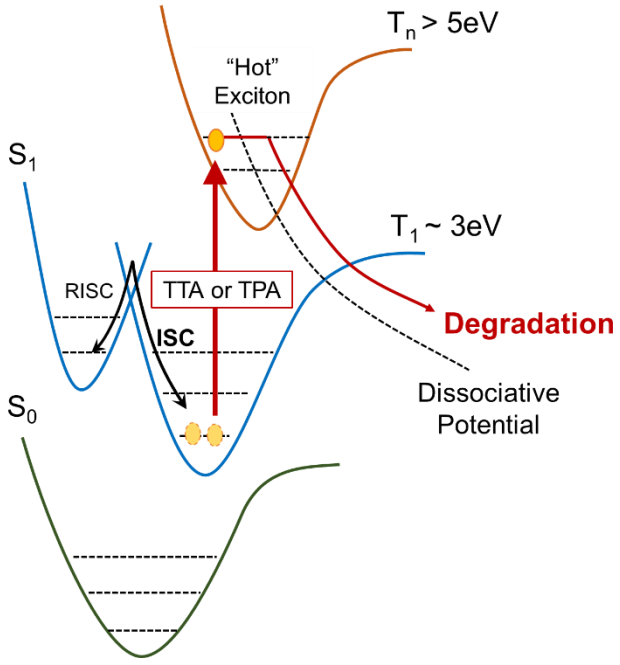

Figure 1.10. Schematic illustration of blue OLED "Death" mechanism.

higher triplet level (i.e., T_2, T_3, etc.). The formation of "Hot excitons" due to the exciton annihilation process increases the likelihood of OLED degradation. Additionally, excitons tend to accumulate at the triplet level due to their long lifetime, which leads to an exponential increase in annihilation processes such as triplet-triplet annihilation (TTA) and triplet-polaron annihilation (TPA). As a result, "Hot exciton" formation is, in fact, accelerated in the blue PHOLEDs and the blue TADF-OLEDs intrinsically, leading to inferior device operational stability.

As one proof, we found that the triplet excited state of a pure blue TADF emitter, namely ν-DABNA[48], which is relatively unstable under optical excitation. According to **Fig. 1.11**, ν-DABNA remains more stable under air conditions than under N_2 conditions. A triplet of oxygen molecules immediately quenches the triplet excitons of ν-DABNA. In contrast, when oxygen is absent, the triplet excitons of ν-DABNA are forced to upconvert to the singlet excited state, resulting in delayed fluorescence. However, since the k_{ISC} of ν-DABNA (1.1×10^8 s^{-1}) is genuinely three orders of magnitude larger than the k_{RISC} (2.0×10^5 s^{-1}), the excitons would accumulate in the triplet state for a long time, causing the exciton annihilation events such as TTA or TPA that trigger the molecular degradation events.

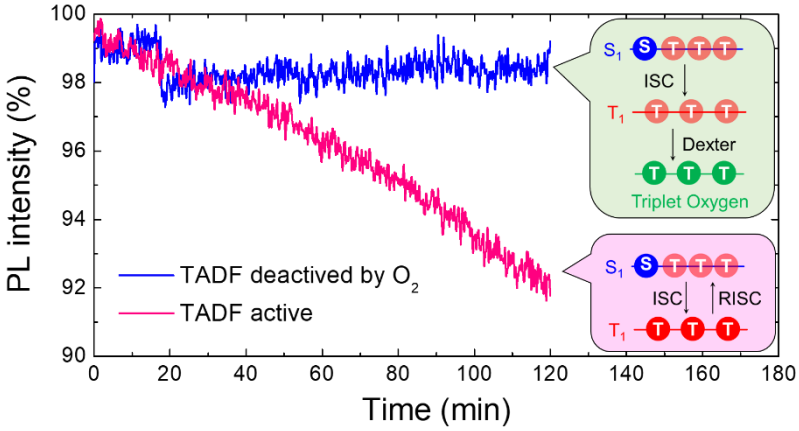

Figure 1.11. Photo-stability characteristics of ν-DABNA in solution over 2 hours and the degradation mechanism.

In attempting to solve the problems, many research works have been done regarding blue PHOLEDs. Several early works focused on understanding the degradation model. In 2007, Prof. Forrest and his team proposed an intrinsic annihilation model for blue phosphorescence OLEDs based on bi-molecular interaction kinetic[49]. Assuming defects inside EML originated from many scenarios, such as exciton-exciton interaction, polaron-polaron interaction, and exciton-polaron interaction, a mathematical model was built to fit the experimental device's lifetime. They found the best fitting corresponding to the exciton-

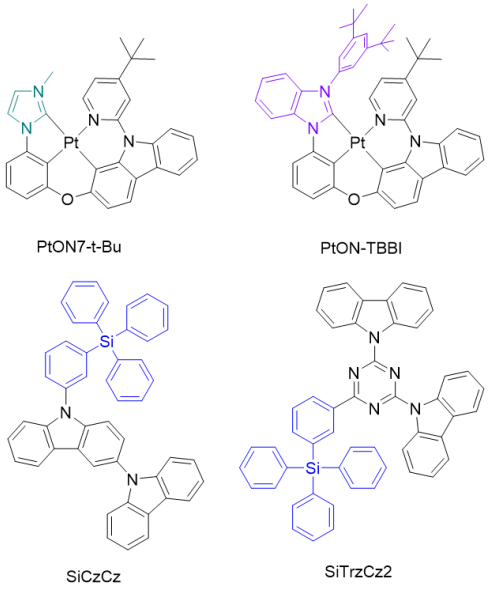

Figure 1.12. Blue Pt complexes and triphenylsilyl based exciplex hosts.

polaron quenching process. This finding later led to the team's publication of hot exciton management in 2017[47]. They demonstrated two strategies to mediate exciton-polaron interaction, including gradient doping and triplet manager. By gradient doping the guest molecule, there can be precise control of the mobility of charge carriers within the EML, ultimately causing the expansion of the recombination zone. Triplet manager was chosen as a high T_1-energy-level phosphorescence assistant dopant to mediate hot exciton. With these methods, Prof. Forrest and colleagues achieved a more than three-fold increase in blue PHOLEDs' operational lifetime. In 2018, Samsung Advanced Institute of Technology and Ewha Womans University collaborated to create a stable blue emitter design concept. They found evidence of polaron-pair formation between the radical cation of a blue Ir complex and the radical anion of the host material[50]. The team later focused on Pt(II) complex, which has the ability to realize high EL efficiency, as well as a bulky triphenyl silyl exciplex host to eliminate emitter-host interactions (**Fig. 1.12**). Some Pt complexes have been reported as a potential candidate for blue PHOLED, but the square planer structure makes it likely to form a polaron-pair with host molecule[15]. The team then address it with ligand's rigid substitutional groups, and robust exciplex host for better carrier transporting, leading to one of the best LT_{95} of 150 hours for blue PHOLEDs[15].

Limited but crucial research has been conducted on improving the stability of blue TADF-based OLEDs. Because typical blue TADF emitters have a long-delayed fluorescence lifetime in μs ~ ms range, it is assumed that minimizing τ_{delay} would also improve the device stability. For instance, H. Noda et al. solidified this viewpoint by engineering delayed fluorescence lifetime as well as k_{RISC}. Aiming to achieve a better CT-LE mixing triplet state, a hetero electron donating moieties (carbazole and diphenyl-carbazole) was employed[25]. This strategy reduces the energy gap between a triplet CT state (^{3}CT) and triplet LE state (^{3}LE), significantly improving the RISC process according to the El-Sayed rule. Indeed, the modified 3Cz2DPhCzBN TADF not only exhibits a shorter τ_{delay} than the template 5CzBN but also offers over a 30-fold increase in OLED operational time. Following the design concept, C-Y. Chan et al. reported a modification of

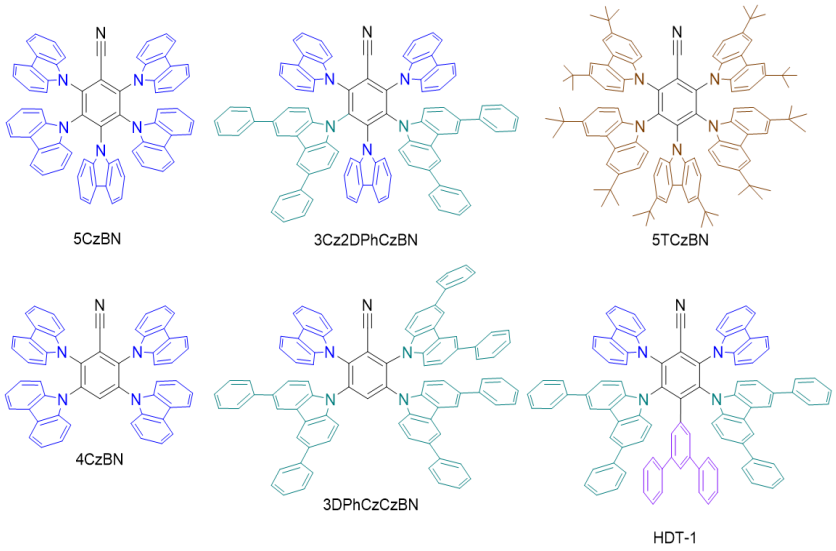

Figure 1.13. 5CzBN and 4CzBN motifs and their modified TADF structures.

4CzBN showing blue-to-sky-blue emission with respectable device stability[16]. Another strategy employing the 5CzBN template was to introduce a steric shield to create 5TCzBN[51]. Thanks to it, L. Duan and his team achieved a nearly 5-times increase in OLEDs stress test. The molecular structures of these TADF can be found in **Fig. 1.13**. Understanding in TADF-OLEDs architecture also improved the OLED stability. For example, a standard host, mCBP, was shown to be the principal OLED lifetime limiting factor due to an imbalance in carrier transport ability[52]. N-type host featuring triazine and fluorene unit, then, demonstrated to significantly expand the recombination zone as well as TADF-OLEDs lifetime.

Significant research is being done on blue multi-resonance TADF (MR-TADF) technology to achieve stable pure blue OLEDs[53,54]. Unlike conventional TADF's molecular design, MR-TADF achieves HOMO-LUMO separation at the atomic level thanks to the effect from the B-N core, leading to a sharp PL spectrum (**Figs. 1.14** and **1.15**). MR-TADF is a promising candidate for a blue emitter due to its highly sharp PL spectrum.

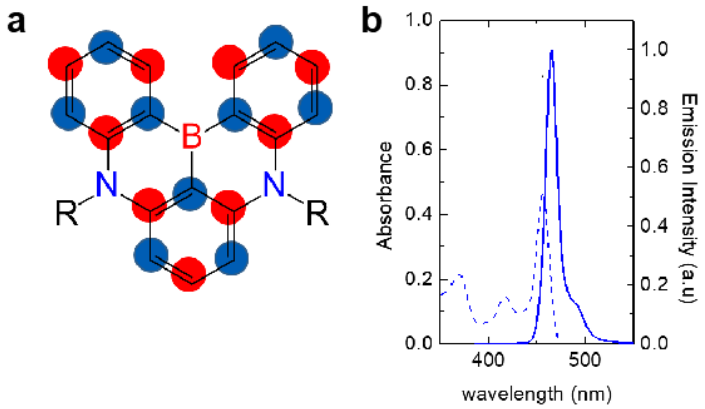

Figure 1.14. a) Schematic illustration of multiple resonance effect. Red dots show LUMO distribution while blue dots show HOMO distribution. b) Absorption spectrum (blue dash line) and PL spectrum (blue solid line) of *ν*-DABNA in toluene.

One successful example is *ν*-DABNA[48]. Early work showed that pairing MR-TADF with conventional TADF indeed improves OLEDs' lifetime. This hyperfluorescent concept is currently yielding some of the best LT_{95} for blue TADF-OLEDs based on *ν*-DABNA[16,55]. Not only

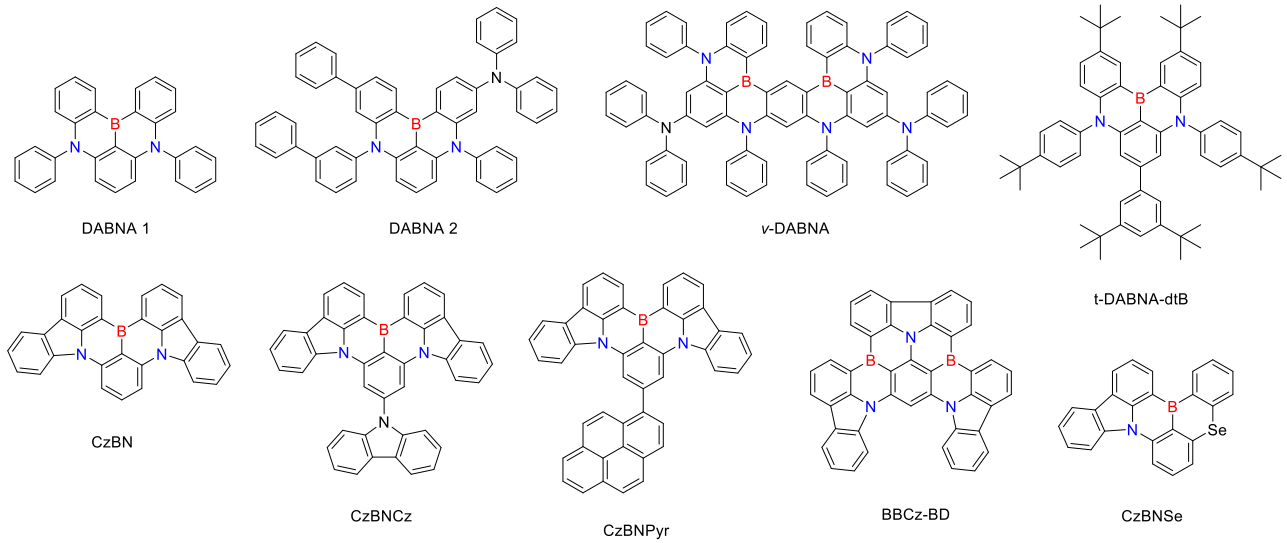

Figure 1.15. Several examples of MR-TADFs.

conventional TADF but PHOLEDs are also shown to benefit from MR-TADF dopant[56]. However, the main mechanism for such a device is still poorly understood. In addition, MR-TADF is also widely used in blue Flu-OLEDs with anthracene-based host[57]. Because of such a large amount of application, effort has been put in to improve the stability of MR-TADF itself. Noticeable works by T.-T. Lee demonstrated how both the carbazole derivative and pyrene derivative of CzBN enhance the stability of the emitter greatly[58]. Meanwhile, Prof. Yasuda and his team contributed a great effort in finetuning MR-TADF properties. They increase the CT-LE mixing in the BN core by adding several *t*-carbazole groups to the parent molecule CzBN. The result shows sharp DABNA-like emission but with a significant RISC rate thanks to additional electron donors[59]. They later explored the heavy atom effect as another method of increasing the RISC rate constant. Thanks to elements such as S and Se, they reported one of the fastest RISC in MR-TADF, reaching 10^8 s^{-1} while maintaining the deep blue emission[60].

On the other hand, blue Flu-OLEDs are well-known to show significantly longer device lifetimes. One of the early reports on blue Flu-OLED by C. Y. Tang mentioned the contraption of a non-nitrogen-atom substitution host-guest system[24]. The paper illustrated an extremely stable blue device using a di-naphthalene anthracene host and TBPe emitter, completing EML with only C and H elements. Later research focused on improving anthracene-based material to achieve higher EQE but mostly below 6%[61,62]. Even with the introduction of the triplet-triplet upconversion mechanic, the progress is still lagging. While rubrene-based OLED cases have achieved an EQE of around 12% [63,64], anthracene derivatives have proven to be a significant challenge in fully improving EQE in blue OLED. Carbazole modification such as PCAn or benzonitrile substitution such as m2CzAntBzt are reported as good candidates for efficient anthracene-based host[65,66], yet no device stability was recorded. Prof J. J. Kim demonstrated over 12% EQE, but his device was unstable due to the material choice[57]. Unfortunately, there is no knowledge about what type of material can satisfy the criteria while being stable. The best overall up-to-date combination between moderate EQE of 10% and moderated operational lifetime LT_{95}~1,000 hour in blue-fluorescent OLED was reported by Sato et al. [14]. **Figure 1.16** summarizes

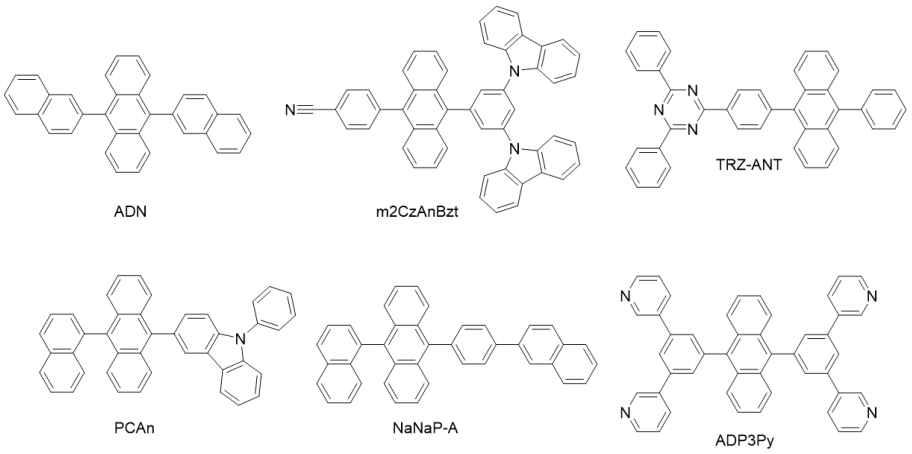

Figure 1.16. Several anthracene-based materials for blue Flu-OLEDs.

the structure of the above anthracene derivatives. Extensive research has been conducted to make blue OLEDs commercially viable. However, PHOLEDs and TADF-OLEDs are not stable enough, and further development is necessary for blue Flu-OLEDs to improve their EQE.

1-6. Motivation and purpose of this thesis

In this thesis, to realize efficient yet stable blue OLEDs, we focused on utilizing CT interactions as our main strategy to conquer the task. Unlike conventional TADF design, exciplex does not require the D-A pair to be connected via an aromatic bridge. Thus, the fabrication method is more straightforward while abundant well-known carrier transporting materials can be tested. Notably, the exciplex system offers all these benefits without requiring an expensive, rare-earth metal complex. Thanks to the flexible materials chosen for the exciplex system, the triplet energy level can be well controlled by selecting a suitable acceptor. Herein, two classes of exciplex are investigated where one shows clear TADF property while the other shows clear triplet-triplet upconversion (TTU) property. We show that EQE and operational lifetime can be significantly enhanced regardless of system type with a suitable acceptor.

In Chapter 3, a rational choice of a TADF-type acceptor is reported as a new strategy to enhance OLEDs' operating lifetime. A comprehensive study of the exciplex system containing 9,9',9"-triphenyl-9H,9'H,9"H-3,3':6',3"-tercarbazole (tris-PCz) and triazine (TRZ) derivatives clarifies the relationship between unwanted carrier recombination on acceptor molecules, TADF property of acceptors and the device degradation event. Because T_1 of TADF-type Acceptor is typically lower than that of tris-PCz, 'exciton recycling' is possible. A three-fold increased operational lifetime can be achieved while still maintaining high-performance OLED properties.

In Chapter 4, we introduce the usage of the anthracene derivative as the acceptor molecule. Due to its low T_1 energy level (~1.8 eV), the anthracene derivative is a common strategy to produce highly stable blue fluorescence OLEDs. Unfortunately, how to improve the EQE of such a low T_1 system is still unclear. This chapter will attempt to demonstrate that exciplex formation between tris-PCz and anthracene plays an essential role in boosting TTU efficiency and, thus, improving EQE. We clarify that the CT interaction at a hole-transport/emitter-layer interface is an overlooked pathway to enhance TTU yield significantly. Thus, low-triplet materials like anthracene can still be exploited for efficient blue OLEDs while achieving a long operational lifetime by default. Unfortunately, the TTU contribution was yet to reach the theoretical maximum, so we dedicate the following chapter to resolving it.

In Chapter 5, we further enhanced the lifetime of blue TTU OLEDs by doping TADF material directly at the CT interface. The bipolar carrier transport ability of TADF materials enables direct carrier recombination on the molecules, resulting in the expansion of the recombination zone. The TTU efficiency approaches the upper limit. Meanwhile, the operational device lifetime of OLED employing TADF molecules increased by five times compared to the conventional ones.

In the final chapter, we will summarize this study again in order to see the road map for future research.

Chapter 2

Role of reverse intersystem crossing using a TADF-type acceptor molecule on the device stability of exciplex-based organic-light emitting diodes

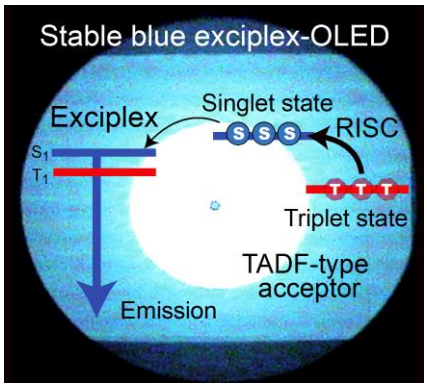

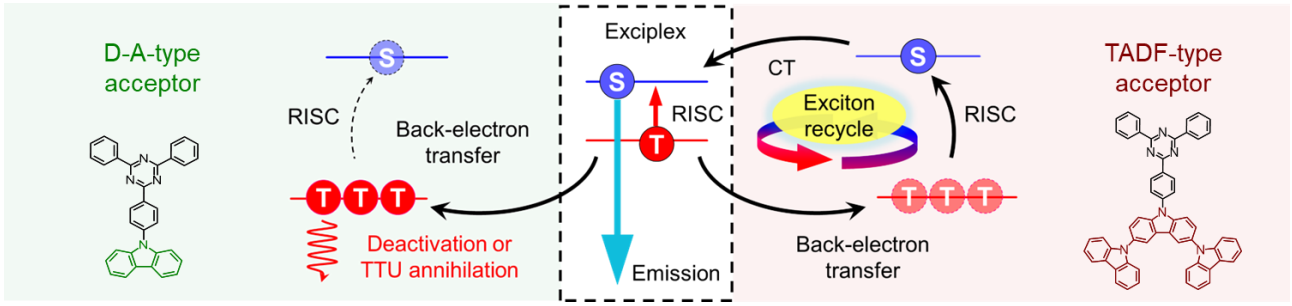

2-1. Introduction

Since the yield of RISC is facilitated by a reduction of the $\Delta E_{S\text{-}T}$, the utilization of radiative exciplexes, created from a spatially separated D-A molecular pair, can provide efficient RISC yield[22,30]. After our very first demonstration of exciplex-based OLED[31], many researchers confirmed the usefulness of exciplexes as an emitter for OLEDs. They vastly decreased the complexity of the device structures. It was also demonstrated that exciplex developments aimed for an efficient host system dragged out the full potential of OLED emitters. Additionally, it was shown that exciplex is achievable even when D-A has spaced away over 10 nm[38,39]. These unique features lead to the ability to add a new functional layer and pioneer other properties of OLEDs.

Looking back at previous exciplex-based OLED studies, it undoubtedly emphasizes improving exciplex systems for advanced OLEDs. However, although one of the critical parameters to evaluate OLED performances is its operating lifetime. The operational device stability of exciplex-based OLEDs still needs to be improved for practical applications. Unfortunately, a clear strategy to choose materials for a stable exciplex system has not yet been established, although some promising progress about a long device lifetime has been reported[67].

Aiming to realize a highly stable exciplex system without any sacrifices, especially to develop a stable blue-OLED, we propose a strategy for choosing the acceptor molecule with two critical hypotheses. First, we introduce a weaker electron-donating group to the 'acceptor' molecule, having no significant change in the exciplex energy. Second, we minimize the instability of exciplexes, which can be ascribed to a large accumulation of long-lived triplet excited states of acceptor molecules after unnecessary carrier recombination events on acceptor molecules. Under device operation, a high-density accumulation of holes inside emitting layer can inject holes into the HOMO of acceptor molecules, leading to unwanted carrier recombination on the acceptor molecules and damaging the exciplex system. Since the electron-donating unit is responsible for the HOMO in acceptor molecules, adding it to the acceptor molecule would form a CT-type excited state with small ΔE_{ST}, *i.e.*, providing a TADF-type acceptor. When unwanted carrier recombination happens on the TADF-type acceptors, the electrically generated triplets can convert to the singlet excited state through RISC, and the singlet excited state of the acceptor molecules then again undergoing energy transfer, *i.e.*, charge-transfer, leading to the exciplex formation again (**Fig. 2.1(a)**). By applying this "dual" triplet exciton recycling strategy, *i.e.*, RISC on both the exciplex and the TADF-type acceptor (**Fig. 2.1(a)**), TADF-type acceptors are found to significantly improve OLED lifetime.

In order to construct a systematic investigation of the proposed concept, several regulations are ensured while a degree of material diversity is promoted. The first invariant factor is the constant

usage of 9,9',9"-triphenyl-9H,9'H,9"H-3,3':6',3"-tercarbazole (tris-PCz), a well-known hole-transporting material possessing a strong electron-donating group of tri-carbazole as a donor molecule for the exciplex system. Second, all acceptor molecules used in this study share the same electron-acceptor unit of phenyl substituted-triazine (TRZ) to avoid any inconsistency in terms of acceptor strength. Since the exciplex formation can be expected to occur between the radical cation of tris-PCz and the radial anion of the TRZ unit incorporated in the acceptors, these regulations should provide a good comparison. Here, a variety of acceptor molecules are

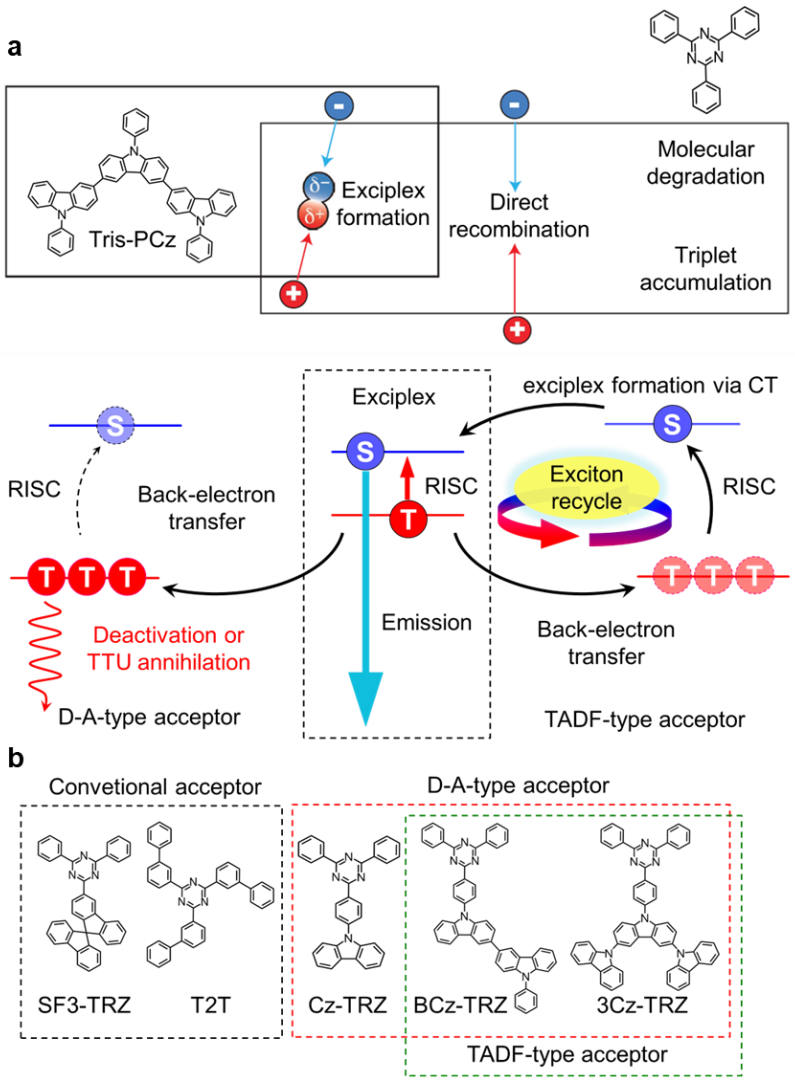

Figure 2.1: (a) Schematic of proposed mechanism to improve exciplex based OLED's stability. (b) Chemical structures of acceptor molecules used in this study.

required to prove our proposed concept, and three types of acceptor molecules were chosen as shown in **Fig. 2.1(b)**; (**Type-1**) Conventional acceptor; 2,4,6-tris(biphenyl-3-yl)-1,3,5-triazine (T2T) and 2-(9,9'-spirobi[fluoren]-3-yl)-4,6-diphenyl-1,3,5-triazine (SF3-TRZ), (**Type-2**) Bipolar-type acceptor; 9-[4-(4,6-diphenyl-1,3,5-triazin-2-yl)phenyl]-9H-carbazole (Cz-TRZ) and (**Type-3**) TADF-type acceptor; 9-(4-(4,6-diphenyl-1,3,5-triazin-2-yl)phenyl)-9'-phenyl-9H,9'H-3,3'-bicarbazole (BCz-TRZ) and 3Cz-TRZ. The conventional acceptor (**Type-1**) is defined to be a molecule without a significant electron-donating group. Here note that the bipolar-type acceptor (**Type-2**) here refers only to non-TADF material even with a D-A structure. On the other hand, while the TADF-type acceptors possess bipolar transport characteristics due to the presence of both donor and acceptor units, placing them in a distinguished category (Type-3) emphasizes the presence of a highly efficient RISC process. With these three types of material choices, the effect of the electron-donating group in acceptor molecules is able to be systematically investigated.

2-2. Experimental Section

2-2-1. Materials

The materials tris-PCz, SF3-TRZ, T2T, Cz-TRZ, BCz-TRZ, and 3Cz-TRZ were synthesized in-house. *v*-DABNA was supplied by JNC corporation.

2-2-2. Sample preparation

Organic films with a thickness of 100 nm for photoluminescence measurements were grown on quartz substrates by thermal evaporation. The organic deposition was performed under vacuum at pressures of below 5 x 10−5 Pa. For OLED fabrication, glass substrates with a pre-patterned, 100-nm-thick tin-doped indium oxide (ITO) coating as anode were used. After pre-cleaning the substrates, effective device areas of 4 mm2 were defined on the patterned-ITO substrates by a polyimide insulation layer using a conventional photolithography technique. Organic layers were formed by thermal evaporation. An OLED based on an exciplex system is as follows: ITO (100 nm) / 1,4,5,9,11-hexaaztriohenyleane hexacarbonitrile (HAT-CN) (10 nm) / tris-PCz (30 nm) / EML (30 nm) / SF3-TRZ (10 nm) / 50wt% Liq:SF3-TRZ (20 nm) / Liq (2 nm) / aluminum (100 nm). The EML consists of 50wt%-tris-PCz and 50wt%-acceptor molecules blended together. After the fabrication, OLEDs were immediately encapsulated with glass lids in a nitrogen-filled glove box (O2 < 0.1 ppm, H2O < 0.1 ppm). Commercial calcium oxide desiccant (Dynic Co.) was included in each encapsulated package.

2-2-3. Optical characterization of organic thin films

The steady-state visible photoluminescence spectra and intensities were measured using a multichannel spectrophotometer (PMA-12, Hamamatsu Photonics). Photoluminescence quantum efficiency was measured using an absolute photoluminescence quantum yield measurement system (Quantaurus-QY Plus, Hamamatsu Photonics) under the flow of argon gas.

2-2-4. Characterization of OLEDs

The current density–voltage–luminance characteristics of the OLEDs were evaluated using a source meter (Keithley 2400, Keithley Instruments Inc.) and an absolute external quantum efficiency measurement system (C9920-12, Hamamatsu Photonics). The operational lifetime was measured using a luminance meter (SR-3AR, TOPCON) with the devices operated at a constant DC current. All measurements were performed in ambient atmosphere at room temperature.

2-2-5. Photo-stability measurement of emissive molecules:

Two 3 mL solution samples of 10^{-5} M concentration in toluene were prepared at room temperature condition. One was exposed to air while the other was bubbled by argon gas for 10 minutes and then capsuled to remove oxygen molecules. Their emission spectrum and intensity were measured continuously by PMA-12 (HAMAMATSU) over 2 hours with a regulated 0.66 mW cm^{-2} of 365 nm excitation light source from MAX-303 (Asahi Spectra USA Inc.).

2-3. Result and discussion

To assess the hypothesis that exciplexes are mainly defined by the interaction of the tris-PCz (donor) and the TRZ unit of the acceptors, the photoluminescence (PL) and EL characteristics of the mixed films were evaluated for all five cases. As summarized in **Table 2.1**, the peak wavelengths varied around 20 nm within the range from 499 nm to 518 nm. For example, although the BCz-TRZ neat film exhibited sky-blue emission, the tris-PCz:BCz-TRZ blend film showed noticeable redshifted emission, indicating the exciplex formation between tris-PCz and BCz-TRZ, *i.e.*, BCz-TRZ acting as an acceptor for tris-PCz (**Fig. 2.2(a)**). Note that the delay fluorescence lifetime (τ_d) and the RISC rate constant (k_{RISC}) of all combinations showed consistent values, *i.e.*, τ_d of 2.6 ~ 3.5 μs and k_{RISC} of ~10^5 s^{-1}, strongly suggesting the presence of a common RISC process among all samples. In addition, the τ_d of the tris-PCz:BCz-TRZ blend is shorter than that of the 50wt%-BCz-TRZ:mCBP film (**Fig. 2.2(b)**), indicating that the TADF component of the blend does not originate from an intrinsic TADF ability of BCz-TRZ molecule. It should be noted that D-A type and TADF type acceptors although show a similar delayed PL profile **(Fig. 2.2(c))**, they have a lower triplet energy level than exciplex singlet energy level. Therefore, those exciplex systems based on the D-A type or TADF type acceptor show a phosphorescence spectrum originating from the electron acceptor molecules **(Fig. 2.2(d))**.

Table 2.1. Photophysical characteristics of 50wt%-tris-PCz:50wt%-acceptor films.

Acceptor	PL [nm]	PLQY [a] [%]	τ_p [ns]	τ_d [μs]	k_r [10^6 s^{-1}]	k_{ISC} [10^7 s^{-1}]	k_{RISC} [10^5 s^{-1}]	k_{nrT} [10^5 s^{-1}]
3Cz-TRZ	511	13 / 32	22	2.8	5.3	3.5	1.6	4.1
BCz-TRZ	499	29 / 21	14	2.8	12	2.8	1.3	4.0
Cz-TRZ	517	9.3 / 31	27	3.0	2.6	2.5	1.3	3.6
T2T	518	8.3 / 37	18	3.5	3.3	3.7	1.7	4.2
SF3-TRZ	504	8.7 / 26	20	2.6	3.5	3.7	1.3	4.2

a) PLQY for prompt (left) and delayed (right) component.

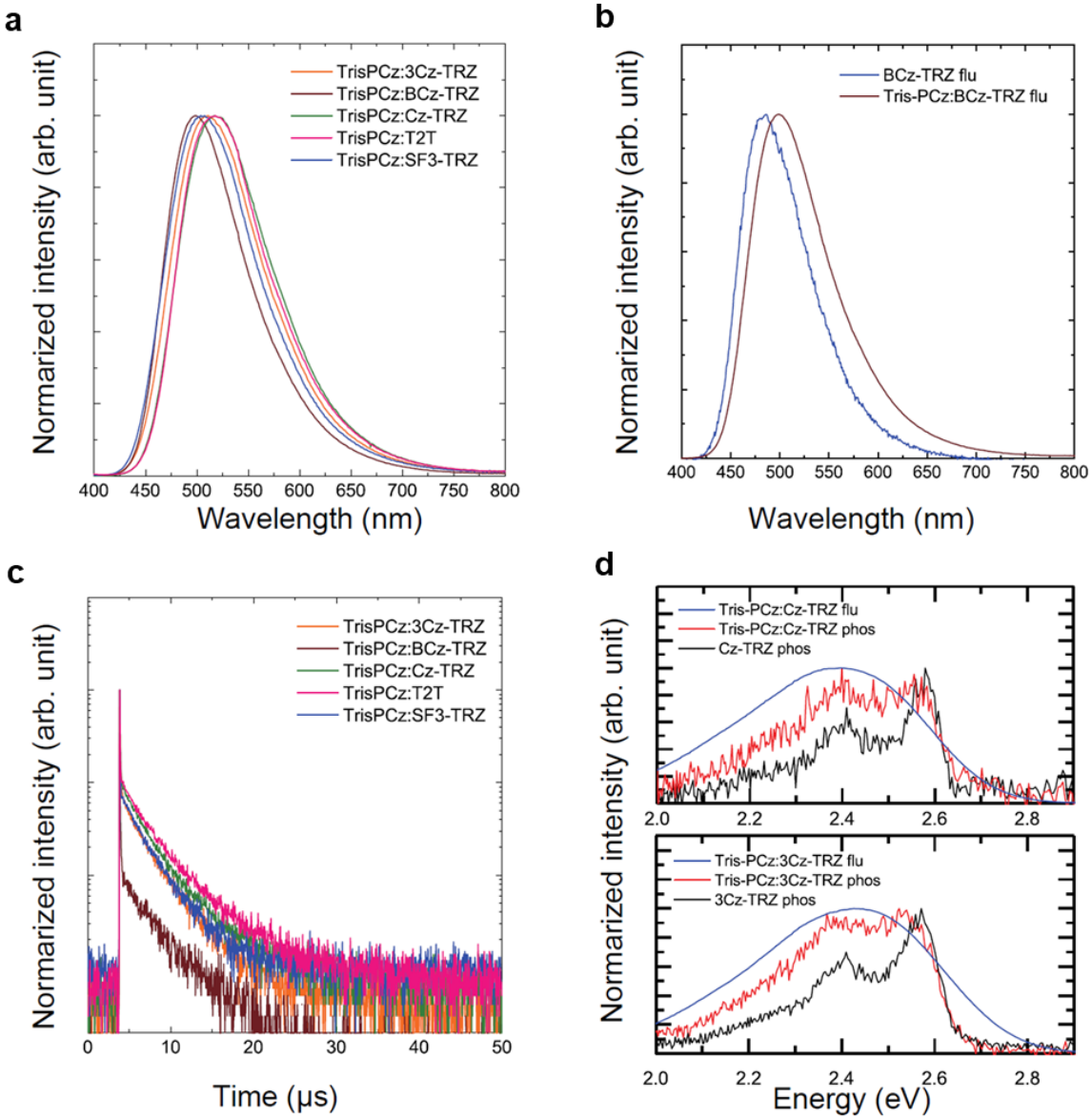

Figure 2.2. (a) PL spectra of tested D-A blend films. (b) PL spectra of BCz-TRZ neat film and BCz-TRZ:tris-PCz blend film. (c) Transient PL decay profiles of tested D-A blend films. (d) Fluorescence and phosphorescence spectra of Cz-TRZ:tris-PCz and 3Cz-TRZ:tris-PCz blend films, and 3Cz-TRZ neat film.

Figure 2.3 shows the device structure as well as 3Cz-TRZ OLED to be our standard device performance. Regarding the EL characteristics, the high similarity of current density (*J*)-voltage (*V*)-luminance (*L*) curves of the fabricated OLEDs as shown in **Fig. 2.4(a)**, highly indicated the common electrical characteristics between all samples. Sharing the on-set voltage (defined to be voltage at L = ~1 cd m^{-2}) value of 2.5 ± 0.05 V in all five devices agrees well with the energy gap between the HOMO of tris-PCz (~5.6 eV) and the lowest-unoccupied-molecular-orbital (LUMO) of the TRZ core (~3.0 eV), suggesting that fundamental carrier transport and the recombination events happened between these two energy levels. Furthermore, the insignificant deviation of the *J-V-L* curves, i.e., voltage stayed around 6.3 ± 0.05 V at 100 mA cm^{-2} supported the investigating hypothesis.

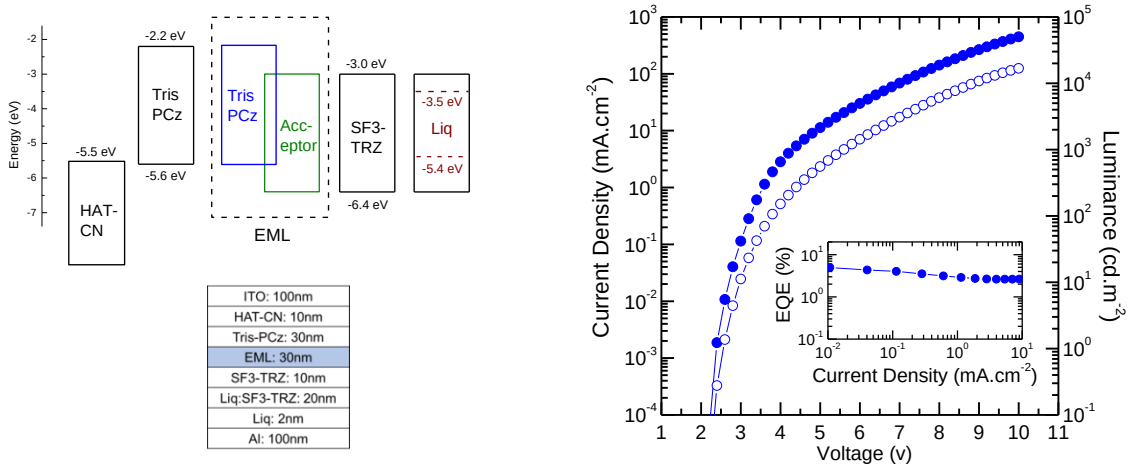

Figure 2.3. Left: Device structure: ITO (100 nm) / 1,4,5,9,11-hexaaztriohenyleane hexacarbonitrile (HAT-CN) (10 nm) / tris-PCz (30 nm) / EML (30 nm) / SF3-TRZ (10 nm) / 50wt% Liq:SF3-TRZ (20 nm) / Liq (2 nm) / aluminum (100 nm). For a control device, the OLED based on the EML consists of 50wt%_3Cz-TRZ:mCBP was used and the OLED performances. Right: Current density (filled circle)-luminance (open circle)-voltage characteristics of the control device. Insert: The EQE-current density characteristics of the control device.

In addition to the low driving voltage in these exciplex-based OLEDs, external EL quantum efficiency (EQE), as well as EL characteristics, were preserved within three types of acceptors. The maximum EQE (EQE_{max}) of around 10% was observed in all devices, while the tris-PCz:3Cz-TRZ and tris-PCz:BCz-TRZ based OLEDs where the EQE peaked at 13-14% (**Fig. 2.4(b)**). In addition, regarding the EL spectra, the emission colors were clearly maintained with their peak wavelengths deviated within only 10 nm (**Fig. 2.4(c)**). It is worth noticing that using the TADF-type acceptors was not the reason for the redshifted spectra since the emission peak at the longest wavelength of 515 nm was obtained by tris-PCz:Cz-TRZ (bipolar-type acceptor case). Meanwhile, tris-PCz:BCz-TRZ shared a similar peak wavelength with tris-PCz:SF3-TRZ (505 nm) and tris-PCz:3Cz-TRZ shared a peak wavelength with tris-PCz:T2T (510 nm). This indicates that changing from conventional acceptor molecules to TADF-type acceptors only slightly affected both recombination and emissive sites.

Despite exhibiting resembling OLED performances, the operational device stability of the different types of exciplex-based OLEDs showed a distinct difference. The operational device stability of each OLED was assessed by monitoring the EL output intensity under the constant current density condition. A constant current density of 3.3 ± 0.01 mA cm^{-2} was set for all devices. **Figure 2.4(d)** shows the EL intensity decay curves with the normalized initial EL intensity before the EL intensities dropped to 50% (LT_{50}) from the initial EL intensity. The OLEDs containing conventional acceptors severely suffered from relatively quick degradation with LT_{50} less than 90 hours. With the introduction of a Cz group to the acceptor molecules, *i.e.*, Cz-TRZ, the OLED lifetime was allowed

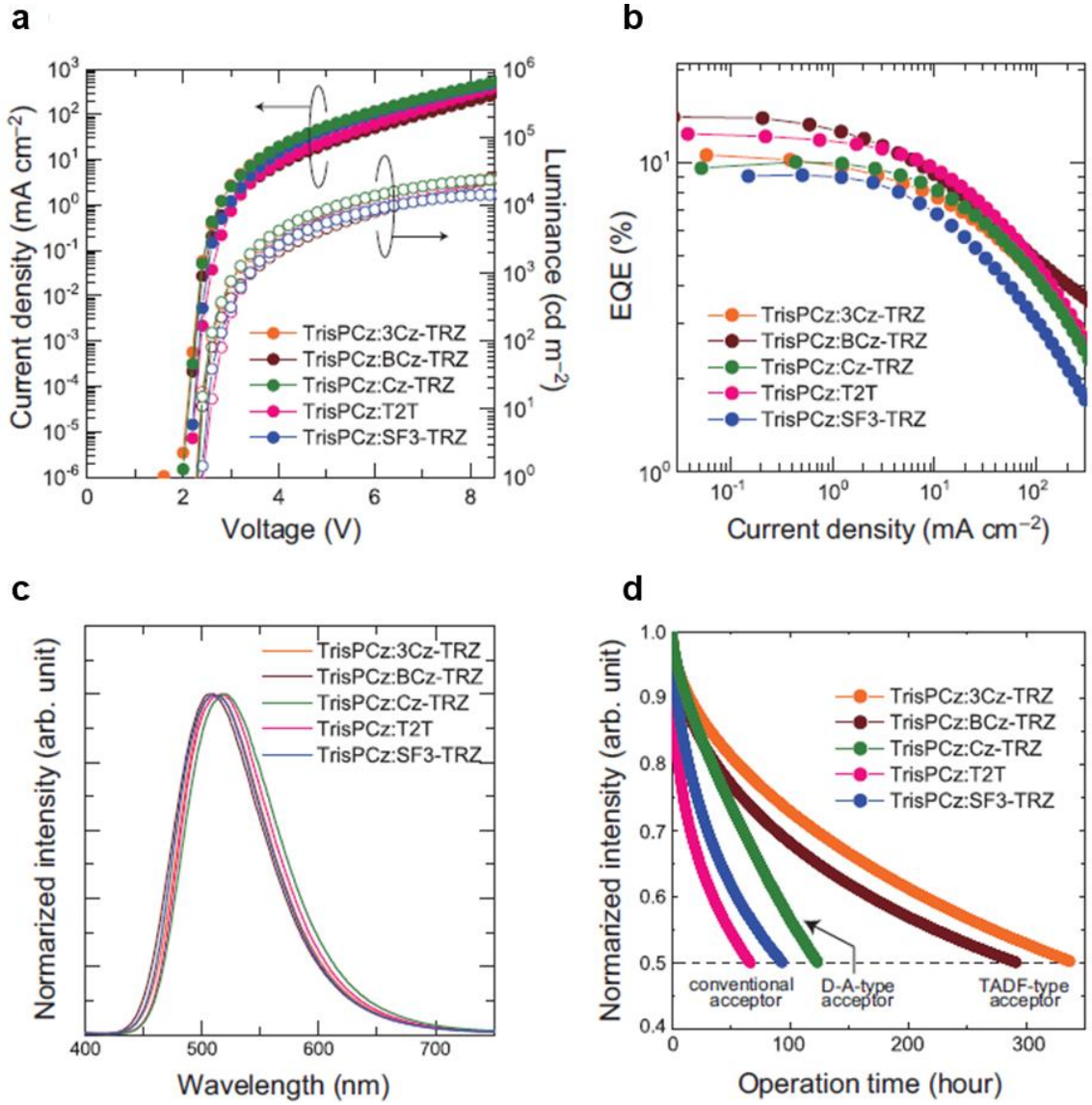

Figure 2.4: (a) Current density-luminance-voltage characteristics and (b) EQE-current density characteristics of fabricated OLEDs. (c) EL spectra in various OLEDs at 3.3 mA cm^{-2}. (d) Normalized OLED luminance as a function of operating time at a constant current density. The constant driving current density was set to 3.3 mA cm^{-2} for each OLED, corresponding to initial luminance at 830, 1050, 920, 1030, and 780 cd m^{-2} for 3Cz-TRZ, BCz-TRZ, Cz-TRZ, T2T, and SF3-TRZ based exciplex OLEDs, respectively.

to reach LT_{50} = 125 hours, resulting in almost double the lifetime of the T2T-based OLED. Remarkably, the usage of the TADF-type acceptors prolonged the LT_{50} more than threefold compared to the conventional acceptors. The LT_{50} of nearly 300 and 350 hours was achieved in the OLEDs based on BCz-TRZ and 3Cz-TRZ, respectively, emphasizing the superiority of the exciplexes utilizing the TADF-type acceptor.

A plot of the EL spectrum at initial, LT_{80}, and LT_{50} provided the fingerprints responsible for the degradation in the exciplex-based OLEDs (**Fig. 2.5**). The tris-PCz: SF3-TRZ-based OLED showed an appearance of the unexpected red emission during the device degradation. Based on our

previous study, this unusual red EL can be assigned to the electromer that originates from SF3-TRZ molecules[68]. On the other hand, the tris-PCz:Cz-TRZ and tris-PCz:3Cz-TRZ-based OLEDs that also

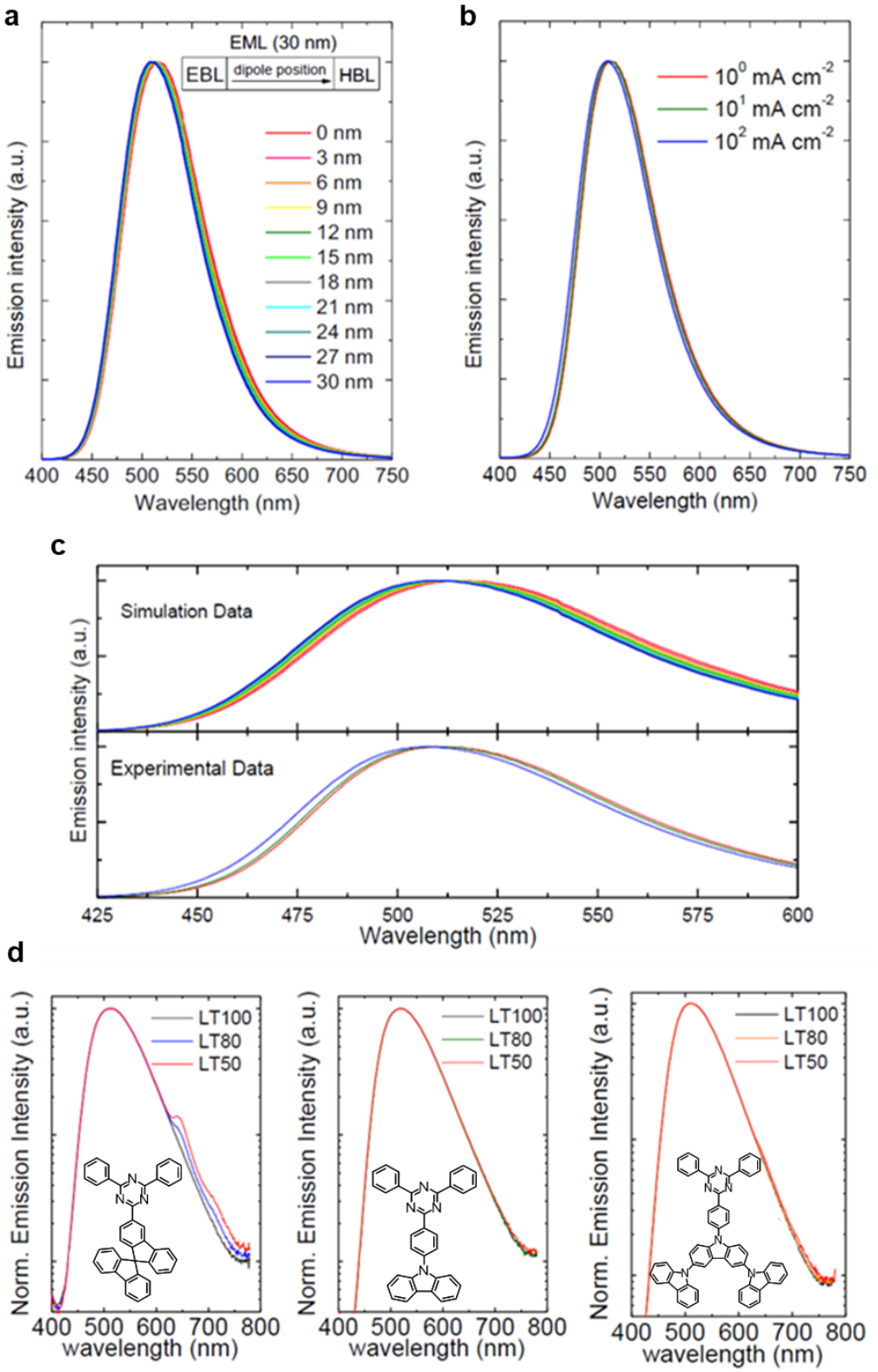

Figure 2.5: (a) Simulated EL spectra for various dipole position inside the EML of exciplex-based OLEDs. Optical simulation was made using Setfos 4.6 software (Fluxim, Germany). (b) Experimental data of the EL at various current density of tris-PCz:3Cz-TRZ device. (c) Expanded simulation and experimental data of EL spectrum. (d) Normalized EL spectra of SF3-TRZ, Cz-TRZ, and 3Cz-TRZ based exciplex-OLED with each driving time.

contained a TRZ unit emitted none of any red EL and experienced almost no EL change during device degradation. The SF3-TRZ electromer emission could only be explained by the presence of SF3-TRZ as an emitter, indicating that holes were injected into the HOMO of the acceptor molecules despite the deeper HOMO level than that of tris-PCz, leading to the degradation of the acceptor molecules. It was shown in the previous section that the initial charge transport and the recombination events occur through the HOMO of tris-PCz and the LUMO of the TRZ unit. Therefore, these exciplex-based OLEDs show comparable EQE. Nonetheless, when the recombination centers, *i.e.*, a D-A pair, are saturated, holes can be accumulated at the EML/HBL interfaces, leading to hole injection into the acceptor molecules and successive degradation. In fact, the normalized EL spectra of the tris-PCz:3Cz-TRZ-based OLED showed a slight blue shift with increasing current density, and it well corresponded to a simulated EL spectrum with a recombination zone shift (**Fig. 2.5**), indicating the accumulation of hole at the EML/HBL interfaces. However, as stated in the introduction, the presence of an electron-donating group in bipolar-type and TADF-type acceptor molecules would act as a receptor for the undesired hole injection and protect the direct carrier recombination event on the TRZ core. This unique strategy proposed here was undeniably supported by the confirmed device stability results.

Although both TADF-type acceptor and bipolar-type acceptor contain the electron-donating group as a receptor for the unexpected injection of holes, the dramatic enhancement of the operational device lifetime in the TADF-type acceptor-based OLED can be ascribed to the efficient TADF mechanism. In fact, the Cz-TRZ-based OLED that has no ability to perform RISC showed a rather short LT_{50} compared to that of the 3Cz-TRZ-based OLED by a factor of two, indicating that triplet exciton upconversion plays an important role in the stability improvement in the exciplex based OLEDs.

The triplet energy level in exciplex can be extremely close to the singlet energy level due to the large spatial separation between the HOMO of a donor unit and the LUMO of an acceptor unit. In the case of the tris-PCz:Cz-TRZ system, the T_1 of Cz-TRZ (2.65 ± 0.05 eV) is slightly lower than the S_1 of the exciplex (2.7 ± 0.05 eV), and very similar to that of the exciplex (2.65 ± 0.05 eV), meaning that some of the triplets of the exciplex can be quenched by the T_1 of Cz-TRZ non radiatively. Although the energy gap between the T_1 of Cz-TRZ and the triplet of the exciplex should be small, the electron transfer, *i.e.*, Dexter-type transfer, from the triplet of Cz-TRZ to the triplet of the exciplex expected to be 'endothermic' process. Therefore, Dexter-type energy transfer is considered to be inefficient. In this case, a part of the Cz-TRZ triplets would not show back energy transfer to the triplet of the exciplex and accumulate because of no TADF activity of Cz-TRZ. Thus, the electrically generated triplets of Cz-TRZ cannot be efficiently utilized as exciplex energy again.

As same as the tris-PCz:Cz-TRZ system, the T_1 of 3Cz-TRZ (2.65 ± 0.05 eV) is very close to that of the exciplex (2.65 ± 0.05 eV) as shown in **Fig. 2.6**. However, thanks to the RISC of 3Cz-TRZ, 3Cz-TRZ can upconvert T_1 excitons to the S_1 of 3Cz-TRZ, contributing to the formation of tris-PCz:3Cz-TRZ exciplexes because the S_1 of 3Cz-TRZ is higher than that of the exciplex (**Fig. 2.1(a)**). Therefore, TADF-type acceptors are expected to have lower accumulated triplet density during OLED operation compared to conventional acceptors and bipolar-type acceptors, leading to long operational device stability. Despite having no positive effect on the EQE, choosing exciplex-type acceptors clearly demonstrated the significant role of the TADF process in enhancing device stability.

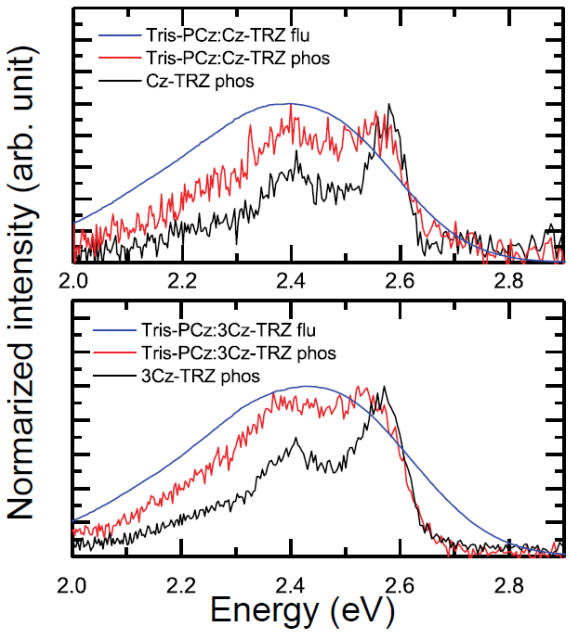

Figure 2.6: Fluorescence and phosphorescence spectra of the Cz-TRZ:tris-PCz and 3Cz-TRZ:tris-PCz blend film, and 3Cz-TRZ neat film.

Next, the utilization of a highly stable exciplex system as a host matrix for pure blue fluorescence emitters is discussed. The highly broad exciplex emission (the full width at half maximum: FWHM = 90 nm) with the greenish sky-blue or green color can be transferred its energy for a pure blue emitter[48]. To achieve such a system, ν-DABNA was chosen as a terminal dopant for a tris-PCz:3Cz-TRZ exciplex system. A device with 1wt%ν-DABNA:49.5wt%-tris-PCz:49.5wt%3Cz-TRZ was prepared to evaluate the possibility of a TADF-type acceptor based exciplex in the blue OLED. A comparison of performances between two OLEDs (with and without ν-DABNA) showed the possibility of a stable pure blue OLED utilizing a TADF-type acceptor-based exciplex. The J-V characteristics of the ν-DABNA doped OLED completely traced the J-V characteristics of the non-doped OLED (**Fig. 2.7(a)**), highlighted that ν-DABNA did not act as any carrier trap sites inside the EML, while the maximum EQE was almost twofold, i.e., 19%, compared with the non-doped OLED (**Fig. 2.7(a)** inset). Further, the EQE at 1,000 cd m^{-2} stayed well above 18%, showing admirable low EL efficiency roll-off characteristics. Not only the significant enhancement of EQE, but also the EL color purity was enhanced (**Fig. 2.7(b)**). By doping ν-DABNA into the exciplex system, the CIE coordinate switched from the green region (CIEy = 0.52) to the blue region (CIEy = 0.36), and FWHM was nearly halved to ~50 nm.

For blue-OLEDs, as already discussed, the very first priority toward practical applications might be an operational device lifetime rather than EQE. **Figure 2.7(c)** clearly demonstrates that the blue OLED could maintain stability after incorporating ν-DABNA. At a constant current density of 3.3 mA cm^{-2}, both devices (with and without ν-DABNA) showed LT50 over 300 hours. Note that the initial luminance of the ν-DABNA doped OLED (1,260 cd m^{-2}) is much higher than that of the non-doped one (830 cd m^{-2}). The blue-OLED possessing a high T_1 dopant (for example, T_1 of ν-DABNA is 2.8 ± 0.05 eV) often suffers from low operational device stability due to a formation of hot excitons due to a large number of accumulated triplet states. However, this is not the case here since no reduction in LT50 was observed, indicating that T_1 of ν-DABNA did not undergo triplet

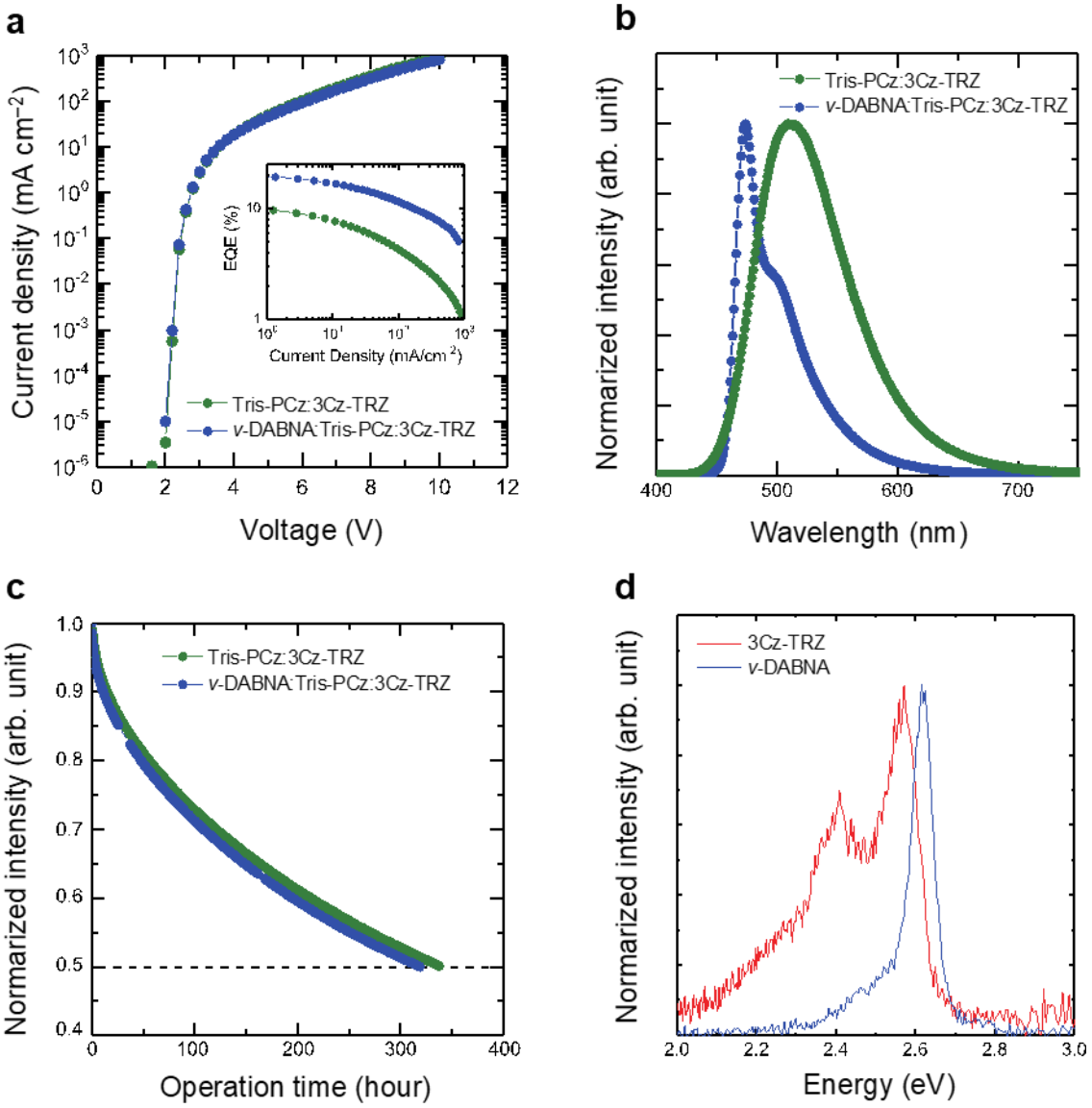

Figure 2.7. (a) Current density-luminance-voltage characteristics of fabricated OLEDs. Inset: EQE-current density characteristics. (b) EL spectra in the OLEDs at 3.3 mA cm^{-2}. (c) Normalized luminance of the OLEDs as a function of operating time at a constant current density. The constant driving current density was set to 3.3 mA cm^{-2} for each OLED, corresponding to initial luminance at 830 and 1260 cd m^{-2} for tris-PCz:3Cz-RTZ and *ν*-DABNA:tris-PCz:3Cz-TRZ based OLED, respectively. (d) Phosphorescence spectra of 3Cz-TRZ and *ν*-DABNA films measured at 77 K.

accumulation inside the EML during OLED operation. With the lower T_1 than the chosen blue dopant, i.e., 2.8 ± 0.05 eV, 3Cz-TRZ (T1=2.65 ± 0.05 eV) was likely to be responsible for the quenching process of the T_1 of ν-DABNA (**Fig. 2.7(d)**). Similar to the previous discussion, 3Cz-TRZ could, in turn, exhibit RISC to recycle triplet excitons to the singlet energy of the exciplex. This exciton recycling circle surely provides the key mechanism for further stable blue-OLEDs. However, we note that the FWHM of the EL is much broader than that of ν-DABNA fluorescence in a doped film state (**Fig. 2.8**), meaning the energy transfer from the S_1 of exciplex to the S_1 of ν-DABNA during the exciton recycling cycle is still incomplete and the spectrum has a green component that originates from the exciplex. Therefore, to improve the color purity of EL, we should develop a bluer exciplex system.

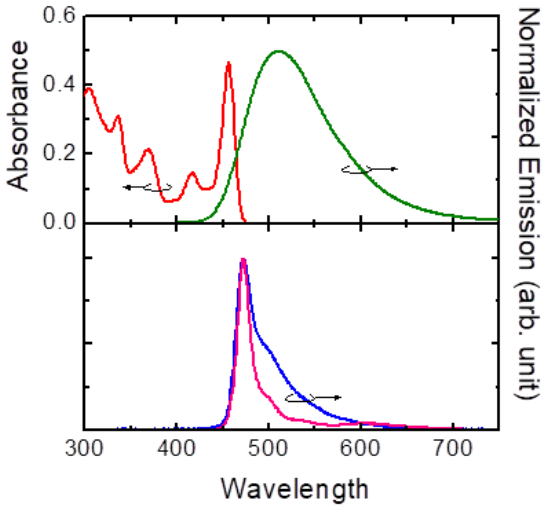

Figure 2.8. Absorption spectrum of *ν*–DABNA (red line), normalized PL spectrum of tris-PCz:3Cz-TRZ (green line) and normalized PL spectra of *ν*–DABNA:tris-PCz:3Cz-TRZ (blue line), and *ν*–DABNA:mCBP (pink line).

2-3 Conclusion

Through an investigation of different types of exciplex acceptors utilizing a TRZ group as a fundamental acceptor unit, an addition of the electron-donating group was found to prolong the operational device lifetime without any loss of the initial OLED performance. The modification preserved the exciplex formation between the tris-PCz and TRZ groups while providing the stabilized acceptor radical cations. The TADF-type acceptors showed great stability thanks to their RISC process. The adaption of TADF-type acceptors to a blue OLED was demonstrated to emphasize that future stable blue-OLEDs could be achieved from a combination of the exciplex exhibiting broad green emission and the pure-blue dopants.

Chapter 3

An overlooked charge-transfer interaction in the interfacial triplet-triplet upconversion process in blue organic light-emitting diodes

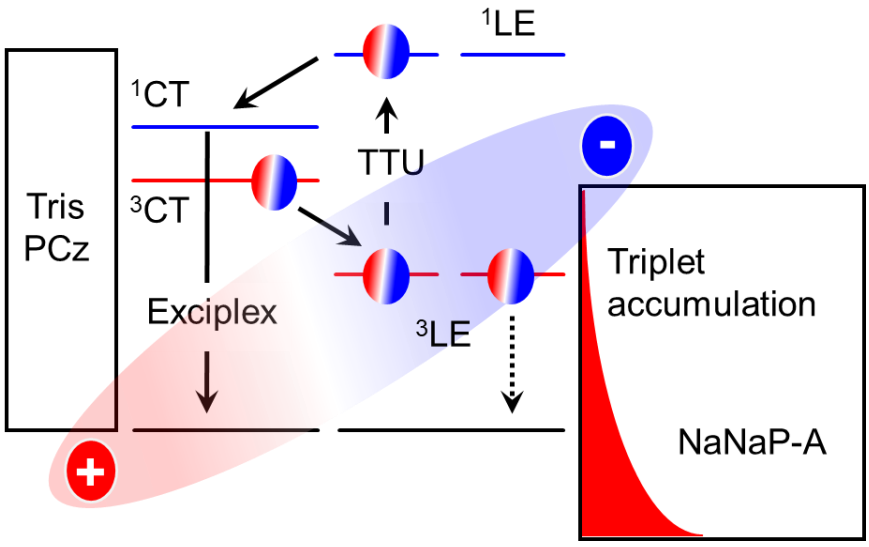

3-1. Introduction

Due to the deadly high T_1 level to produce blue emission, the exciplex system in Chapter 2 failed to meet standard commercial requirements. An alternative triplet-excitonic pathway in blue OLEDs is a triplet-triplet upconversion (TTU), which is a well-established solution for practical applications[14,46]. Anthracene derivatives, a well-known TTU material for blue OLEDs, have the lowest-excited triplet energy level (T_1) of around 1.6 eV, which is close to half of the singlet excited energy. The collision of the two low-energy triplets produces just enough energy for a singlet generation rather than the formation of a hot triplet that partially decays non-radiatively via a dissociation potential curve. For this reason, blue TTU-OLEDs provide a practical solution. Although the IQE in TTU-OLEDs falls short of the theoretical limit, i.e., 100%, TTU-OLEDs can theoretically gain a high singlet exciton production yield of up to 62.5%.

Despite the practical use of pure-blue TTU-OLEDs, TTU's underlying mechanism still remains debated with varied viewpoints. First, from the aspect of the exciton formation process, Monkman's group proposed a family of anthracene derivatives featuring high triplet levels (Tn) exceedingly twice the T_1 levels, leading to nearly 62.5% of IQE in OLEDs in 2013[69]. Recently, our group has proposed that spin-orbit coupling induced by intramolecular CT interaction in anthracene derivatives could facilitate TTU events[70]. Second, from the aspect of device engineering, in 2015, Xiang et al. revealed that the carrier recombination zone in a blue TTU-OLED exists in the EML close to the interface between the EML and the HTL[64], indicating the benefit from a dense triplet accumulation at the interface. Alternatively, the origin of the sub-bandgap EL in rubrene-based OLEDs was explained as the CT-sensitized TTU generating at the rubrene/fullerene interface[63,64]. Further, B.-Y. Lin et al. proposed the CT-sensitized blue TTU-OLEDs to reduce a driving voltage[71]. Although the IQE from these CT-sensitized TTU-OLEDs was far from the theoretical limit, it has been suggested that the

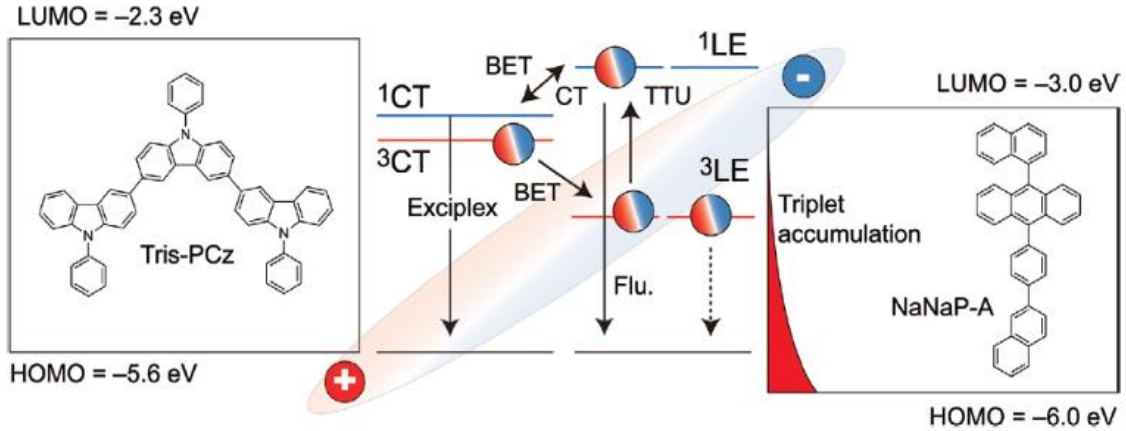

Figure 3.1: Charge-transfer interaction at the donor–acceptor (D-A) interface. Molecular structure of tris-PCz and NaNaP-A, and the related energy level diagram of the molecular system. The abbreviation: BET and Flu. are back energy transfer and fluorescence, respectively.

CT interface can facilitate TTU events at the interface according to the dense triplet accumulation. However, the interfacial CT formation has been claimed as the main reason for the IQE loss in, particularly, blue TTU-OLEDs[72,73]. Therefore, researchers avoided interfacial CT formation by adopting novel efficient TTU materials. As a result, the role of the CT interface in TTU events has been overlooked. In this chapter, we investigate the role of interfacial CT formation in highly efficient blue TTU-OLEDs to unveil the real working mechanism. The schematic of the study is shown in **Fig. 3.1**.

3-2. Experimental Section

3-2-1 Sample preparation

All organic layers were formed by thermal evaporation under high-vacuum conditions (<10−5 Pa). Organic films with a thickness of 50 nm were grown on a quartz substrate for PL measurements. All of the OLEDs were fabricated on clean ITO glass substrates and had an effective device area of 4 mm2. The OLED structure was ITO (100 nm) / HAT-CN (10 nm) / tris-PCz (20 nm) /EBL (10nm) / EML (30 nm) / SF3-TRZ (10 nm) / 50wt%-Liq:SF3-TRZ (20 nm) / Liq (2 nm) / Al (100 nm), with ITO as the anode, HAT-CN as hole-injecting layer, tris-PCz as the electron-transporting layer, EBL (either tris-PCz, mCBP, TPN-DBF) as electron-blocking layer, SF3-TRZ as the hole-blocking layer, Liq:SF3-TRZ as electron-transporting layer, Liq as electron-injecting layer, and Al as the cathode. mCBP was purchased from NARD Institute. 9,9’,9’’-triphenyl-9H,9’H,9’’H-3,3’:6’,3’’-tercarbazole (Tris-PCz) and 9-(1-naphthalenyl)-10-[4-(2-naphthalenyl)phenyl]anthracene (NaNaP-A) was synthesized via previously reported procedures. v-DABNA was supplied by Prof. Takuji Hatakeyama and JNC corporation. After OLED fabrication, the OLEDs were immediately encapsulated with glass lids and epoxy glue in a dry N_2-filled glove box.

3-2-2 Fundamental PL properties

The steady-state PL spectra, absorption spectra, PLQY, and HOMO measurements were similar to Chapter 2. The emission lifetime was measured using a streak camera (C4334, Hamamatsu Photonics) with a Nd:YAG laser (MPL15100, QS Lasers) at an excitation wavelength of λ=355 nm with a pulse width of about 700 ps as an excitation light source under the pressure of ~3 Pa.

3-2-3 Characterization of OLED performances

I-V-L and EQE characteristics are similar to Chapter 2.

3-2-4 Exciplex fitting model

Consider a normal distribution curve with a standard deviation σ and a peak position μ (was set to be exciplex's HOMO-LUMO gap as described in the main text) as follows:

$$f(x) = \frac{1}{\sigma\sqrt{2\pi}} EXP\left(-\frac{1}{2}\left(\frac{x-\mu}{\sigma}\right)^2\right) \quad (3.1)$$

To simplify the calculation, we normalized the curve to get **(Fig. 3.2)**:

$$f_{normalized}(x) = EXP\left(-\frac{1}{2}\left(\frac{x-\mu}{\sigma}\right)^2\right) \quad (3.2)$$

By solving $f_{normalized}(x) = 0.5$, we will get $FWHM = 2\sqrt{2ln2}\sigma$.
(3.3)

The derivative of the function above is:

$$f'_{normalized}(x) = EXP\left(-\frac{1}{2}\left(\frac{x-\mu}{\sigma}\right)^2\right).\left(-\frac{x-\mu}{\sigma^2}\right) = f_{normalized}(x).\left(-\frac{x-\mu}{\sigma^2}\right) \quad (3.4)$$

^{1}CT value is then estimated from the intersection between a tangent line at the on-set point x_0 and the x-axis. The tangent line equation is therefore:

$$y - f_{normalized}(x_0) = f'_{normalized}(x_0).(x - x_o) \quad (3.5)$$

Solving that equation for y=0, we get:

$$^1CT = x = \frac{f'_{normalized}(x_0).x_o - f_{normalized}(x_0)}{f'_{normalized}(x_0)} = x_o - \frac{f_{normalized}(x_0)}{f'_{normalized}(x_0)} = x_o + \frac{\sigma^2}{x_o - \mu} \quad (3.6)$$

Without loss of generalization, we defined on-set point x_0 where $f_{normalized}(x_0) = k$ (k is a constant, $x_0 > \mu$). x_0 can then be expressed as:

$$x_0 = \sqrt{2ln\left(\frac{1}{k}\right)}\sigma + \mu \quad (3.7)$$

Combining **Eq. 3.3**, **3.6**, and **3.7**, we can get the result:

$$^1CT = \sqrt{2ln\left(\frac{1}{k}\right)}\sigma + \mu + \frac{\sigma^2}{\sqrt{2ln\left(\frac{1}{k}\right)}\sigma} \quad (3.8)$$

$$= \sqrt{2ln\left(\frac{1}{k}\right)}\sigma + \mu + \frac{\sigma}{\sqrt{2ln\left(\frac{1}{k}\right)}}$$

$$= \frac{1}{2}\sqrt{\frac{-ln(k)}{ln2}}FWHM + \mu + \frac{FWHM}{4\sqrt{-ln(k)ln2}}$$

As implied by the formula, there is a linear relationship between the ^{1}CT value and FWHM.

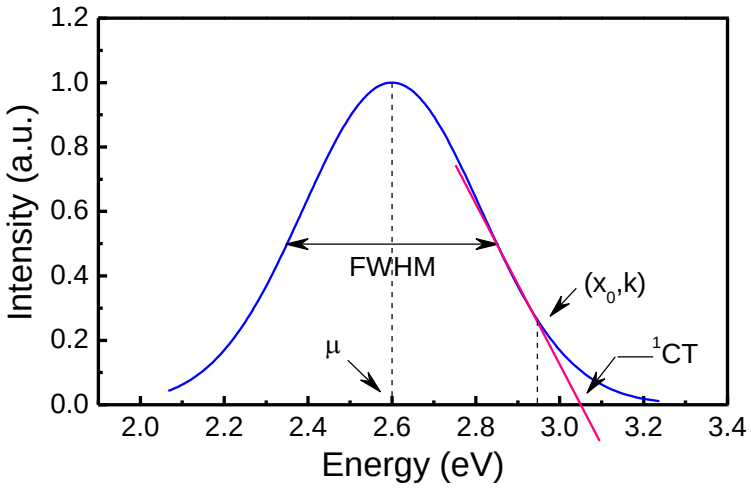

Figure 3.2 Example of a simulated exciplex spectrum.

3-3. Results and discussion

Figure 3.1 shows molecular structures and the related energy level diagram of the molecules used in this study. To systematically research the proposed hypothesis for exciton decay and upconversion processes, we selected NaNaP-A as the TTU material based on the well-established characteristics for high TTU efficiency[74]. NaNaP-A has the HOMO and the LUMO energies of –6.0 and –3.0 eV, respectively. Here, we selected tris-PCz as the hole-transport material, since tris-PCz possesses the HOMO/LUMO levels of –5.6/–2.3 eV, indicating the possibility of exciplex formation between tris-PCz and NaNaP-A. Thus, when the CT excited state is formed between the tris-PCz and NaNaP-A interface, the formation of a high singlet CT energy level (~2.6 eV) close to the NaNaP-A emission peak (~2.7 eV, ~450 nm) can be expected. Further, in order to remove such interfacial CT interaction, we also insert a thin wide-energy bandgap mCBP layer into the tris-PCz/NaNaP-A interface. Due to the wide-energy bandgap of mCBP (HOMO/LUMO of –6.1/–2.6 eV), there is virtually no energy offset at the mCBP/ NaNaP-A interface, thus leading to no CT interaction at the mCBP/ NaNaP-A interface in the mCBP-inserted OLED.

Table 3.1. Photophysical properties of the neat, blended, and stacked films.

Compound	PL Peak [nm]	FWHM [nm]	PLQY [%][a)]	τ_p [ns]	τ_d [μs]
NaNaP-A neat	453	62	53±2	2.0	2.2
Tris-PCz:NaNaP-A blend	452	64	50±2	1.8 / 8.1	N.D.
mCBP:NaNaP-A blend	450	61	57±2	2.2	N.D.
Tris-PCz/NaNaP-A stack	451	68	–	2.6 / 8.6	1.8
mCBP/NaNaP-A stack	445	63	–	2.7	1.9

a) Photoluminescence quantum efficiency under Argon atmosphere.

In order to address the detailed CT interaction, a tris-PCz:NaNaP-A blend film was also investigated in comparison with an mCBP:NaNaP-A blend film and a NaNaP-A neat film. **Table 3.1** summarizes the related photoluminescence (PL) characteristics of all films. The PL spectra of these films (**Fig. 3.3(a)**) showed only a very slight difference across samples with similar PL peaks at around 450 nm. In particular, the mCBP:NaNaP-A blend expressed almost the same FWHM as that of the NaNaP-A neat film (~61 nm). Conversely, the tris-PCz:NaNaP-A blend had a noticeably wider FWHM (~64 nm), suggesting the CT interaction between tris-PCz and NaNaP-A. To validate the contribution of CT interaction, the exciplex spectrum was inferred from an emission spectrum simulation. Assuming the exciplex peak energy is 2.6 eV, we fitted all spectra under the equation: Total PL spectrum = A1 (pure NaNaP-A emission) + A2 (exciplex emission), where A1 and A2 are the fitting constants. The singlet energy level of the exciplex (1CT: estimated from the spectrum onset) and the coefficient of determination for each fitting are plotted in **Fig. 3.3(b)**. It was clarified that the best-fit region ($R2 > 0.998$) corresponded well with the 1CT ranging from 2.87 eV to 3.00 eV with A1 and A2 being 0.89 and 0.11, respectively.

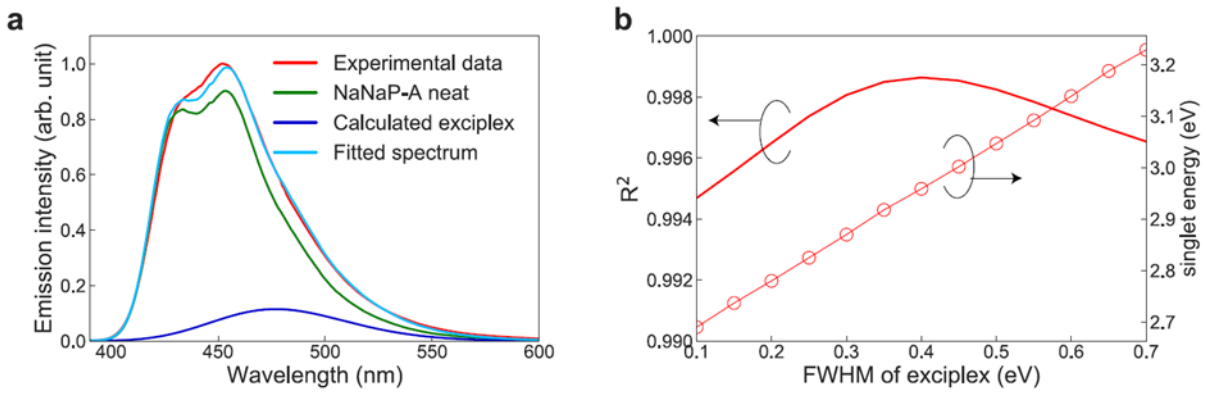

Figure 3.3: (a) PL spectra of the experimentally obtained NaNaP-A neat film (green), and tris-PCz:NaNaP-A blend film (red). The sky-blue line indicating the restoration of the PL spectrum of the tris-PCz:NaNaP-A blend using the NaNaP-A neat spectrum and the simulated exciplex emission spectrum (blue). (b) The relationship between a simulated ^{1}CT energy level (open circle: spectrum on-set value) and a coefficient of determination for each fitting (solid line).

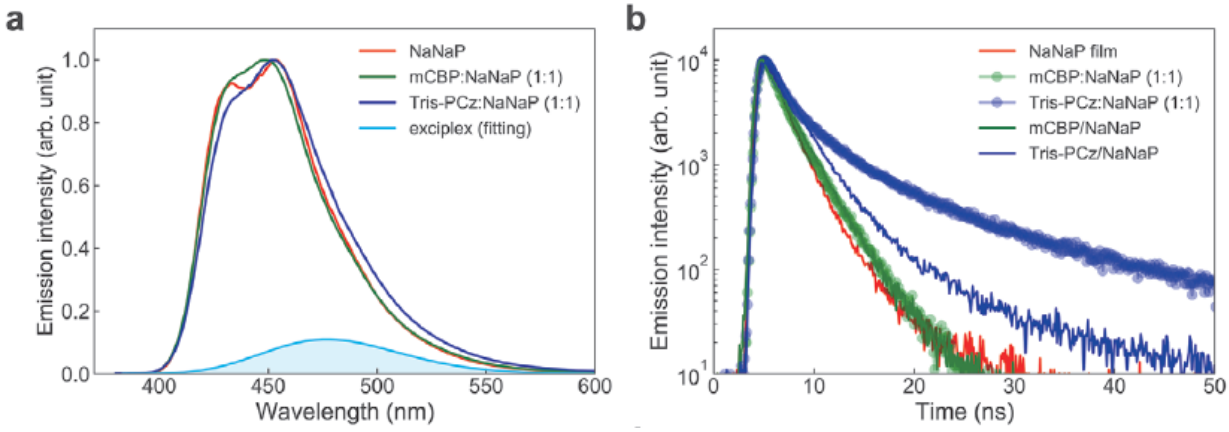

Figure 3.4: (a) PL spectra of the NaNaP-A, mCBP:NaNaP-A, and tris-PCz:NaNaP-A film. The sky-blue line indicating the simulated exciplex emission spectrum in the tris-PCz:NaNaP-A film. The fitting constant A1 and A2 were 0.89 and 0.11, respectively. (b), (c) Transient PL decay profiles of the NaNaP-A neat film, mCBP:NaNaP-A and tris-PCz:NaNaP-A blend films, and mCBP/NaNaP-A and tris-PCz/NaNaP-A-stacked films for 50 ns time range, respectively.

The CT interaction also affects the sample's PL decay profiles. Compared to the fitted exciplex PL spectrum, NaNaP-A neat and mCBP:NaNaP-A blend film shows a slightly narrower spectrum **(Fig. 3.4(a))**. The transient PL decay curves (**Fig. 3.4(b)**) yielded a completely distinct decay profile for the tris-PCz:NaNaP-A due to the presence of the prolonged second-order decay curve (τ_1~1.8 ns, and τ_2~8.1 ns). On the other hand, the other samples gave a single-exponential decay profile with a lifetime of ~2.0 ns. The PL wavelength of the tris-PCz film is much shorter than that of the blend, and the tris-PCz emission completely disappeared in the blend film, indicating the efficient CT from tris-PCz to NaNaP-A. We, therefore, assigned τ_1 to the fluorescence of NaNaP-A (^{1}LE) and the relatively long τ2 to the CT component (^{1}CT). Furthermore, compared with an mCBP:NaNaP-A system showing only ^{1}LE emission, the CT component accounted for 41% in tris-PCz:NaNaP-A system, denoting a significant contribution of the exciplex. While one would assume that such contribution of the CT emission should be somewhat prominent, it is not the case here based on the A1:A2 ratio above. The CT interaction seems to be overshadowed because the LE and CT energy levels are very close to each other. In fact, it enables the back electron transfer (BET) process from ^{1}CT to ^{1}LE, evidenced by the near identical spectrum between nanosecond-time-scale prompt and delay emission (**Fig. 3.5**).

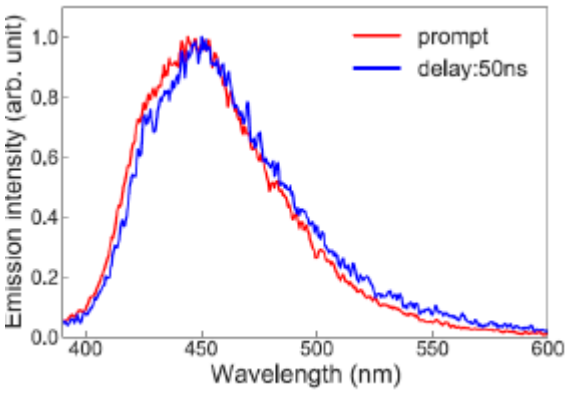

Figure 3.5: The prompt (red line) and nanosecond time scale delayed (blue line) PL spectra of the tris-PCz:NaNaP-A blend film.

After confirming the CT interaction between tris-PCz and NaNaP-A molecules in the blend, the interfacial CT interaction was studied

to clarify the actual situation in OLEDs. A multi-stacked-layer structure was employed as a valid replacement to detect a clear PL signal from the interface. By alternating a 10-nm-thick tris-PCz (or mCBP) layer and a 10-nm-thick NaNaP-A layer, the total 100-nm-thick stacked film (containing nine interfaces) was prepared. After studying the transient PL of these stacked films, again, only the combination of the tris-PCz/NaNaP-A system showed the characteristic extended decay curve, while the mCBP/NaNaP-A stacked film and NaNaP-A neat film showed a similar emission lifetime (**Fig. 3.4(b)**). Notably, triplets are generated in the NaNaP-A neat film originating from the intersystem crossing (ISC) process. This result reinforced our hypothesis of the interfacial CT excited-state formation between tris-PCz and NaNaP-A molecules. Noticeably, the blend film had a more intense delay component than the stacked film, since it only forms exciplex pairs at their interfaces, decreasing the total number of the D-A pairs under optical excitation.

By extending the transient PL measurement time range to 10 μs, the delayed emission component could be recognized in all stacked films. The mCBP/NaNaP-A stacked film expressed the decay profile exactly coincided with that of the NaNaP-A neat film (**Fig. 3.6(a)**). In both cases, the delayed emission spectra closely resembled the prompt emission spectrum (**Fig. 3.6(b)**). We assigned this delayed signal to the TTU process in the NaNaP-A layers. Regarding the tris-PCz/NaNaP-A case, on the other hand, the delayed curve is once again distinguished from the other two cases. Although the transient lifetime is close to those of the mCBP and neat films' cases, the tris-PCz/NaNaP-A stacked film gave a much more intense delayed component. The strengthened delayed signal could be a product of the additional contribution of the CT interaction. It was also recognized that the delayed emission of the tris-PCz/NaNaP-A stacked film showed a slightly broadened spectrum. The spectral broadening indicates an additional contribution of ^{1}CT. There are

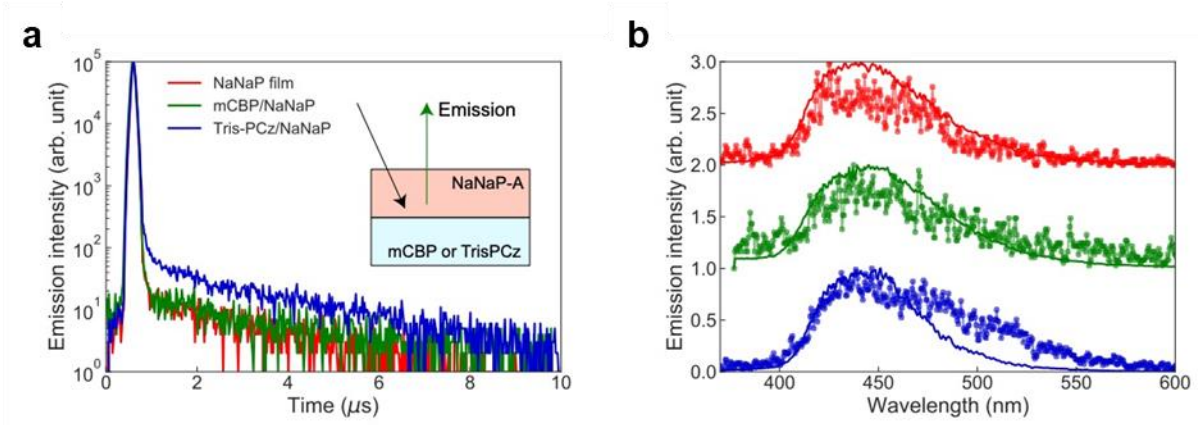

Figure 3.6: (a) Transient PL decay profiles of the NaNaP-A neat film, mCBP:NaNaP-A and tris-PCz:NaNaP-A blend film, and mCBP/NaNaP-A and tris-PCz/NaNaP-A-stacked film for 10 μs time range, respectively. (b) The prompt (line) and delayed (Delayed time: 1.5–10 μs, circle symbol) PL spectra of the NaNaP-A neat film, mCBP/NaNaP-A film, and tris-PCz/NaNaP-A-stacked film.

two pathways to generate the ^{1}CT in microsecond order: from the ^{3}CT via a RISC process to the ^{1}CT; from the ^{3}LE via a TTU process to the ^{1}LE and then to the ^{1}CT. As we can expect a fast relaxation from the ^{3}CT to the low energy level ^{3}LE[74], the second pathway is significantly more probable than the first one. It leads to the conclusion of a re-CT interaction between the singlet exciton of NaNaP-A and a ground state of the tris-PCz molecule after the TTU event. Overall, these PL characteristics of the stacked films highlight the role of interfacial CT interaction between the HTL (tris-PCz) and the TTU-host (NaNaP-A) on the TTU yield. It also provided that mCBP is a fair candidate to remove the exciplex formation completely. Therefore, these PL results alert that this overlooked interaction is presenting at the interface and should be addressed.

Figures 3.7(a) and **3.7(b)** show materials and OLEDs structure in this study. Although it has been previously pointed out that the NaNaP-A-based OLED accumulates dense electrons at the

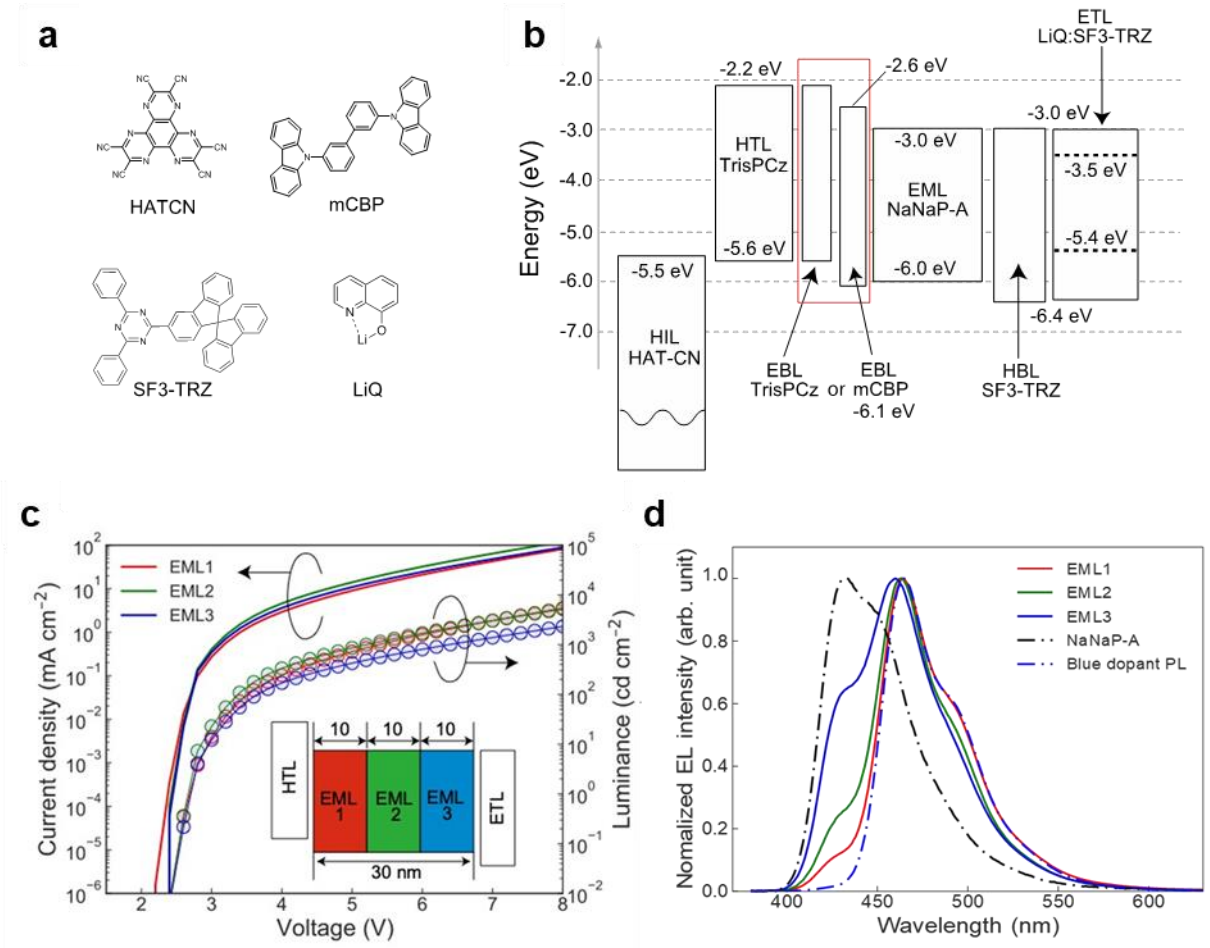

Figure 3.7: (a) Chemical structures of the hole injection material HAT-CN, the wide-bandgap EBL mCBP, and the hole blocking / electron transport material SF3-TRZ use in the TTUOLEDs. (b) HOMO and LUMO energy level diagram of the fabricated TTU-OLEDs. The dashed lines represent the HOMO and LUMO energies of LiQ. (c) Current density-luminance-voltage, and (d) Normalized EL spectrum in the OLEDs at 1.0 mA cm^{-2}. Inset: Schematic illustration of the EML structure. The blue dopant, (N1,N6-bis(4-dibenzofuranyl)-3,8-diisopropyl-N1, N6-bis(4-isopropylphenyl)-1,6-pyrenediamine[14], was doped into NaNaP-A host with a doping concentration of 1.0 % for each device.

electron blocking layer (EBL)/EML interface[14], we re-confirmed it in our OLED structure (**Fig. 3.7(c)**) via the well-established partial emitter doping method. By dividing the EML into three layers with the 10 nm thickness (**Fig. 3.7(c)**), a blue dopant was then doped with the doping concentration of 1.0 mol% in each section to give three different testing OLEDs. **Figure 3.7(d)** demonstrated that the dopant's emission was increased when the doped position was located closer to the tris-PCz/EML interface. This result indicated that our device also possesses a similar charge recombination zone as those in T. Sato e.al despite different material sets[14]. It is due to a remarkedly unbalanced carrier transport ability of the NaNaP-A layer, i.e., dominant electron current and negligible small hole current.

Figure 3.8(a) shows the current density-voltage-luminance (I-V-L) curves of two OLEDs (without the blue dopant) and **Fig. 3.8(b)** shows the OLEDs EQE performance. A clear difference of driving voltage of about 1.0 V between two OLEDs was observed, i.e., 1.0 mA cm–2 at 3.2 V for the tris-PCz/NaNaP-A based OLED and 1.0 mA cm^{-2} at 4.2 V for the mCBP/NaNaP-A based OLED. Since the unbalanced carrier transport ability of the NaNaP-A layer limits hole injection from the tris-PCz layer to the NaNaP-A layer, holes were accumulated at the tris-PCz's HOMO, while electrons were accumulated at NaNaP-A's LUMO. Since the CT interface between two molecules has been confirmed, some holes and electrons are consumed directly as the interfacial CT exciton formation. This fact eliminated the requirement of direct hole injection into the NaNaP-A layer, escaping a large voltage drop at the interface. Indeed, the EL was observed at below 2.6 V, corresponding to the CT energy, in the tris-PCz/NaNaP-A-based OLED. On the other hand, the situation is not similar in the case of the mCBP/NaNaP-A system. No CT interaction was confirmed at the mCBP/NaNaP-A interface, indicating that hole injection into the HOMO of a NaNaP-A layer or electron injection into the LUMO of an mCBP layer is expected to happen. The mCBP/NaNaP-A-based OLED showed a small EL component below 400 nm corresponding to the mCBP emission (**Fig. 3.8(c)**). This implies that the absence of interfacial exciplex could easily lead to electron leakage even though the mCBP layer has a wide energy bandgap material (3.5 eV for optical gap) with a shallow LUMO of –2.6 eV. Indeed, the turn-on of EL was observed at 3.5 V, which corresponds well to the mCBP bandgap in the mCBP/NaNaP-A-based OLED.

While an interfacial exciplex is generally viewed as an exciton leakage, our interfacial CT interaction-based TTU-OLED exhibited an exceptionally high EQE with a maximum EQE reaching 6% at 7 mA cm–2 (**Fig. 3.8(b)**). Since the PLQY of the NaNaP-A neat film is 53±2%, the singlet exciton production yield surpassed 50±2%, approaching the theoretical singlet exciton production limit (62.5%)[69]. To confirm the contribution of the TTU on the high EQE, we evaluated a transient

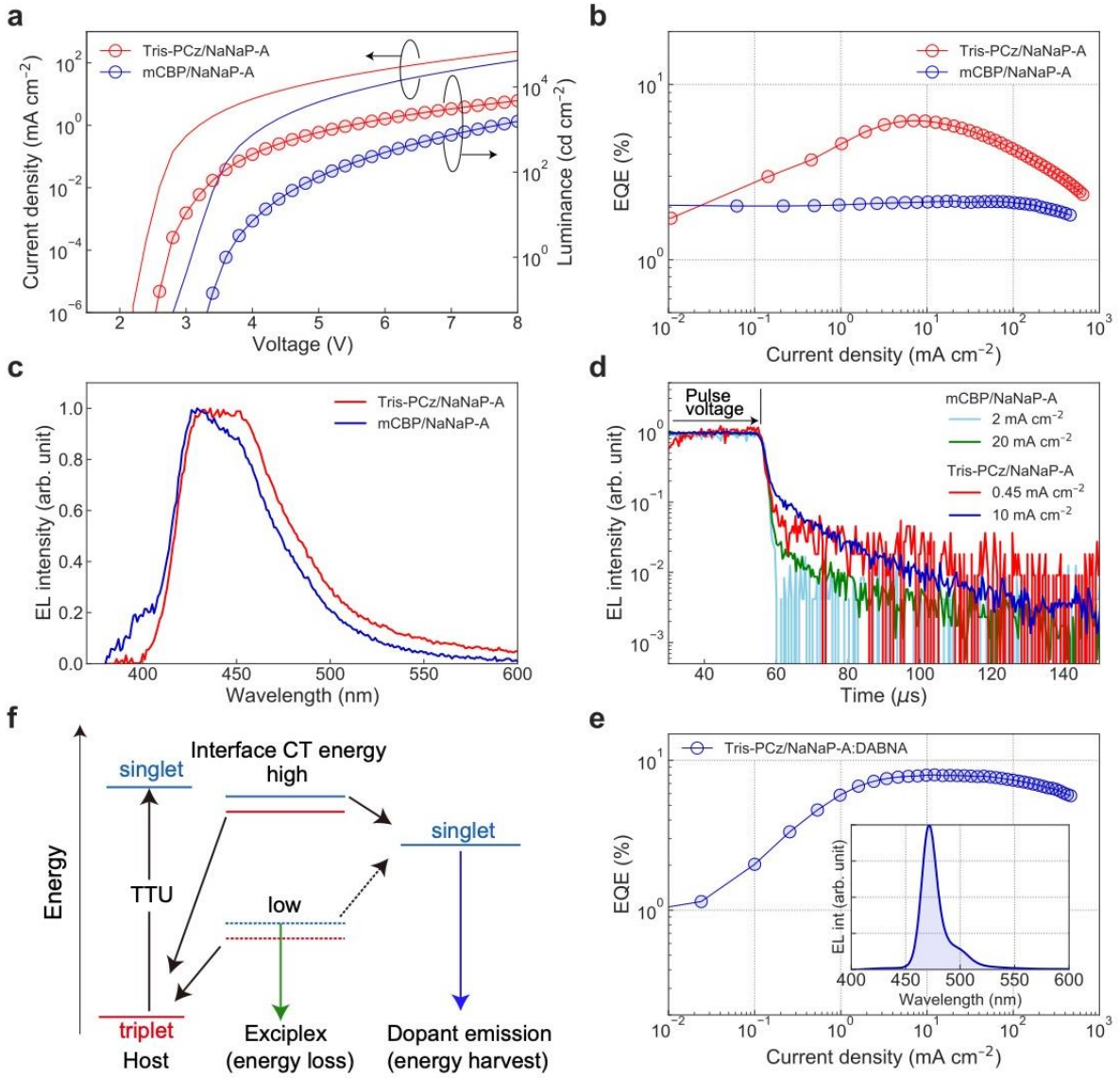

Figure 3.8: (a) Current density–luminance–voltage, and (b) EQE–current density characteristics of the tested OLEDs. (c) Normalized EL spectra in the OLEDs at 0.1 mA cm^{-2}. (d) Transient EL profiles of the OLEDs at various current density. (e) Schematic illustration of the requirement energy level diagram to exploit the singlet CT energy as blue emission. (f) EQE–current density characteristics of the pure blue TTU-OLEDs. Inset: Normalized EL spectrum in the OLED at 1.0 mA cm^{-2}.

EL in OLEDs, as shown in **Fig. 3.8(d)**. The OLED exhibited a clear delayed EL component that shares the identical EL spectrum with the prompt one even at a low current density region (0.45 mA cm^{-2}), indicating the presence of an efficient TTU in the OLED and the CT interaction which is not harmful to TTU-OLED's performance. Conversely, the mCBP/NaNaP-A-based OLED only showed a maximum EQE of around 2% and almost no delayed EL component even at 2.0 mA cm^{-2}, similar to conventional fluorescence OLEDs. However, note that a very slight efficiency rollup and the delay EL component was observed at around 20 mA cm^{-2} (**Figs. 3.8(b)** and **3.8(d)**), indicating the small contribution of the TTU event to the EQE in the OLED. With the horizontal orientation of NaNaP-A measured to be 79% **(Fig. 3.9(a))**, the maximum EQE can be estimated to be 7.8% (outcoupling

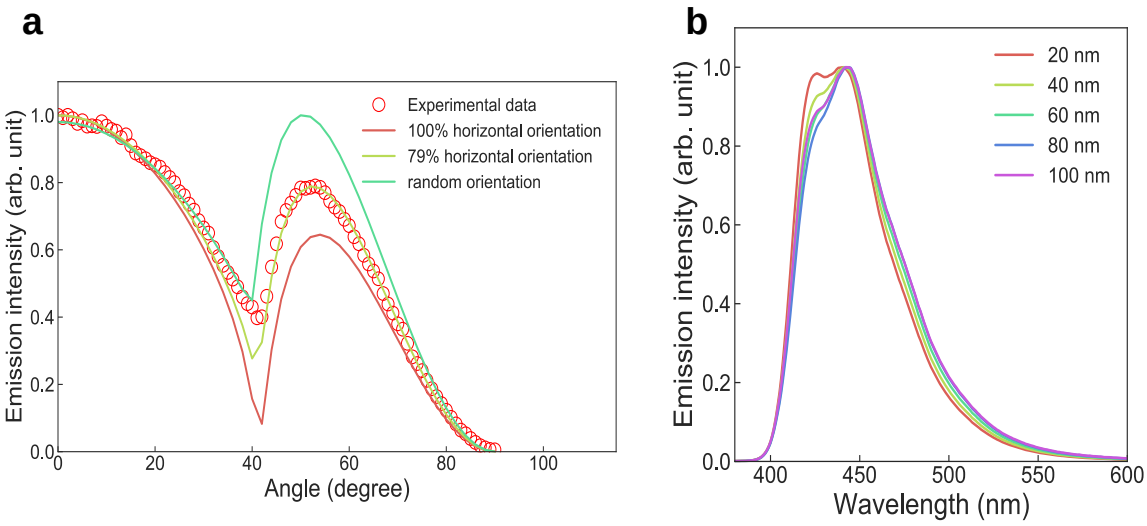

Figure 3.9: (a) Angular dependance of PL intensity of the NaNaP-A and horizontal orientation fitting. (b) Simulated NaNaP-A PL spectrum based on film thickness. Both simulations were obtained from Setfos 6.

factor is around 25%), which is close to the actual measured value. Notice that a slight difference between the PL spectrum and the EL spectrum of NaNaP-A can be explained by the optical interference effect because the film thickness for the PL measurement is 100 nm while the EML thickness in the OLED is 30 nm (**Fig. 3.9(b)**).

Here, we propose an explanation for the carrier accumulation at the HTL/EML interface. During electrical excitation, the tris-PCz/NaNaP-A interface accumulates tris-PCz's radical cations and NaNaP-A's radical anions at the HTL side and EML side, respectively. It provides an effective carrier recombination site through the CT interaction (**Fig. 3.1**). Although the electrically generated singlet CT (^{1}CT) decays as exciplex emission or upconverts to ^{1}LE, the triplet CT (^{3}CT) would non-radiatively decay to the localized excited triplet state (^{3}LE) of NaNaP-A. Thus, the CT interface builds up high-density hole-electron pairs, successively leading to an exceedingly dense amount of the ^{3}LE excitons. They, in turn, accelerate triplet-triplet collision to yield TTU at the interface. This was confirmed by the difference in the EL spectra from both OLEDs (**Fig. 3.5(c)**) and an enhancement of the EL delayed component (**Fig. 3.5(d)**). The tris-PCz/NaNaP-A based OLED showed the broadened FWHM, indicating the additional contribution of the exciplex as same as the PL (**Fig. 3.2(a)**). Note that the singlet excited state of NaNaP-A that is generated via TTU has a possibility to undergo CT interaction with the tris-PCz again. Further, we should also consider another potential process at the HTL/EML interface. The high density of holes and electrons at the interface can dramatically change the hole injection barrier, facilitating holes to inject directly into the NaNaP-A layer. Although it is difficult to quantitatively conclude which process is dominated at

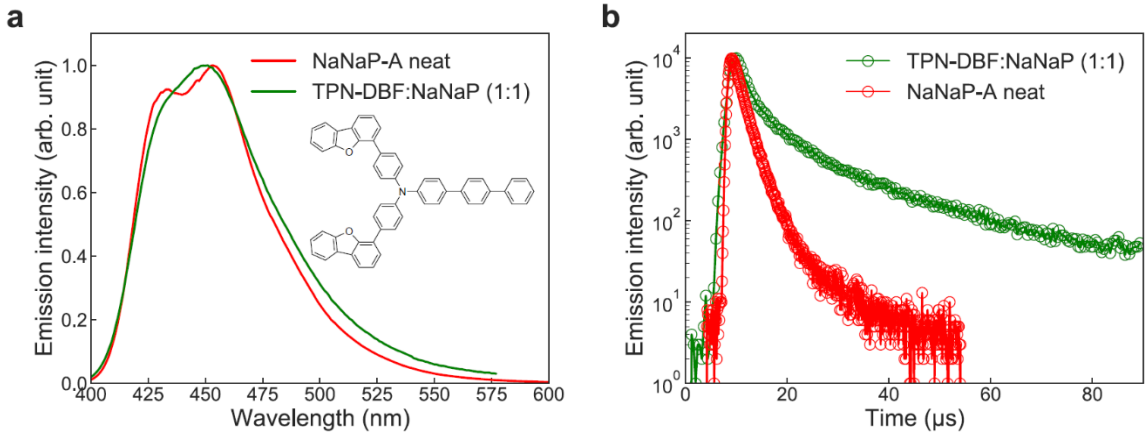

Figure 3.10: (a) PL spectrum of the NaNaP-A, and TPN-DBF:NaNaP-A film. The PLQY of the blend was 31%, which is lower than that of the NaNaP-A neat film, indicating the CT interaction between TPN-DBF and NaNaP-A. Inset: Chemical structure of TPN-DBF. The HOMO and LUMO of the TPN-DBF was estimated to –5.7 eV and –2.7 eV, respectively. (b) Transient PL decay profiles of the NaNaP-A neat film, and TPN-DBF:NaNaP-A film for 90 ns time range.

this stage, the CT-sensitized TTU at the interface should undoubtedly occur even in the OLEDs as observed for the optical excitation.

The generalization of our proposed mechanism was furtherly solidified with an N,N-bis[4-(dibenzofuran-4-yl)phenyl]-p-terphenyl-4-amine (TPN-DBF) that was used as an electron-blocking layer[14]. The high energy CT formation is also confirmed in the TPN-DBF:NaNaP-A molecular system as shown in **Figs. 3.10** and **3.11**. The TPN-DBF:NaNaP-A blend exhibited a very clear ^{1}CT peak at 460 nm. We suppose that its intense CT emission originates from the strong CT interaction between electron-donating group triphenylamine and NaNaP-A. The HOMO energy level of TPN-

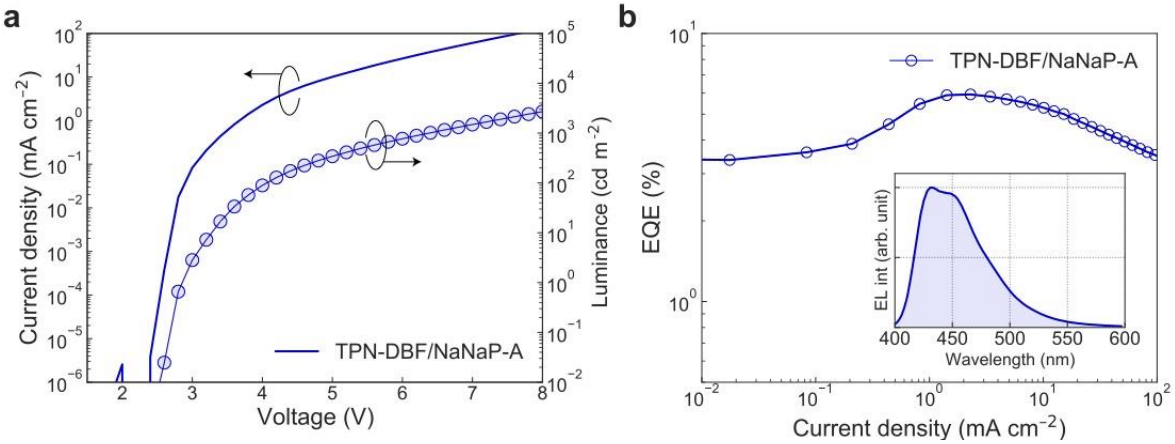

Figure 3.11: (a) Current density-luminance-voltage, and (b) EQE-current density characteristics in the TPN-DBF/NaNaP-A based OLED. Inset: Normalized EL spectrum in the OLEDs at 1.0 mA cm^{-2}. The OLED structure was ITO (100 nm) / HAT-CN (10 nm) / tris-PCz (20 nm) / TPN-DBF (10nm) / NaNaP-A (30 nm) / SF3-TRZ (10 nm) / 50wt%_Liq:SF3-TRZ(20 nm) / Liq(2 nm) / Al (100 nm). Maximum EQE of 5.9% was obtained at 2.3 mA cm^{-2}.

DBF (~5.7eV) is also similar to tris-PCz (~5.6eV). We hypothesize that our research is applicable to prominent hole-transporting material with HOMO ranging from 5.5eV to 5.8eV. Note that HOMO>5.9eV creates a zero-energy offset like mCBP and thus should be avoided. Importantly, since the blue TTU-OLED based on a NaNaP-A host and TPN-DBF possesses remarkably high operational stability (LT95 > 1,000 hours, initial luminance = 1,000 cd m^{-2}) with high EQE (around 10%), it is expected that the formation of the CT interface would not trigger the degradation event.

It is a common strategy to dope fluorescence emitters in TTU-OLEDs to boost EL efficiency. In our interfacial CT system, the ^{1}CT stays at the lowest singlet energy level of ~2.87 eV based on the simulation results above. To fully exploit the electrically generated singlet excitons via the TTU event, the efficient energy transfer from ^{1}CT to S_1 of a blue dopant is crucial. An energy miss-match would inevitably lead to inefficient energy transfer between them (**Fig. 3.12**). Here, ν-DABNA was selected as the fluorescent dopant for pure-blue TTU-OLEDs and not as the TADF dopant[48]. The ν-DABNA molecule has a high S_1 energy of 2.7 eV, satisfying the required energy alignment condition. The EL spectrum presented distinct features from the dopant with narrow FWHM (18 nm), corresponding to the Commission Internationale de l' Eclairage coordinates (0.12, 0.12). It, therefore, indicated a complete energy transfer from both ^{1}CT (from CT interface) and ^{1}LE (from NaNaP-A) to S_1 of ν-DABNA without any changing of the turn–on voltage. The maximum EQE of the OLEDs was improved appreciably (8% for ν-DABNA, as shown in **Fig. 3.5(f)**) because of an improvement of PLQY (67% for 1wt%-ν-DABNA:NaNaP-A).

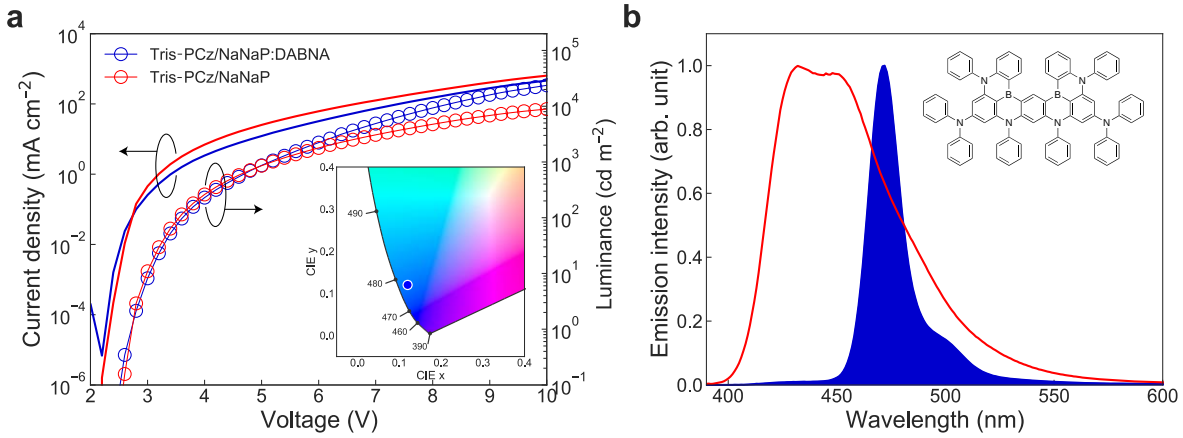

Figure 3.12: (a) Current density-luminance-voltage, and (b) Normalized EL spectrum at 1.0 mA cm^{-2} in the OLED with and without blue dopant (*ν*-DABNA). Inset: Chemical structure of *ν*-DABNA.

3-4. Conclusion

In summary, the "overlooked" real role of interfacial CT formation in pure-blue TTU-OLEDs was revealed, and we clarified the actual contribution to OLED performance. The triplet energy can

be well harvested based on the cascade energy alignment of the S_1 of NaNaP-A > ^{1}CT state > the S_1 of *v*-DABNA with the aid of a TTU process in NaNaP-A, ensuring all singlet excitons can be transferred to the blue dopant. Thus, the mechanism we proposed here highlights a new aspect regarding the material selection and OLED design architectures required for high-performance pure-blue TTU-OLEDs. It should be noted that opposite interfaces, i.e., the EML/electron transporting layer, could also have a similar effect depending on the host's carrier transportability.

Chapter 4

Enhancing triplet-triplet upconversion efficiency and operational lifetime in blue organic light-emitting diodes by utilizing thermally-activated delayed fluorescence materials

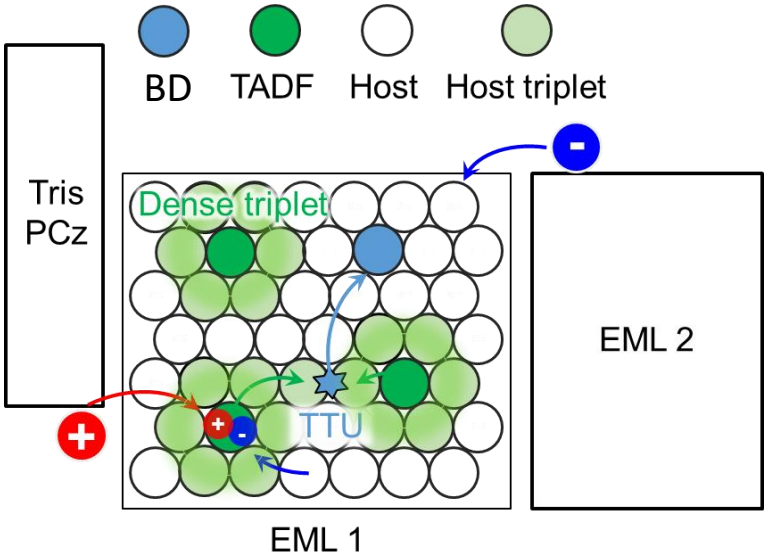

4-1. Introduction

In Chapter 3, we utilized the interfacial CT interaction at the HTL/EML interface in the blue TTU-OLED, which improved its EQE. However, the TTU contribution to the total EL intensity is still restricted. In this chapter, we demonstrate a proof-of-concept to attaining maximum TTU contribution yield in blue fluorescence TTU-OLEDs, achieved through the doping of TADF molecules at the carrier recombination zone as carrier recombination center. Generally, TADF materials have an electron-donating unit (D) and an electron-accepting unit (A) in their backbone to ensure a small singlet-triplet energy gap through the CT interaction. Therefore, the D-A type materials naturally possess a bipolar carrier transport ability[22]. Since the low hole transport ability of anthracene derivatives naturally restricts the hole carrier penetration inside the EML[14], the bipolar carrier transport ability of TADF materials enables direct carrier recombination on the molecules, expanding the recombination zone. Despite the slightly lower EQE of the OLED (~5%) compared to that of conventional blue TTU-OLEDs (~7%), owing to the low photoluminescence quantum yield (PLQY) of the TADF-doped layer (~25%), the TTU efficiency reaches its upper limit. Additionally, the operational device lifetime (LT90) of tested blue OLEDs employing TADF molecules exceeds 120 hours at an initial luminance of 1,000 cd m^{-2}, which is five times longer than that of conventional ones, highlighting the expansion of the recombination zone as a crucial factor in enhancing overall OLED performance in TTU-OLEDs.

4-2. Experimental section

4-2-1. Sample preparation

Same as Chapter 2.

4-2-2. Fundamental PL properties

The steady-state PL spectra were recorded by a spectrofluorometer (FP-8600, JASCO). The PLQY was measured using an absolute photoluminescence quantum yield measurement system (Quantaurus-QY Plus, Hamamatsu Photonics) under the argon gas flow. HOMO levels were measured by photoelectron spectroscopy method using a Riken Keiki, AC-3. Optical energy gaps of these materials were obtained from the absorption edges of films. The emission lifetime was measured using a fluorescence lifetime measurement system (C11367-03 Quantaurus-Tau, Hamamatsu Photonics).

4-2-3. Characterization of OLED performances

Same as Chapter 2.

4-2-4. TTU model

In our system, there are 3 components: TADF (HDT-1), host (1,2-ADN), and blue dopant DB (ν-DABNA). The recombination event happens at TADF to generate singlet (S_{TADF}) and triplet (T_{TADF}) excitons with the rate of G/4 and 3G/4, respectively (whereas G is the charge recombination rate). TADF singlet is then quenched by BD singlet via FRET energy transfer with a coefficient rate of k_{FRET}^1, as well as ISC process with a coefficient rate of k_{ISC}. TADF triplet is first generated by recombination event and ISC process. After that, it is quenched by the host triplet via Dexter energy transfer with a coefficient rate of k_{DET}.

$$\frac{d[S_{TADF}]}{dt} = \frac{G}{4} - (k_{FRET}^1 + k_{ISC})[S_{TADF}] \tag{4.1}$$

$$\frac{d[T_{TADF}]}{dt} = \frac{3G}{4} + k_{ISC}[S_{TADF}] - k_{DET}[T_{TADF}] \tag{4.2}$$

Host triplet can undergo the TTU process with a bimolecular annihilation rate γ_{TTU}, as well as non-radiative decay with a rate constant k_{nr}. The host singlet is then formed by the TTU process, before being quenched by the BD singlet via FRET energy transfer with a coefficient rate of k_{FRET}^2.

$$\frac{d[S_{host}]}{dt} = \frac{1}{2}\gamma_{TTU}[T_{host}]^2 - k_{FRET}^2[S_{host}] \tag{4.3}$$

$$\frac{d[T_{host}]}{dt} = k_{DET}[T_{TADF}] - \gamma_{TTU}[T_{host}]^2 - k_{nr}[T_{host}] \tag{4.4}$$

Blue dopant singlet is formed by the FRET process from both TADF and host, before radiative decay with coefficient k_r.

$$\frac{d[S_{BD}]}{dt} = k_{FRET}^1[S_{TADF}] + k_{FRET}^2[S_{host}] - k_r[S_{BD}] \tag{4.5}$$

Equation 4.5 clearly indicates that emission from blue dopant singlet consists of a prompt component from S_{TADF} and a delayed component from S_{host}. The delay contribution can then be defined as:

$$TTU\ con\ tribution = \frac{Delayed\ EL\ intensity}{Total\ EL\ intensity} \tag{4.6}$$

Regarding the transient EL data, we can choose the moment pulse off at t=0, total EL intensity is normalized to 1, i.e., $I(0) = 1$. In addition, the recombination rate G drops to 0 as no more exciton is electrically generated. The entire system evolves into:

$$\frac{d[S_{TADF}]}{dt} = -(k_{FRET}^1 + k_{ISC})[S_{TADF}] \tag{4.7}$$

$$\frac{d[T_{TADF}]}{dt} = k_{ISC}[S_{TADF}] - k_{DET}[T_{TADF}] \tag{4.8}$$

$$\frac{d[S_{host}]}{dt} = \frac{1}{2}\gamma_{TTU}[T_{host}]^2 - k_{FRET}^2[S_{host}] \tag{4.9}$$

$$\frac{d[T_{host}]}{dt} = k_{DET}[T_{TADF}] - \gamma_{TTU}[T_{host}]^2 - k_{nr}[T_{host}] \tag{4.10}$$

$$\frac{d[S_{BD}]}{dt} = k_{FRET}^1[S_{TADF}] + k_{FRET}^2[S_{host}] - k_r[S_{BD}] \tag{4.11}$$

An assumption was made to simplify the calculation as follows. FRET and DET processes are 3 orders of magnitude higher than the TTU process. It is supported by the time scale of the PL system where emission was only observed in the nanosecond range but not in the microsecond range. Meanwhile, transient EL showed delayed emission at microsecond rage, originating from the TTU process. Thus, when considering delayed EL, other processes can be regarded as immediately finished, transforming equation (9) into:

$$\frac{d[T_{host}]}{dt} = -\gamma_{TTU}[T_{host}]^2 - k_{nr}[T_{host}] \tag{4.12}$$

This equation has a solution in the form of $[T_{host}(t)] = [a + b.\exp(ct)]^{-1}$ where a, b, and c are constant. The substitution method will then yield:

$$[T_{host}(t)] = \left\{-\frac{\gamma_{TTU}}{k_{nr}} + \left\{\frac{1}{[T_{host}(0)]} + \frac{\gamma_{TTU}}{k_{nr}}\right\}\exp(-k_{nr}t)\right\}^{-1} \tag{4.13}$$

In addition, due to our assumption, all generated S_{host} from the TTU process is transferred to S_{BD}. Thus equation (9) is at a steady state, meaning:

$$[S_{host}(t)] = \frac{1}{2k_{FET}}\gamma_{TTU}[T_{host}(t)]^2 \tag{4.14}$$

$$[S_{host}(t)] = \frac{1}{2k_{FET}}\gamma_{TTU}\left\{-\frac{\gamma_{TTU}}{k_{nr}} + \left\{\frac{1}{[T_{host}(0)]} + \frac{\gamma_{TTU}}{k_{nr}}\right\}\exp(-k_{nr}t)\right\}^{-2} \tag{4.15}$$

After prompt emission, the delayed EL purely originates from $S_{host,}$ thus $[S_{BD}] \propto [S_{host}]$. Therefore, the delayed intensity at time t is calculated with a scaling factor L:

$$\frac{I_{Delayed}(t)}{I(0)} = I_{Delayed}(t) = \frac{[S_{BD}(t)]}{[S_{BD}(0)]} \tag{4.16}$$

$$\propto \frac{[S_{host}(t)]}{[S_{BD}(0)]} \tag{4.17}$$

$$\propto \frac{\gamma_{TTU}}{2k_{FET}[S_{BD}(0)]}\left\{-\frac{\gamma_{TTU}}{k_{nr}} + \left\{\frac{1}{[T_{host}(0)]} + \frac{\gamma_{TTU}}{k_{nr}}\right\}\exp(-k_{nr}t)\right\}^{-2} \tag{4.18}$$

$$= \frac{L \times \gamma_{TTU}}{2k_{FET}[S_{BD}(0)]}\left\{-\frac{\gamma_{TTU}}{k_{nr}} + \left\{\frac{1}{[T_{host}(0)]} + \frac{\gamma_{TTU}}{k_{nr}}\right\}\exp(-k_{nr}t)\right\}^{-2} \tag{4.19}$$

Combining our normalization of transient EL data and equation 4.5, we can obtain the following equality:

$$TTU\ contribution = I_{Delayed}(0) = \frac{L \times \gamma_{TTU}}{2k_{FET}[S_{BD}(0)]}[T_{host}(0)]^2 \quad (4.20)$$

Experimental data were therefore fitted with equation 15. Unfortunately, it is not possible to obtain all constants due to the scaling factor L. Thus, we extrapolated the fitting line to get $I_{delayed}(0)$ value (**Fig. 4.1**).

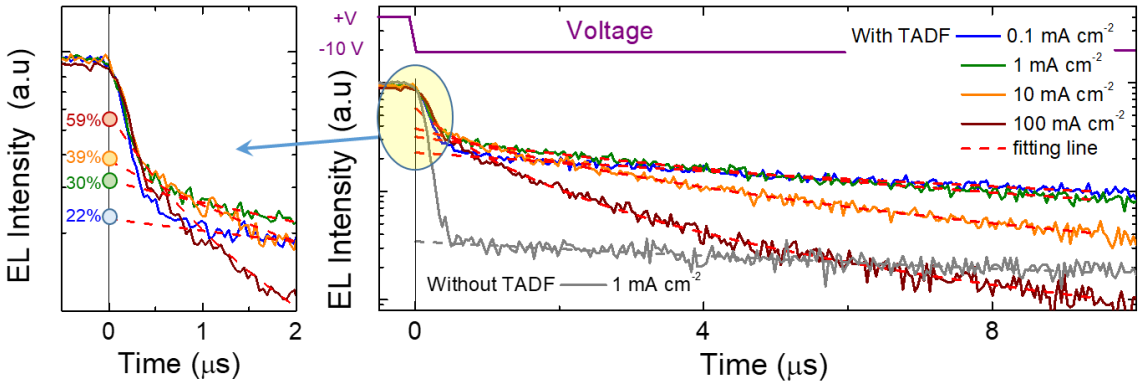

Figure 4.1: Prompt and delayed EL intensity under pulse excitation for OLEDs with and without TADF. Voltage pulse corresponds to pre-set current density (from 0.1 to 100 mA cm^{-2}). The read and gray dash lines are fitting results.

4-3. Results and discussions

Figures 4.2 and 4.3 illustrate the energy level diagram of the OLEDs tested in this study. We employed HDT-1[16], which possesses TADF activity, and v-DABNA as an assistant dopant and final blue emitter for TTU-OLED, respectively[44,48]. Two devices with either a conventional EML structure

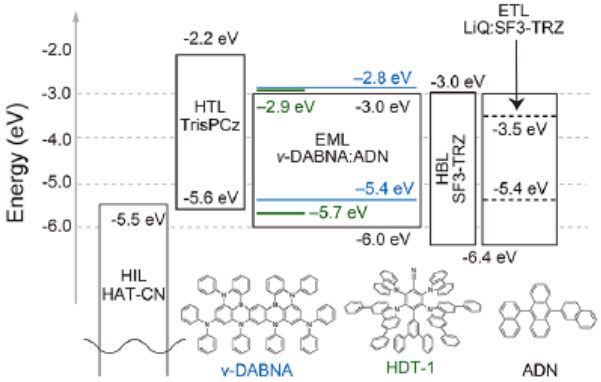

Figure 4.2: Related HOMO and LUMO energy level diagram of the tested OLED and the molecular structures of the key materials used in this study.

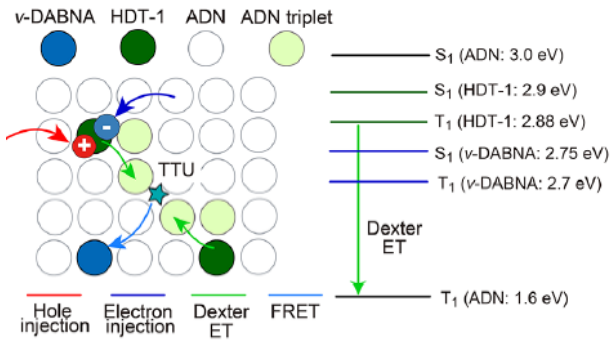

Figure 4.3: Schematic illustration of the proposed TTU events inside the extended EML structure.

or a modified EML structure were fabricated and evaluated for OLED performance. The modified EML structure was divided into two parts: 1) an interface extension area (3 nm-thick 1wt%-v-DABNA: 5 wt%-HDT-1: 1,2-ADN layer) and 2) the main EML portion (27 nm-thick 1wt%-*v*-DABNA : 1,2-ADN layer)[75]. The current density-voltage-luminance (I-V-L) curves of both OLEDs are shown in **Fig. 4.4(a)**. While the turn-on voltage (driving voltage at 1 cd m^{-2}) of both devices exhibited a similar value of around 2.8 V, the driving voltage of the OLED with a modified EML was slightly higher than the conventional one by around 0.2 V. This difference implies the formation of additional carrier recombination sites, in the modified EML compared to the conventional EML structure, which is attributed to the HDT-1 doping. Since the HOMO energy level of HDT-1 is slightly deeper than that of tris-PCz by 0.1 eV, there is a 0.1 eV hole-injection barrier between HTL and HDT-1 doped EML. Further, because the HDT-1 doping concentration in the EML is limited to 5 wt%, it is not expected to have efficient hole carrier hopping between HDT-1 molecules. Therefore, the driving voltage is slightly increased by the HDT-1 doping. Thus, the driving voltage is increased by 0.2 V in total. Both OLEDs shared a similar EL spectrum that displayed distinct features originating from the v-DABNA with a narrow FWHM (21 nm), corresponding to the Commission Internationale de l'Éclairage coordinates (CIE) of (x = 0.12, y = 0.13) as depicted in the inset of Fig. 1b. The EL spectrum of the OLED with an extended EML remained stable even with increasing

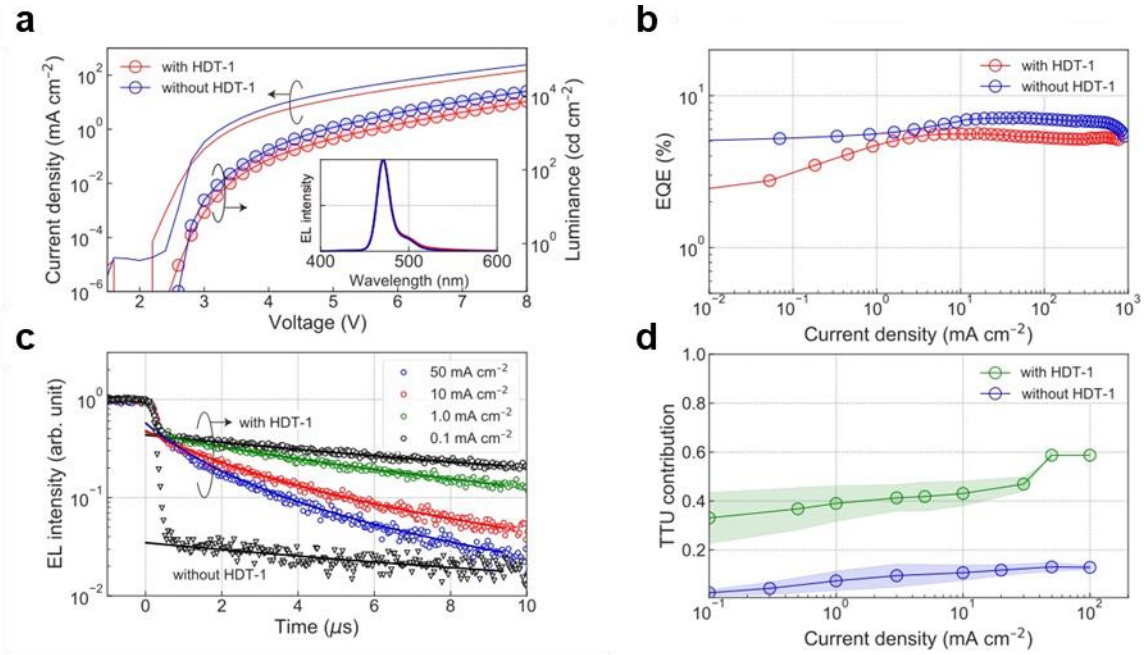

Figure 4.4: (a) Current density−luminance−voltage and (b) EQE−current density characteristics of the tested OLEDs. Inset: Normalized EL spectrum in the OLEDs at 1 mA cm^{-2}. (c) Transient EL profiles of the OLEDs with and without HDT-1 doping at various current densities. The triangle symbol is a transient EL profile of the OLED without HDT-1 at 0.1 mA cm^{-2}. (d) Dependence of the TTU contribution in the OLEDs with and without HDT-1 doping on an injected current density.

current density (Fig. S2), indicating an efficient energy transfer from both the excited singlet state of HDT-1 and 1,2-ADN to the excited singlet state of ν-DABNA.

The maximum EQE was slightly diminished from 7% to 5% (**Fig. 4.4(b)**), when introducing HDT-1 to the 1wt%-ν-DABNA: 1,2-ADN matrix, corresponding to the reduction of PLQY in the 1wt%-ν-DABNA: 5 wt%-HDT-1: 1,2-ADN layer (total PLQY = 25%). Despite the fact that the triplet exciton diffusion in the EML should be considered, the IQE of the OLED clearly exceeded the theoretical maximum for conventional fluorescence OLEDs and was expected to be higher than that of the OLED without HDT-1. To study the impact of TADF assistant dopant in more detail, transient EL was taken for both OLEDs under 2 kHz pulse driving voltage. The pulse consists of 100 μs positive voltage to reach the targeted current density, and 400 μs of –10 V to remove any charge accumulation inside the OLED after applying the positive voltage. At the window of 10 μs during the voltage switch, a streak camera was set up to capture the EL from these OLEDs, showing delayed emission. The OLEDs with modified EML exhibited much more intense delayed EL intensity than that of the OLED without HDT-1 (**Fig. 4.4(c)**). For example, at 0.1 mA cm^{-2}, the delayed EL intensity of the OLED with modified EML was over 10 times larger than that of the conventional one. Since a ratio of delayed EL intensity over total EL intensity is one of the indicators to evaluate the TTU efficiency[57,62,69], these transient EL signals were then fitted by the conventional TTU model to asset the TTU contribution to total EL efficiency.

With such a significant delayed-EL component, the OLED with modified EML yielded a much higher TTU contribution than conventional OLEDs across all current density regions (**Fig. 4.4(d)**). As a general feature of TTU-OLEDs, both types of OLEDs demonstrated increasing TTU contribution with increasing current density. Devices with HDT-1 reached nearly 60% TTU contribution at 50 mA cm–2 before saturation, marking one of the highest TTU contributions recorded in recent blue TTU-OLEDs. Meanwhile, OLED without HDT-1 only plateaued at around 18% even at 100 mA cm–2. In fact, 60% contribution is the theoretical limit for TTU-OLEDs, implying that the extent of carrier recombination site by HDT-1 was able to exploit the full potential of TTU ability of the EML. While researchers have been studying 100% TTU contribution, their systems work under the strict condition of an outstandingly strong ISC process and no FRET process[71]. In our system, the FRET energy transfer process rate constant from the singlet state of HDT-1 to the singlet state of ν-DABNA is expected to be out-competing with the ISC process. Similar evidence also has been reported earlier[16], resulting in 60% for the TTU theoretical limit.

In order to validate such a high TTU efficiency in the OLED with modified EML, we propose a possible mechanism that can yield favorable conditions for the TTU process (**Fig. 4.3**). As HDT-1

is doped near the HTL/EML interface, according to a low hole transport ability of anthracene derivatives 25, direct hole injections to the HOMO of HDT-1 (–5.7 eV) are highly expected to happen. This process leads to direct carrier recombination and generation of triplet excitons on HDT-1 molecules. Since the excited triplet energy of HDT-1 (2.7 eV) surpasses that of the 1,2-ADN (1.6 eV), the triplet exciton of HDT-1 is immediately quenched by the triplet state of nearby 1,2-ADN molecules. Consequently, a localized region surrounding each HDT-1 dopant provides a high concentration of triplet excitons, owing to the prolonged triplet lifetime of the anthracene unit. Therefore, the local triplet density around TADF molecules should be exceedingly high, facilitating efficient TTU events. These regions, characterized by a diameter of two or three molecules, can be referred to as triplet accumulation spots. The important point is that TADF concentration is only 5wt%, the number of the spots is very limited, leading to highly dense triplets around TADF molecules. Since the thickness of the HDT-1 doped layer is as thin as 3 nm, it is expected that such spots effectively cover nearly all the extended recombination zone. Then, this allows a substantial quantity of triplet excitons to be diffused from the narrow interfacial region to the bulk of the EML (i.e., 1wt%-v-DABNA: 1,2-ADN layer), thereby increasing the likelihood of triplet-triplet exciton collisions, and maximizing the contribution of TTU. Although showing a nearly 60% delay contribution, the transient EL profile of the OLED with extended EML at 100 mA cm^{-2} is steeper and decay faster than that of 0.1 mA cm^{-2}. While the reason behind such behavior is still unclear, we hypothesize that exciton-polaron annihilation processes could be the culprits because of the penetration of radical cation of HDT-1 into the EML.

Even though doping of carrier recombination sites to the system significantly boosts TTU contribution, it results in the PLQY reduction, hence reduced EQE. To gain insight into the photoluminescence properties of the blend film, PL characterization was conducted. The blend films of 1wt%-v-DABNA: x wt%-HDT-1: 1,2-ADN layer were fabricated with x% = 0%, 5%, 10%, and 20%. All films exhibit the same peak wavelength originating from v-DABNA which is distinctively different from both the PL spectrum of 1,2-ADN and HDT-1 (**Fig. 4.5(a)**). Further, the samples with TADF show longer emission lifetime in the ns range, regardless of TADF concentration (**Fig. 4.5(b)**). No delayed fluorescence that originates from the TADF activity of HDT-1 was observed because of 1,2-ADN low triplet energy level (**Fig. 4.5(c)** and **Fig. 4.3**). Among all three materials, v-DABNA has the lowest S_1 energy level while 1,2-ADN has the lowest T_1 energy level. Thus, in this system, all of the optically generated singlet excitons of 1,2-ADN are transferred to a v-DABNA singlet state while the triplet excitons are confined to the 1,2-ADN triplet state. Interestingly, the PLQY decreases correspondingly with increasing the HDT-1 doping concentration. Notably, the PLQY without HDT-1 is around 55% while the 5wt%-HDT-1 doped film only shows 25%. This phenomenon can be

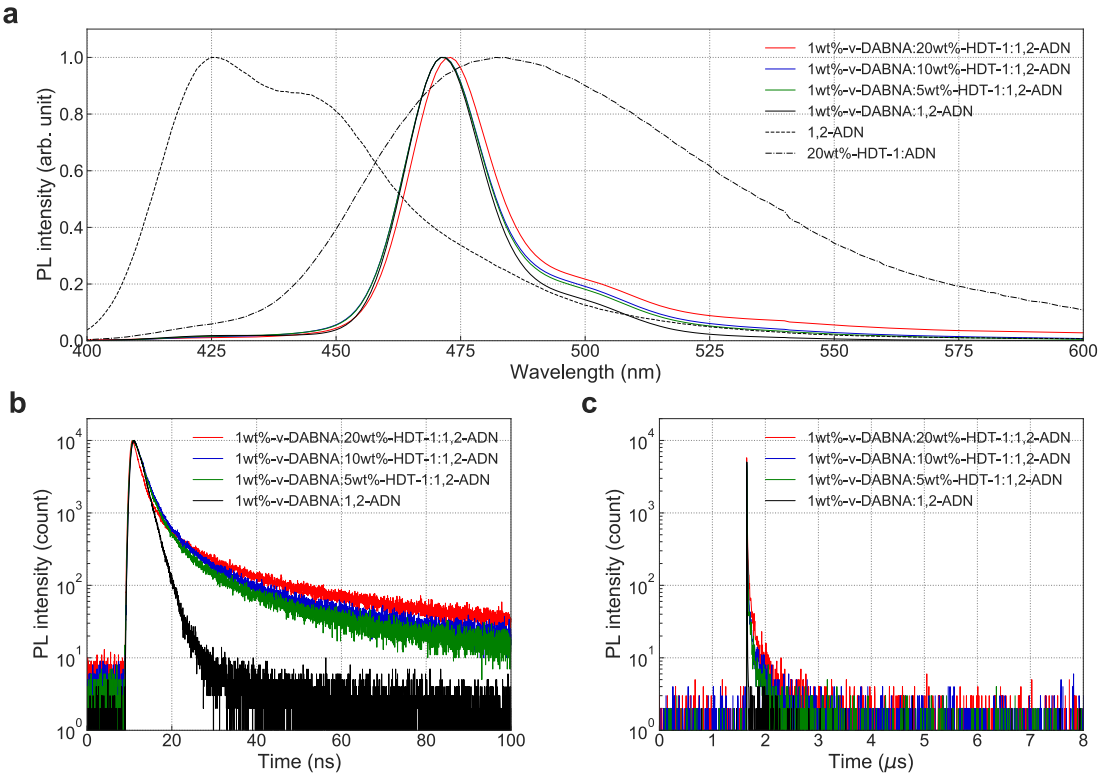

Figure 4.5: (a) Steady-state PL spectra of 1,2-ADN film, 20wt%-HDT-1: 1,2-ADN blend film, and 1wt%-*ν*-DABNA: x wt%-HDT-1: 1,2-ADN blend film with various HDT-1 doping concentrations (x% = 0, 5, 10, and 20). (b, c) Transient PL decay profiles of 1wt%-*ν*-DABNA: x wt%-HDT-1: 1,2-ADN blend film with various HDT-1 doping concentrations (x% = 0, 5, 10, and 20).

explained by the intersystem-crossing (ISC) process in HDT-1. As the concentration of HDT-1 is higher than ν-DABNA, the Förster-type resonance energy transfer from the TTU singlet state (1,2-ADN) is more likely to happen to the HDT-1 singlet state first before reached to the ν-DABNA excited singlet state. **Figure 4.5** clearly shows that HDT-1 is capable of harvesting singlet excitons from 1,2-ADN because of its lower S_1 energy level compared to that of 1,2-ADN. Therefore, the ISC process on an HDT-1 molecule can happen successively, converting the excitons to the triplet excited state. These excited triplets are then quenched by the TTU host triplet state, decreasing the total PLQY of the system. It is worth noting that there is a key difference between PL and EL processes. While triplet generation needs an ISC process from HDT-1 in the PL process, it happens directly in the EL process. In addition, TTU is generally inactive in PL studies due to low excitation light intensity, while it dominates in EL thanks to high current density. As a result, although PLQY with HDT-1 is halved compared to the one without HDT-1, the EQE only drops by 30%.

Importantly, the operational device lifetime of the OLED employing the extended EML structure was augmented by a factor of five in comparison to conventional OLEDs even though much triplet excitons contribute to the EL process, as demonstrated in **Fig. 4.6**. Both devices were put under

accelerated test with the same initial luminance of 1,000 cd m^{-2}. The LT95, which is the amount of running time before the luminance failed to 95% (950 cd m^{-2}) from the initial luminance, of conventional OLED was only 12 hours. Meanwhile, with 5wt% HDT-1 doped at the extended CT interface, the LT_{95} was able to exceed 60 hours. Similarly, when operating both OLEDs at the same current density of 10 mA cm^{-2}, a similar trend can be observed. Specifically, while LT97 of conventional devices was only around 8 hours, the OLED employing the extended EML showed LT97 of nearly 80 hours. This substantial improvement implies that facilitating direct recombination onto HDT-1 molecules at the HTL/EML interface is crucial in enhancing OLED stability. It is commonly believed that charge carrier accumulation can lead to several degradation processes because of the generation of high-energy polaron via singlet-polaron annihilation or triplet-polaron annihilation. By moving the recombination site away from the CT interface (HTL/EML interface in this case), we can expect the separation of the exciton generation region from the charge accumulation region, resulting in less annihilation probability.

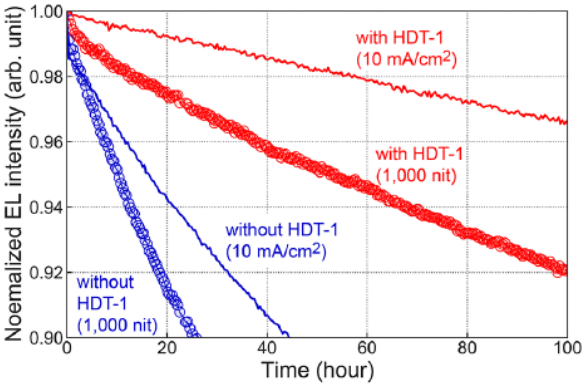

Figure 4.6: Normalized EL intensity of the OLEDs as a function of operating time at a constant current density. The constant driving current density was set to reach 1000 cd m^{-2} and 10 mA cm^{-2} for each OLED.

4-4. Conclusion

In conclusion, we demonstrated here a proof-of-concept of an extended CT interface that can enhance both TTU contribution and operational device lifetime simultaneously. By employing a sky-blue TADF material (HDT-1) as the assistant dopant in a 3-nm-thick layer near the HTM/EML interface, the recombination zone was successfully expanded, allowing for direct charge injection onto TADF molecules. As a result, although EQE was slightly diminished, a considerable enhancement in delayed EL intensity was recorded with almost one order of magnitude, approaching the theoretical maximum for TTU contribution. Additionally, the expansion of the recombination zone also led to a fivefold improvement in the OLED's operational lifetime. This study offers a straightforward and simple method for developing highly efficient and stable blue TTU-OLEDs. It should be noted, however, that these achievements are still in the preliminary stage and further optimization, as well as future studies on assistant dopant choices, may overcome the EQE reduction. As discussed above, the one major efficiency inhibitor is the low PLQY coming from TADF's ISC

process. It can thus be expected that future deep blue TADF with ultrafast FRET energy transfer process from TADF's S_1 to emitter's S_1 can outcompete with ISC, hence improving PLQY as well as EQE.

Chapter 5

Summary and Outlook

5-1. Summary

This study provided a comprehensive understanding of blue OLED improvement based on CT interaction, i.e., exciplex. We explored TRZ derivatives and anthracene derivatives as acceptors for tris-PCz-based exciplex. It was revealed that regardless of which OLED mechanism, exciplex shows the general trend of enhancing both EQE and device lifetime **(Fig. 5.1)**.

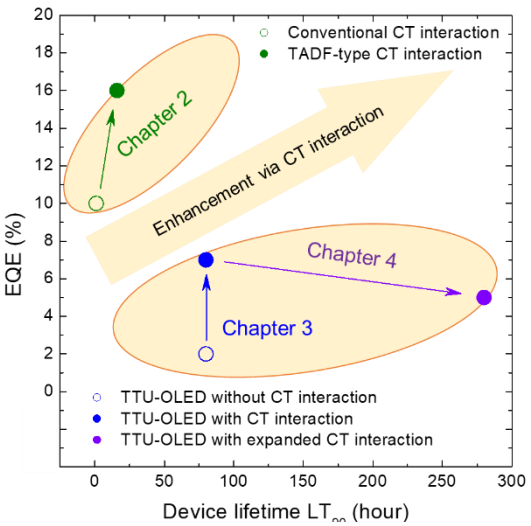

Figure 5.1: Summary of Chapters 2-4 with respect to EQE and device lifetime LT_{90}.

In Chapter 2, the conventional TRZ derivatives with a high triplet energy level were shown to possess extremely low device stability when used as acceptor molecules for tris-PCz donors. On the other hand, utilizing the D-A type molecule as an acceptor significantly improved the OLED stability while maintaining a high EL performance even when tris-PCz is used as the donor. Interestingly, the TADF-type acceptor yielded the best OLED performances. We concluded that the significant improvement in OLED stability is due to "exciton recycling" in the TADF-type acceptor-based exciplex system. This process is possible because T_1 of the TADF-type acceptor is the lowest in the whole system, allowing for the triplet confinement and the RISC process directly on the TADF-type acceptor.

In Chapter 3, we clarify that the charge-transfer (CT) interaction at a hole-transport/emitter-layer interface is an overlooked pathway to enhance TTU yield significantly. This interaction was hypothesized as the main mechanism behind the efficient TTU process in the tris-PCz/NaNaP-A-based blue fluorescence OLED. First, a small energy offset at the interface enables the formation of a high-energy CT exciton. Second, the lower energy triplet state (~1.8 eV) originated from an anthracene moiety collects the interfacial triplet CT excitons. Third, due to the high-density triplet formation at the interface, TTU at the interface contributes to the efficient EL even at low current density. As evidence, a significant drop in OLED performance was confirmed when blocking the CT interface with the mCBP layer. Thus, this finding underlines the important role of the CT interface in exploiting the full potential of TTU in pure-blue OLEDs.

Chapter 4 presents a proof-of-concept for realizing the maximum TTU contribution yield in blue fluorescence OLEDs through doping TADF molecules as carrier recombination centers. The bipolar carrier transport ability of TADF materials enabled direct carrier recombination on the

molecules, resulting in the expansion of the recombination zone. Although the EQE of the OLED is slightly lower than that of conventional TTU-OLEDs due to the low PLQY of the doped layer, the TTU efficiency approaches the upper limit (~60%). Further, the operational device lifetime of OLED employing TADF molecules increased by five times compared to the conventional ones, highlighting the expansion of the recombination zone as a crucial factor for enhancing overall OLED performance in TTU-OLEDs.

5-2. Future perspective

While this study focused on examining various acceptor materials, it would be beneficial to explore the role of various donor materials in future research. The findings and strategies discussed in Chapters 2, 3, and 4 for acceptors could also be applied to donors. Specifically, Chapter 2 introduced the concept of using a TADF-type acceptor, and applying a TADF-type donor could lead to similar enhancements. This will create a promising new target: TADF donor-TADF acceptor exciplexes. Optimizing the donor materials could also reduce the driving voltage for TTU-OLEDs, as shown in Chapters 3 and 4. The CT interaction has already achieved an ultra-low turn-on voltage for blue TTU-OLEDs. The exciplex system will provide a valuable methodology for increasing EQE and stability in blue OLED research.

5-2-1. TADF donor-TADF acceptor based exciplex

In Chapter 2, we addressed the concern of unwanted hole-injection from the exciplex's donor to the exciplex's acceptor. Our solution was to introduce an electron donating group to exciplex's acceptor to stabilize radical cation. Although the system showed a positive result, it should be recognized that inside OLEDs both holes and electrons will be eventually transported through all materials of the EML. This is because even with an energy barrier, such as the LUMO-LUMO gap of the exciplex's donor and exciplex's acceptor, charge injection is possible with thermal energy and high operating voltage. Therefore, there should also be a concern about unwanted electron-injection from the exciplex's acceptor to the exciplex's donor. In our exciplex system between tris-PCz and TRZ, the mechanism can be described as follows. Tris-PCz's LUMO energy level is around –2.4 eV while TRZ's is –3.0 eV. Due to thermal probability and/or an additional 0.6 eV to the operation voltage, electrons can overcome the energy gap and directly be injected into tris-PCz's LUMO. Unfortunately, due to the electron-rich nature of tris-PCz, this unwanted injection significantly destabilized the molecule, leading to potential degradation cause. In fact, carbazole moieties has been reported to show irreversible cyclic voltage after each reduction step[76]. By introducing electron-

accepting moiety, unwanted electrons can be located away from the tris-PCz core, leading to increased stability. However, there is a crucial criterion for the extra moiety. In order to not disturb the overall exciplex system between tris-PCz and TRZ, the additional electron-accepting group needs to have a shallower LUMO than TRZ's. Possible candidates are pyrimidine, pyridine, ketone, benzonitrile, and so on. This modification will transform tris-PCz, a p-type molecule, into a D-A type molecule similar to Cz-TRZ, promising to enhance OLEDs operational lifetime over tris-PCz. As we discussed in Chapter 2, changing from D-A type to TADF type will result in further device stability improvement thanks to the local RISC process. Thus, we propose that TADF-TADF type exciplex has the potential to significantly improve upon what TADF-type acceptor has shown (**Fig. 5.2**). The problem is how to design a tris-PCz based TADF with the listed acceptor moieties. Tris-PCz and benzonitrile have been reported before but their TADF property remains poor with less than 10^4 RISC rate constant[77]. We also tried to synthesize tris-PCz with the pyrimidine group (**Fig. 5.3**). Unfortunately, the large molecular weight prevented us from purifying the material. The problem might come from the imbalance between the electron-donating strength of tris-PCz over the electron-accepting capability of benzonitrile or pyrimidine. If so, employing a multi-acceptor such as the A-D-A motif might be the answer to obtaining good tris-PCz-based TADF.

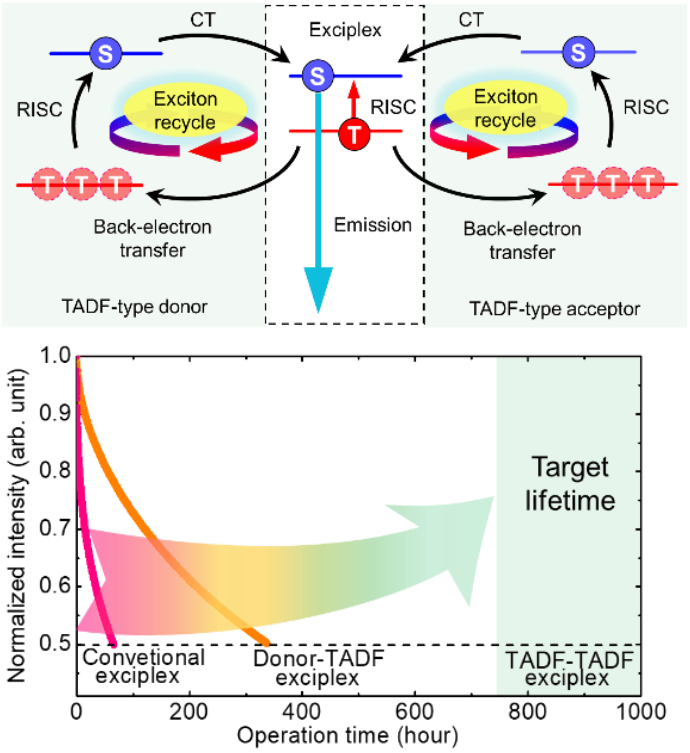

Figure 5.2. TADF-TADF interfacial CT OLED concept and target lifetime of future research.

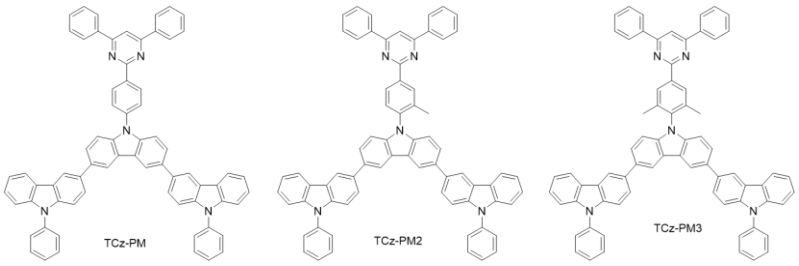

Figure 5.3: Examples of potential tris-PCz based TADF materials for TADF-TADF exciplex.

5-2-2. Ternary TADF Exciplex

In the final section of Chapter 2, we discussed the possibility of utilizing *v*-DABNA as a dopant for the exciplex host. It was shown that the device lifetime did not change significantly with the doping of *v*-DABNA, hence no further stability improvement. However, *v*-DABNA itself is not a stable molecule. Developing a

stable MR-TADF-type emitter would significantly accelerate stable blue OLED realization. It is noted that *v*-DABNA is yet to meet the CIE_y requirement of 0.05 for deep blue devices. Future emitters should overcome this problem by raising the energy level to around 0.1 eV. However, we must also develop a higher energy exciplex system to completely confine energy (**Fig. 5.4**).

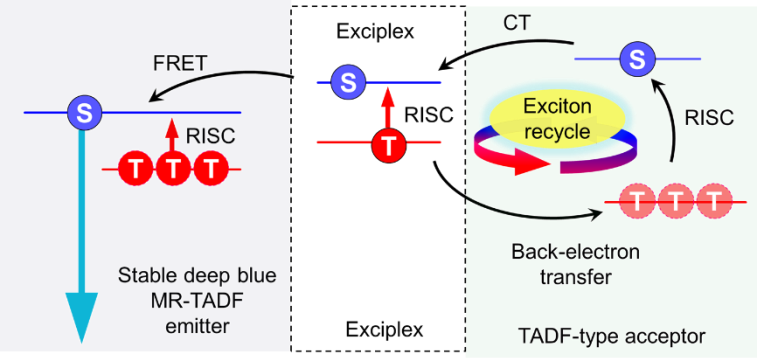

Figure 5.4: Schematic proposal of ternary TADF exciplex.

5-2-3. Ultra-low-driving-voltage and highly efficient blue TTU-OLEDs

We demonstrated the importance of exciplex formation for realizing high EQE TTU-OLEDs in Chapter 3. In which, holes are located at the tris-PCz side of the HTL/EML interface, while electrons are located at the NaNaP-A side of the HTL/EML interface. Thus, OLED turn-on voltage (where EL intensity equals 1 cd m^{-2}) corresponds well with the gap between tris-PCz HOMO and NaNaP-A LUMO (i.e., CT energy level). It means that if we reduce this gap, a much lower operating voltage is possible (**Fig. 5.5**). Thanks to ADN-derivative's low triplet energy level (~1.6 eV), it is theoretically possible to have fully operating blue TTU-OLEDs at 1.6 V. In fact, such a device has been reported recently by S. Izawa et al.[78]. However, their approach was to generate CT interaction between ADN and a strong electron-accepting molecule such as perylene diimide (PDI), forcing them to inject holes directly onto a ADN-derivative. While it is possible to do so with the MoO_3 charge injecting layer, we have shown in Chapter 3 that EQE drops significantly when hole injection must happen. Indeed, Izawa's devices exhibited only 3% EQE, much lower than the theoretical 10%. Thus, we propose a different way to reduce driving voltage while maintaining a relatively high EQE: modifying tris-PCz to have a shallower HOMO level. NaNaP-As' LUMO is around –3.0 eV, so the theoretical target is –4.6 eV for the HOMO of HTL.

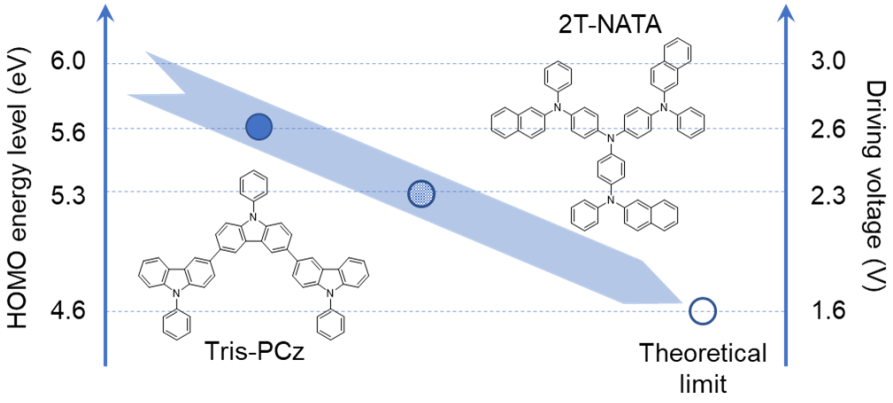

Figure 5.5: Schematic proposal of blue OLEDs with ultra-low driving voltage.

Several shallow HOMO (around –5.0 eV) candidates can be 2T-NATA, Spiro-TTB, and Spiro-OMeTAD. They are common commercialized hole-transporting materials for both OLEDs and organic solar cells, so it is relatively convenient to incorporate them into TTU-OLEDs. The outcoming OLEDs are expected to show a turn-on voltage of sub 2 V. Although it is not as low as the theoretical minimum, a much higher EQE than the reported one can be promised.

References

1. Pierret, R. F. *Advanced Semiconductor Fundamentals second edition*. vol. 1 (Pearson Education, Inc., 2003).
2. Sparkes, J. J. *Semiconductor Devices*. (Van Nostrand Reinhold (UK) Co. Ltd., 1987).
3. Brütting, W. *Physics of Organic Semiconductors*. (Wiley-VCH, 2005).
4. Gaspar, D. & Polikarpov, E. *OLED Fundamentals: materials, devices, and processing of organic light-emitting diodes*. (CRC press, 2015).
5. Okumoto, K. & Shirota, Y. Development of high-performance blue–violet-emitting organic electroluminescent devices. *Appl. Phys. Lett.* **79**, 1231–1233 (2001).
6. Tang, C. W., Vanslyke, S. A. & Chen, C. H. Electroluminescence of doped organic thin films. *J. Appl. Phys.* **65**, 3610–3616 (1989).
7. Shi-Jian Su, B., Chiba, T., Takeda, T., Kido, J., Su, S., Takeda, T., Kido, J. & Chiba, T. Pyridine-Containing Triphenylbenzene Derivatives with High Electron Mobility for Highly Efficient Phosphorescent OLEDs. *Adv. Mater.* **20**, 2125–2130 (2008).
8. Anthopoulos, T. D., Markham, J. P. J., Namdas, E. B., Samuel, I. D. W., Lo, S. C. & Burn, P. L. Highly efficient single-layer dendrimer light-emitting diodes with balanced charge transport. *Appl. Phys. Lett.* **82**, 4824–4826 (2003).
9. Chen, H. F., Yang, S. J., Tsai, Z. H., Hung, W. Y., Wang, T. C. & Wong, K. T. 1,3,5-Triazine derivatives as new electron transport–type host materials for highly efficient green phosphorescent OLEDs. *J. Mater. Chem.* **19**, 8112–8118 (2009).
10. Chang, C. C., Hsieh, M. T., Chen, J. F., Hwang, S. W. & Chen, C. H. Highly power efficient organic light-emitting diodes with a p-doping layer. *Appl. Phys. Lett.* **89**, 253504 (2006).
11. Kijima, Y., Asai, N. & Tamura, S. I. A Blue Organic Light Emitting Diode. *Japanese J. Appl. Physics, Part 1 Regul. Pap. Short Notes Rev. Pap.* **38**, 5274–5277 (1999).
12. Schols, S. *Device Architecture and Materials for Organic Light-Emitting Devices*. (Springer, 2011).
13. Tang, C. W. & Vanslyke, S. A. Organic electroluminescent diodes. *Appl. Phys. Lett.* **51**, 913–915 (1987).
14. Sato, T., Miyamae, T., Ohata, H. & Tsutsui, T. Direct observations of the charge behavior of a high-efficiency blue organic light-emitting diode under operating conditions using electric-field-induced doubly resonant sum-frequency-generation vibrational spectroscopy. *Org. Electron.* **74**, 118–125 (2019).

15. Sun, J., Ahn, H., Kang, S., Ko, S. B., Song, D., Um, H. A., Kim, S., Lee, Y., Jeon, P., Hwang, S. H., You, Y., Chu, C. & Kim, S. Exceptionally stable blue phosphorescent organic light-emitting diodes. *Nat. Photonics* **16**, 212–218 (2022).

16. Chan, C. Y., Tanaka, M., Lee, Y. T., Wong, Y. W., Nakanotani, H., Hatakeyama, T. & Adachi, C. Stable pure-blue hyperfluorescence organic light-emitting diodes with high-efficiency and narrow emission. *Nat. Photonics* **15**, 203–207 (2021).

17. Kim, D. J., Lee, S., Lee, Y. H., Jang, H., Ahn, K. H. & Han, W. S. Triazine-dibenzofuran-based n-type host materials for high-efficiency and long-lifetime green phosphorescent organic light-emitting diodes. *J. Mater. Chem. C* **9**, 12102–12110 (2021).

18. Mac Ciarnáin, R., Mo, H. W., Nagayoshi, K., Fujimoto, H., Harada, K., Gehlhaar, R., Ke, T. H., Heremans, P. & Adachi, C. A Thermally Activated Delayed Fluorescence Green OLED with 4500 h Lifetime and 20% External Quantum Efficiency by Optimizing the Emission Zone using a Single-Emission Spectrum Technique. *Adv. Mater.* **34**, 2201409 (2022).

19. Margulies, E. A., Boudreauit, P. L. T., Adamovich, V. I., Alleyne, B. D., Weaver, M. S. & Brown, J. J. Narrow spectrum deep red emitters for OLED lighting and display. *Dig. Tech. Pap. - SID Int. Symp.* **50**, 911–913 (2019).

20. Kothavale, S., Chung, W. J. & Lee, J. Y. High efficiency and long lifetime orange-red thermally activated delayed fluorescent organic light emitting diodes by donor and acceptor engineering. *J. Mater. Chem. C* **9**, 528–536 (2021).

21. Ha, J. M., Hur, S. H., Pathak, A., Jeong, J. E. & Woo, H. Y. Recent advances in organic luminescent materials with narrowband emission. *NPG Asia Mater.* **13**, 1–36 (2021).

22. Uoyama, H., Goushi, K., Shizu, K., Nomura, H. & Adachi, C. Highly efficient organic light-emitting diodes from delayed fluorescence. *Nature* **492**, 234–238 (2012).

23. Nakanotani, H., Masui, K., Nishide, J., Shibata, T. & Adachi, C. Promising operational stability of high-efficiency organic light-emitting diodes based on thermally activated delayed fluorescence. *Sci. Rep.* **3**, 1–6 (2013).

24. Shi, J. & Tang, C. W. Anthracene derivatives for stable blue-emitting organic electroluminescence devices. *Appl. Phys. Lett.* **80**, 3201–3203 (2002).

25. Noda, H., Nakanotani, H. & Adachi, C. Excited state engineering for efficient reverse intersystem crossing. *Sci. Adv.* **4**, eaao6910 (2018).

26. Hosokai, T., Matsuzaki, H., Nakanotani, H., Tokumaru, K., Tsutsui, T., Furube, A., Nasu, K., Nomura, H., Yahiro, M. & Adachi, C. Evidence and mechanism of efficient thermally activated delayed fluorescence promoted by delocalized excited states. *Sci. Adv.* **3**, e1603282

(2017).

27. Baldo, M. A., O'Brien, D. F., You, Y., Shoustikov, A., Sibley, S., Thompson, M. E. & Forrest, S. R. Highly efficient phosphorescent emission from organic electroluminescent devices. *Nature* **395**, 151–154 (1998).

28. Fleetham, T., Li, G. & Li, J. Phosphorescent Pt(II) and Pd(II) Complexes for Efficient, High-Color-Quality, and Stable OLEDs. *Adv. Mater.* **29**, 1601861 (2017).

29. Adachi, C., Baldo, M. A., Forrest, S. R. & Thompson, M. E. High-efficiency organic electrophosphorescent devices with tris(2-phenylpyridine)iridium doped into electron-transporting materials. *Appl. Phys. Lett.* **77**, 904–906 (2000).

30. Tanaka, H., Shizu, K., Miyazaki, H. & Adachi, C. Efficient green thermally activated delayed fluorescence (TADF) from a phenoxazine–triphenyltriazine (PXZ–TRZ) derivative. *Chem. Commun.* **48**, 11392–11394 (2012).

31. Goushi, K., Yoshida, K., Sato, K. & Adachi, C. Organic light-emitting diodes employing efficient reverse intersystem crossing for triplet-to-singlet state conversion. *Nat. Photonics* **6**, 253–258 (2012).

32. Goushi, K. & Adachi, C. Efficient organic light-emitting diodes through up-conversion from triplet to singlet excited states of exciplexes. *Appl. Phys. Lett.* **101**, 023306 (2012).

33. Li, J., Nomura, H., Miyazaki, H. & Adachi, C. Highly efficient exciplex organic light-emitting diodes incorporating a heptazine derivative as an electron acceptor. *Chem. Commun.* **50**, 6174–6176 (2014).

34. Mamada, M., Tian, G., Nakanotani, H., Su, J. & Adachi, C. The Importance of Excited-State Energy Alignment for Efficient Exciplex Systems Based on a Study of Phenylpyridinato Boron Derivatives. *Angew. Chemie - Int. Ed.* **57**, 12380–12384 (2018).

35. Chapran, M., Pander, P., Vasylieva, M., Wiosna-Salyga, G., Ulanski, J., Dias, F. B. & Data, P. Realizing 20% External Quantum Efficiency in Electroluminescence with Efficient Thermally Activated Delayed Fluorescence from an Exciplex. *ACS Appl. Mater. Interfaces* **11**, 13460–13471 (2019).

36. Zhang, L. & Cheah, K. W. Thermally Activated Delayed Fluorescence Host for High Performance Organic Light-Emitting Diodes. *Sci. Rep.* **8**, 8832 (2018).

37. Seino, Y., Sasabe, H., Pu, Y. J. & Kido, J. High-performance blue phosphorescent OLEDs using energy transfer from exciplex. *Adv. Mater.* **26**, 1612–1616 (2014).

38. Nakanotani, H., Furukawa, T., Morimoto, K. & Adachi, C. Long-range coupling of electron-

hole pairs in spatially separated organic donor-acceptor layers. *Sci. Adv.* **2**, e1501470 (2016).

39. Pu, Y. J., Koyama, Y., Otsuki, D., Kim, M., Chubachi, H., Seino, Y., Enomoto, K. & Aizawa, N. Exciplex emissions derived from exceptionally long-distance donor and acceptor molecules. *Chem. Sci.* **10**, 9203–9208 (2019).

40. Colella, M., Danos, A. & Monkman, A. P. Less is more: Dilution enhances optical and electrical performance of a TADF exciplex. *J. Phys. Chem. Lett.* **10**, 793–798 (2019).

41. Zhang, C., Lu, Y., Liu, Z., Zhang, Y., Wang, X., Zhang, D. & Duan, L. A π–D and π–A Exciplex-Forming Host for High-Efficiency and Long-Lifetime Single-Emissive-Layer Fluorescent White Organic Light-Emitting Diodes. *Adv. Mater.* **32**, 1–10 (2020).

42. Fukagawa, H., Shimizu, T., Kamada, T., Yui, S., Hasegawa, M., Morii, K. & Yamamoto, T. Highly efficient and stable organic light-emitting diodes with a greatly reduced amount of phosphorescent emitter. *Sci. Rep.* **5**, 1–7 (2015).

43. Song, W., Yeob Lee, J., Joo Cho, Y., Yu, H., Aziz, H., Mun Lee Song, K. W., Lee, J. Y., Cho, Y. J., Yu, H., Aziz, H. & Lee, K. M. Electroplex as a New Concept of Universal Host for Improved Efficiency and Lifetime in Red, Yellow, Green, and Blue Phosphorescent Organic Light-Emitting Diodes. *Adv. Sci.* **5**, 1700608 (2018).

44. Nakanotani, H., Higuchi, T., Furukawa, T., Masui, K., Morimoto, K., Numata, M., Tanaka, H., Sagara, Y., Yasuda, T. & Adachi, C. High-efficiency organic light-emitting diodes with fluorescent emitters. *Nat. Commun.* **5**, 1–7 (2014).

45. Furukawa, T., Nakanotani, H., Inoue, M. & Adachi, C. Dual enhancement of electroluminescence efficiency and operational stability by rapid upconversion of triplet excitons in OLEDs. *Sci. Rep.* **5**, 8429 (2015).

46. Sasaki, T., Hasegawa, M., Inagaki, K., Ito, H., Suzuki, K., Oono, T., Morii, K., Shimizu, T. & Fukagawa, H. Unravelling the electron injection/transport mechanism in organic light-emitting diodes. *Nat. Commun.* **12**, 1–8 (2021).

47. Lee, J., Jeong, C., Batagoda, T., Coburn, C., Thompson, M. E. & Forrest, S. R. Hot excited state management for long-lived blue phosphorescent organic light-emitting diodes. *Nat. Commun.* **8**, 15566 (2017).

48. Kondo, Y., Yoshiura, K., Kitera, S., Nishi, H., Oda, S., Gotoh, H., Sasada, Y., Yanai, M. & Hatakeyama, T. Narrowband deep-blue organic light-emitting diode featuring an organoboron-based emitter. *Nat. Photonics* **13**, 678–682 (2019).

49. Giebink, N. C., D'Andrade, B. W., Weaver, M. S., MacKenzie, P. B., Brown, J. J., Thompson, M. E. & Forrest, S. R. Intrinsic luminance loss in phosphorescent small-molecule

organic light emitting devices due to bimolecular annihilation reactions. *J. Appl. Phys.* **103**, 44509 (2008).

50. Kim, S., Bae, H. J., Park, S., Kim, W., Kim, J., Kim, J. S., Jung, Y., Sul, S., Ihn, S. G., Noh, C., Kim, S. & You, Y. Degradation of blue-phosphorescent organic light-emitting devices involves exciton-induced generation of polaron pair within emitting layers. *Nat. Commun.* **9**, (2018).

51. Zhang, D., Cai, M., Zhang, Y., Zhang, D. & Duan, L. Sterically shielded blue thermally activated delayed fluorescence emitters with improved efficiency and stability. *Mater. Horizons* **3**, 145–151 (2016).

52. Cui, L. S., Ruan, S. Bin, Bencheikh, F., Nagata, R., Zhang, L., Inada, K., Nakanotani, H., Liao, L. S. & Adachi, C. Long-lived efficient delayed fluorescence organic light-emitting diodes using n-type hosts. *Nat. Commun.* **8**, 1–8 (2017).

53. Hatakeyama, T., Shiren, K., Nakajima, K., Nomura, S., Nakatsuka, S., Kinoshita, K., Ni, J., Ono, Y. & Ikuta, T. Ultrapure Blue Thermally Activated Delayed Fluorescence Molecules: Efficient HOMO-LUMO Separation by the Multiple Resonance Effect. *Adv. Mater.* **28**, 2777–2781 (2016).

54. Oda, S., Kumano, W., Hama, T., Kawasumi, R., Yoshiura, K. & Hatakeyama, T. Carbazole-Based DABNA Analogues as Highly Efficient Thermally Activated Delayed Fluorescence Materials for Narrowband Organic Light-Emitting Diodes. *Angew. Chemie - Int. Ed.* **60**, 2882–2886 (2021).

55. Jeon, S. O., Lee, K. H., Kim, J. W. J. S., Ihn, S. G., Chung, Y. S., Kim, J. W. J. S., Lee, H., Kim, S., Choi, H. & Lee, J. Y. High-efficiency, long-lifetime deep-blue organic light-emitting diodes. *Nat. Photonics* **15**, 208–215 (2021).

56. Wang, X., Wang, L., Meng, G., Zeng, X., Zhang, D. & Duan, L. Improving the stability and color purity of a BT.2020 blue multiresonance emitter by alleviating hydrogen repulsion. *Sci. Adv.* **9**, eadh1434 (2023).

57. Lim, H., Woo, S. J., Ha, Y. H., Kim, Y. H. & Kim, J. J. Breaking the Efficiency Limit of Deep-Blue Fluorescent OLEDs Based on Anthracene Derivatives. *Adv. Mater.* **34**, 2100161 (2022).

58. Lee, Y. T., Chan, C. Y., Tanaka, M., Mamada, M., Goushi, K., Tang, X., Tsuchiya, Y., Nakanotani, H. & Adachi, C. Tailor-Made Multi-Resonance Terminal Emitters toward Narrowband, High-Efficiency, and Stable Hyperfluorescence Organic Light-Emitting Diodes. *Adv. Opt. Mater.* **10**, 1–9 (2022).

59. Yang, M., Shikita, S., Min, H., Park, I. S., Shibata, H., Amanokura, N. & Yasuda, T. Wide-Range Color Tuning of Narrowband Emission in Multi-resonance Organoboron Delayed Fluorescence Materials through Rational Imine/Amine Functionalization. *Angew. Chemie - Int. Ed.* **60**, 23142–23147 (2021).

60. Park, I. S., Min, H. & Yasuda, T. Ultrafast Triplet–Singlet Exciton Interconversion in Narrowband Blue Organoboron Emitters Doped with Heavy Chalcogens. *Angew. Chemie* **134**, e202205684 (2022).

61. He, X., Ren, S., Liu, H., Zhao, S., Liu, F., Du, C., Min, J., Zhang, H. & Lu, P. Efficient Nondoped Pure Blue Organic Light-Emitting Diodes Based on an Anthracene and 9,9-Diphenyl-9,10-dihydroacridine Derivative. *Chem. - An Asian J.* **15**, 163–168 (2020).

62. Chiang, C. J., Kimyonok, A., Etherington, M. K., Griffiths, G. C., Jankus, V., Turksoy, F. & Monkman, A. P. Ultrahigh efficiency fluorescent single and bi-layer organic light emitting diodes: The key role of triplet fusion. *Adv. Funct. Mater.* **23**, 739–746 (2013).

63. Pandey, A. K. & Nunzi, J. M. Rubrene/fullerene heterostructures with a half-gap electroluminescence threshold and large photovoltage. *Adv. Mater.* **19**, 3613 (2007).

64. Xiang, C., Peng, C., Chen, Y. & So, F. Origin of Sub-Bandgap Electroluminescence in Organic Light-Emitting Diodes. *Small* **11**, 5439 (2015).

65. Cho, I., Kim, S. H., Kim, J. H., Park, S. & Park, S. Y. Highly efficient and stable deep-blue emitting anthracene-derived molecular glass for versatile types of non-doped OLED applications. *J. Mater. Chem.* **22**, 123–129 (2012).

66. Wang, Y., Liu, W., Ye, S., Zhang, Q., Duan, Y., Guo, R. & Wang, L. Molecular engineering of anthracene-based emitters for highly efficient nondoped deep-blue fluorescent OLEDs. *J. Mater. Chem. C* **8**, 9678–9687 (2020).

67. Shih, C. J., Lee, C. C., Chen, Y. H., Biring, S., Kumar, G., Yeh, T. H., Sen, S., Liu, S. W. & Wong, K. T. Exciplex-Forming Cohost for High Efficiency and High Stability Phosphorescent Organic Light-Emitting Diodes. *ACS Appl. Mater. Interfaces* **10**, 2151–2157 (2018).

68. Tanaka, M., Noda, H., Nakanotani, H. & Adachi, C. Effect of Carrier Balance on Device Degradation of Organic Light-Emitting Diodes Based on Thermally Activated Delayed Fluorescence Emitters. *Adv. Electron. Mater.* **5**, 1800708 (2019).

69. Monkman, A. P. Singlet Generation from Triplet Excitons in Fluorescent Organic Light-Emitting Diodes. *ISRN Mater. Sci.* **2013**, 1–19 (2013).

70. Ieuji, R., Goushi, K. & Adachi, C. Triplet–triplet upconversion enhanced by spin–orbit

coupling in organic light-emitting diodes. *Nat. Commun.* **10**, 5283 (2019).

71. Lin, B. Y., Easley, C. J., Chen, C. H., Tseng, P. C., Lee, M. Z., Sher, P. H., Wang, J. K., Chiu, T. L., Lin, C. F., Bardeen, C. J. & Lee, J. H. Exciplex-Sensitized Triplet-Triplet Annihilation in Heterojunction Organic Thin-Film. *ACS Appl. Mater. Interfaces* **9**, 10963–10970 (2017).

72. Suzuki, T., Nonaka, Y., Watabe, T., Nakashima, H., Seo, S., Shitagaki, S. & Yamazaki, S. Highly efficient long-life blue fluorescent organic light-emitting diode exhibiting triplet-triplet annihilation effects enhanced by a novel hole-transporting material. *Jpn. J. Appl. Phys.* **53**, 052102 (2014).

73. Salehi, A., Dong, C., Shin, D. H., Zhu, L., Papa, C., Thy Bui, A., Castellano, F. N. & So, F. Realization of high-efficiency fluorescent organic light-emitting diodes with low driving voltage. *Nat. Commun.* **10**, 2305 (2019).

74. Senevirathne, C. A. M., Yoshida, S., Auffray, M., Yahiro, M., Karunathilaka, B. S. B., Bencheikh, F., Goushi, K., Sandanayaka, A. S. D., Matsushima, T. & Adachi, C. Recycling of Triplets into Singlets for High-Performance Organic Lasers. *Adv. Opt. Mater.* **10**, 1 (2022).

75. Tasaki, S., Nishimura, K., Toyoshima, H., Masuda, T., Nakamura, M., Nakano, Y., Itoi, H., Kambe, E., Kawamura, Y. & Kuma, H. Realization of ultra-high-efficient fluorescent blue OLED. *J. Soc. Inf. Disp.* **30**, 441–451 (2022).

76. Hsiao, S. H. & Lin, S. W. Electrochemical synthesis of electrochromic polycarbazole films from N-phenyl-3,6-bis(N-carbazolyl)carbazoles. *Polym. Chem.* **7**, 198–211 (2016).

77. Zhang, W., Zhang, Y. X., Zhang, X. Q., Liu, X. Y., Fan, J. & Liao, L. S. Blue thermally activated delayed fluorescence materials based on bi/tri-carbazole derivatives. *Org. Electron.* **58**, 238–244 (2018).

78. Izawa, S., Morimoto, M., Fujimoto, K., Banno, K., Majima, Y., Takahashi, M., Naka, S. & Hiramoto, M. Blue Organic Light-Emitting Diode with a Turn-on Voltage at 1.47 V. *ChemRxiv* (2023) doi:10.26434/CHEMRXIV-2023-TNHT6.

List of Publication

1. "The Role of Reverse Intersystem Crossing Using a TADF-Type Acceptor Molecule on the Device Stability of Exciplex-Based Organic Light-Emitting Diodes" **Thanh Ba Nguyen**, Hajime Nakanotani, Takuji Hatakeyama, Chihaya Adachi, *Adv. Mater.*, **2020**, 32, 9, 1906614.
2. "An Overlooked Charge-Transfer Interaction in the Interfacial Triplet-Triplet Upconversion Process in Blue Organic Light- Emitting Diodes" **Thanh Ba Nguyen**, Hajime Nakanotani, Chihaya Adachi, *Adv. Opt. Mater.*, **2022**, 10, 18, 2200704.
3. "Enhancing Triplet–Triplet Upconversion Efficiency and Operational Lifetime in Blue Organic Light-Emitting Diodes by Utilizing Thermally Activated Delayed Fluorescence Materials" **Thanh Ba Nguyen**, Hajime Nakanotani, Chin-Yiu Chan, Shunta Kakumachi, Chihaya Adachi, *ACS Appl. Mater. Interfaces*, **2023**, 15, 19, 23557.

List of Conference

1. "Enhancing Stability of Exciplex-based OLED by Utilizing TADF-Type Acceptor" **T. B. Nguyen**, H. Nakanotani, T. Hatakeyama, C. Adachi, The 68th JSAP Spring Meeting 2020 (2020/02/28, Japan).
2. "Study on the Role of TADF-Type Molecules for Exciplex-Based OLEDs" **T. B. Nguyen**, H. Nakanotani, T. Hatakeyama, C. Adachi, A-COE 2020 (2020/11/08, Korean).
3. "Role of a charge-transfer interface in blue TTU-OLEDs" **T. B. Nguyen**, H. Nakanotani, C. Adachi, The 82nd JSAP Autumn Meeting 2021 (2021/09/13, Japan).
4. "Role of a charge-transfer interface in blue TTU-OLEDs" **T. B. Nguyen**, H. Nakanotani, C. Adachi, A-COE 2021 (2021/09/03, Japan).
5. "Enhancing OLEDs Lifetime by Expanding CT Interface with TADF Assistant Dopant" **T. B. Nguyen**, H. Nakanotani, C. Adachi, The 70th JSAP Spring Meeting 2023 (2023/03/15, Japan).

Acknowledgement

This writing summarizes the research over three years from September 2018 at Adachi Laboratory, Graduate School of Engineering, Kyushu University.

First of all, I am deeply indebted to my family in Vietnam. Without the emotional and financial support from them, there would not be a slim chance for me to be here.

I would like to state my deepest sincere thanks to Professor Adachi for always listening, motivating as well as providing enthusiastic guidance. In addition, I also would like to express my greatest gratitude toward Associate Professor Nakanotani for kind supervision, insightful discussions and lots of important suggestions throughout the research. Moreover, I would like to thank Associate Professor Tsuchiya, Associate Professor Matsushima, Assistant Professor Mamada, Assistant Professor Kabe, Assistant Professor Goushi for endless helpful advices.

I would like to send my deepest acknowledgement to all seniors from Master Students to Doctor Students student as well as Post-Doctoral Fellows in Adachi Laboratory for providing the warmest welcome. Especially, I would like to thank Dr. Noda for following and guiding me throughout not only experiments but also my concerns, Mr. Nagata for helping me regarding Clean Room equipment, and others fellow members of Nakanotani group.

Finally, I would like to thank all technical staffs and officers for their hard-working to ensuring everything is organized and flows smoothly.

It is such an honor for me to be a part of Adachi Laboratory. Even though things happened unexpectedly over the last two years, even though people had to leave, everyone surely took place in this wonderful memory.

Nguyen Ba Thanh